

Gene Regulation Strategies Underlying Skeletal Muscle Atrophy
in Cancer Cachexia

Geysson Javier Fernandez Garcia

UNIVERSIDADE ESTADUAL PAULISTA

“Júlio de Mesquita Filho”

INSTITUTO DE BIOCÊNCIAS DE BOTUCATU

Gene Regulation Strategies Underlying Skeletal Muscle Atrophy
in Cancer Cachexia

M.Sc. GEYSSON JAVIER FERNANDEZ GARCIA

Thesis advisor:

Prof. Dr. ROBSON F. CARVALHO

Thesis presented to the Institute of Biosciences of Botucatu, Sao Paulo State University "Júlio de Mesquita Filho" - UNESP, as a requirement to obtain the PhD Degree in Biological Sciences - Field: Genetics.

BOTUCATU – SP

2018

FICHA CATALOGRÁFICA ELABORADA PELA SEÇÃO TÉC. AQUIS. TRATAMENTO DA INFORM.
DIVISÃO TÉCNICA DE BIBLIOTECA E DOCUMENTAÇÃO - CÂMPUS DE BOTUCATU - UNESP
BIBLIOTECÁRIA RESPONSÁVEL: ROSANGELA APARECIDA LOBO-CRB 8/7500

Fernandez Garcia, Geysson Javier.

Gene regulation strategies underlying skeletal muscle atrophy in cancer cachexia / Geysson Javier Fernandez Garcia. - Botucatu, 2018

Tese (doutorado) - Universidade Estadual Paulista "Júlio de Mesquita Filho", Instituto de Biociências de Botucatu

Orientador: Robson Francisco Carvalho
Capes: 20202008

1. Expressão gênica. 2. Atrofia muscular. 3. Caquexia. 4. Câncer. 5. MicroRNAs.

Palavras-chave: cancer cachexia; gene expression; miRNA profile; muscle atrophy.

*I dedicate this dissertation to the loves of my life:
My parents, my brothers and my wife Luz Ochoa,
For all the love, affection and encouragement.*

*“Satisfaction of one’s curiosity is one of the greatest
sources of happiness in life”*

Linus Pauling.

Acknowledgements

Over the last few years, the journey I have been embarked on was possible thanks to a wonderful crew that provided me of guidance and support not only from an academic point of view but also from a more family-oriented perspective. Therefore, I am using this opportunity to express my deepest appreciation to all those who encouraged me and provided me the possibility to complete this thesis. First of all, I am deeply thankful to Brazil because it has welcomed me as another of its citizens and has given me the opportunity to grow, specially to the Foundation for Research Support of the State of São Paulo (FAPESP) for the financial assistance granted (Grants: 2014/13941-0 and 2016/08294-1). To my advisers, the professors Dr. Robson Carvalho and Alexander Hoffmann for their ambitious and inestimably constructive criticisms and friendly advice, as well as for their truthful and enlightening views on a series of issues related to this project. Secondly, I'm greatly indebted to Prof. Dr. Claudia Aparecida Rainho, and Prof. Dr. Guilherme Targino Valente for serving as my qualifying exam members, for your remarks, invaluable comments and positive criticism. Furthermore, I thank the members of the current examination committee of my PhD thesis, for agreeing to read this manuscript and taking the time to evaluate its content. I would also like to thank the impressive and efficient group of professionals behind the LBME lab at Sao Paulo State University as well as the Signaling systems lab at University of California, Los Angeles, whose help has been critical for the realization of this work. A big thank you as well to Dr. Jayson Gutierrez at Ghent University, a great colleague and my close friend, who motivated me to study systems biology and from whom I received so much great feedback and advice.

A special thanks to God and my family. Words cannot express how grateful I am to my brother, my mother, my father and my sister. Your prayer for me was what sustained me thus far. I would also like to thank my friends, Cintia, Adewunmi, Marie Metzsig, Catera Wilder, Quen Cheng, Kim, Sho, Chen Seng, Leonardo, Juarez, Talita, Tassiana, Mariana Ribeiro, Ivan, Carlos and Paulinha who supported me with their friendship and incented me to strive towards my goal. At the end, I would like to express my great appreciation to my wife Luz Ochoa, for her loving support through this trip (near or far), who spent sleepless nights, for all the sacrifices you have made in my name. For all the love you have given me

To all of you, a big thank you!

Gene Regulation Strategies Underlying Skeletal Muscle Atrophy in Cancer Cachexia

by

Geysson Javier Fernandez Garcia

Abstract

Cancer cachexia is a syndrome characterized by the severe skeletal muscle wasting tissue; that affects more than 50% of all cancer patients and results in lower quality of life due to compromised fatigue, weakness, decreased immune function, insulin resistance and poor tolerance and response to radio and chemotherapy. Remarkably, approximately 20% of cancer-related deaths are estimated to be directly caused by cachexia. There is currently no effective targeted therapy and the main limitation lays on the traditional approaches that not deal with the inherent complexity, characterized by non-linear interactions, of gene regulatory networks (GRN). Thus, a clear identification of the components of gene regulation, and a quantitative understanding of their temporal integration to control cellular responses is fundamental for capture essential mechanistic details that will ultimately enable the development of direct therapeutic strategies for the treatment of cancer cachexia. Here, we examine genome-wide gene expression of muscle wasting under two different frameworks, using static and dynamic gene expression data. We structure this approach as follow: Chapter 1 presents a quantitative characterization of the signaling pathways and a GRN reconstruction of muscle wasting in Lewis Lung Carcinoma (LLC) tumor-bearing mice by integrating static mRNAs and microRNAs expression profiles. The results show that LLC mice reduced body weight in 20% and presented muscle and fat tissue wasting after 23 days of tumor induction. In addition, we found 1008 differential expressed mRNAs (487 up-regulated and 521 down-regulated) and eighteen deregulated miRNAs (13 up-regulated and 5 down-regulated). Our data suggest activation of the transcriptional factor NF- κ B and Stat3, which have been described in the activation of atrophic gene programs. Moreover, we ident potential posttranscriptional regulation by miRNAs of three important biological process: extracellular matrix organization, cell migration and transcription factor binding. Overall our results identify a set of signaling pathways that may contribute to muscle wasting in cancer cachexia, between them extracellular matrix genes with potential regulatory mechanism mediated by miRNAs.

Chapter 2 provides further dissection of the NF- κ B signaling pathway in atrophying muscle cells. Here, we examine quantitatively the genome-wide dynamic gene expression effects of the activation of NF- κ B by the exposure of tumor necrosis factor – alpha (TNF- α) on skeletal muscle cells (C2C12). We characterize the regulatory strategies of gene induction and repression by measuring both mRNA transcription and degradation rates and connecting these processes via mathematical modeling. Our data points to a dominant role of transcription dynamics in the regulation of both gene induction and repression programs in response to TNF; and unveils a decrease in mRNA degradation rate as strategy for genes of late response to increase their intracellular concentrations. Furthermore, our analysis shows constitutive degradation as an intrinsic characteristic of genes that determines most of temporal ranks of gene expression profiles. Using a non-degradable form of inhibitor kappa B alpha and RelA knockout C2C12 cells we found that NF- κ B is responsible for both gene induction and gene repression during muscle cell atrophy induced by TNF- α . Our fine-grained data highlights the importance of signaling dynamics in mediating the TNF- α effects on skeletal muscle cells and reveals a critical interplay between synthesis and degradation control in that regulates dynamic gene expression programs.

Estratégias de regulação de genes subjacentes a atrofia do músculo esquelético na cachexia associada ao câncer

por

Geysson Javier Fernandez Garcia

Resumo

A caquexia associada ao câncer é uma síndrome caracterizada pela grave perda de tecido musculo esquelético; que se estima que afeta mais de 50% de todos os pacientes com câncer e resulta em menor qualidade de vida devido a fadiga, fraqueza, redução da função imune, resistência à insulina e baixa tolerância e resposta à quimioterapia. Notavelmente, 20% das mortes relacionadas ao câncer são diretamente causadas pela caquexia. A principal limitação de que atualmente não há terapia direcionada, é o uso de abordagens tradicionais que não tratam a complexidade em sistemas biológicos, caracterizada por interações não-lineares de redes de regulação genética (GRN, do inglês *Gene Regulatory Networks*). Por esse motivo, ainda é necessária uma identificação dos componentes da GRN e uma compreensão quantitativa de sua integração temporal no controle das respostas celulares. Adquirir tal conhecimento é fundamental para capturar detalhes mecanicistas essenciais para direcionar estratégias terapêuticas para uma doença complexa, como a caquexia do câncer. Neste trabalho, examinamos a expressão genética do músculo esquelético em dois abordagens metodológicos diferentes: usando dados de expressão de genes estáticos e dinâmicos. Estruturamos nosso trabalho da seguinte maneira: o Capítulo 1 apresenta uma caracterização quantitativa das vias de sinalização e uma reconstrução de GRN no tecido musculo esquelético em ratos portadores de carcinoma de pulmão de Lewis (LLC, do inglês Lewis lung carcinoma) através da integração de perfis de expressão de mRNAs e miRNAs em um tempo. Os resultados mostram que os camundongos LLC reduziram o peso corporal em 20% e apresentaram perda de tecido muscular e adiposo após 23 dias de indução tumoral. Além disso, encontramos 1008 mRNAs expressos diferencialmente (487 induzidos e 521 reprimidos) e 18 miRNAs desregulados (13 induzidos e 5 reprimidos). Nossos dados sugerem a ativação do fator transcricional NF- κ B e Stat3, que foram descritos na ativação de programas genéticos atróficos no musculo esquelético. Além disso, identificamos a potencial regulação pós-transcricional por miRNAs de três processos biológicos importantes: organização da matriz extracelular, migração celular e ligação do fator de transcrição. Em geral, nossos resultados identificam um conjunto de caminhos de sinalização que podem contribuir na perda

de tecido musculo esquelético na caquexia associada ao câncer, entre eles genes da matriz extracelular com potencial mecanismo regulatório mediado por miRNAs.

O Capítulo 2 fornece uma dissecção da via de sinalização de NF- κ B em células musculares atrofiadas. Neste capítulo, examinamos quantitativamente os efeitos dinâmicos na expressão gênica pela ativação de NF- κ B após exposição ao fator de necrose tumoral alfa (TNF- α) nas células do músculo esquelético (C2C12). Caracterizamos as estratégias reguladoras de indução e repressão de genes, medindo as taxas de transcrição e degradação para cada mRNA e conectando esses processos através de modelagem matemática. Nossos dados apontam para um papel dominante da transcrição na regulação dos programas de indução e repressão de genes em resposta ao TNF; e revela uma diminuição da taxa de degradação de mRNA como estratégia para genes de resposta tardia para aumentar suas concentrações intracelulares. Além disso, nossa análise mostra a degradação constitutiva como uma característica intrínseca dos genes que determina a ordem temporal dos perfis de expressão gênica. Usando uma forma não degradável do inibidor kappa B alfa e um knockout de RelA, descobrimos que o fator NF- κ B é responsável por indução de genes e repressão de genes durante a atrofia de células musculares induzida por TNF. Nossos dados destacam a importância da dinâmica de sinalização na mediação dos efeitos do TNF nas células do músculo esquelético e revela uma interação crítica entre o controle de síntese e degradação, que regula os programas dinâmicos de expressão gênica.

Contents

1 Genomic Profile of mRNAs and microRNAs of Skeletal Muscle Atrophy in Cancer Cachexia	1
1.1 Introduction.....	2
1.1.1 Skeletal Muscle	2
1.1.2 Cancer Cachexia.....	3
1.1.3 Molecular pathways in cachexia	4
1.1.4. Genome wide studies.....	6
1.1.5 Transcriptome	6
1.1.6 MicroRNome	7
1.2. Question to be answered.....	9
1.3 Characterization of Lewis Lung Cancer (LLC) tumor bearing mice.....	9
1.4 Muscle atrophy in cancer cachexia is associated with heterogeneity in transcriptome changes	13
1.5 Muscle atrophy in cancer cachexia is discriminate by a reduced set of genes.....	16
1.6 Identification of regulatory pathways associated with muscle wasting in cancer cachexia	17
1.7 Transcriptional regulation during muscle atrophy.....	20
1.8 miRNAs associated with muscle wasting in cancer cachexia.....	21
1.9 Integrative analyses of miRNA and mRNA expression profiles identified signaling pathways enriched with predicted miRNA targets	23
1.10 Discussion.....	25
1.11 Methods	29
2 Integrated regulation of mRNA transcription and degradation decodes TNF signaling during inflammatory muscle-atrophy	33
2.1 Introduction.....	34
2.2 Question to be answered.....	36
2.3 TNF stimulation induces skeletal muscle cell atrophy	37
2.4 Dynamic response of cytoplasmic mRNA.	37
2.5 Integration of temporal mRNA degradation and transcription rates reveal the dynamics of gene expression in response to TNF	40
2.5.1 mRNA degradation rates correlate with the temporal ordering of gene expression clusters.	40

2.5.2 Changes in transcription rates correlates with cytoRNA expression levels....	42
2.6 Coupling transcription and degradation dynamic through a mathematical model.	44
2.6.1 Model accurately describes dynamic changes in gene expression	44
2.6.2 Synthesis control dominates but degradation control is critical for some genes	46
2.7 Molecular Regulatory Mechanisms of cytoRNA levels.	49
2.7.1. Transcriptional control is dependent of RelA transcription factor	49
2.7.2 Transcriptional control dependent of MAPK.	52
2.8 Discussion.....	53
2.9 Methods	54
A Supplementary information.....	62
B Bibliography	71

“The way to get good ideas is to get lots of ideas, and throw the bad ones away”

Linus Pauling

1

Genomic Profile of mRNAs and microRNAs of Skeletal Muscle Atrophy in Cancer Cachexia

1.1 Introduction

1.1.1 Skeletal Muscle

Skeletal muscles comprise approximately 40-50% of body mass and are responsible for basic functions such as locomotion, metabolism and respiration¹. In order to allow movement, the organization of muscle cells is highly structured which enable generation and sustaining mechanical tension. Myofiber may have several centimeters in length and can contain hundreds of nuclei. The myofibers cytoplasm is filled with contractile proteins that are assembled into repetitive structures, sarcomeres, the basic contraction unit. These structures are made up of highly ordered actin and myosin filaments, as well as hundreds of regulatory proteins such as the troponin–tropomyosin complex, and scaffolding and cytoskeletal crosslinking proteins such as α -actinin, myomesin and the kinase titin² (**Figure 1-1**).

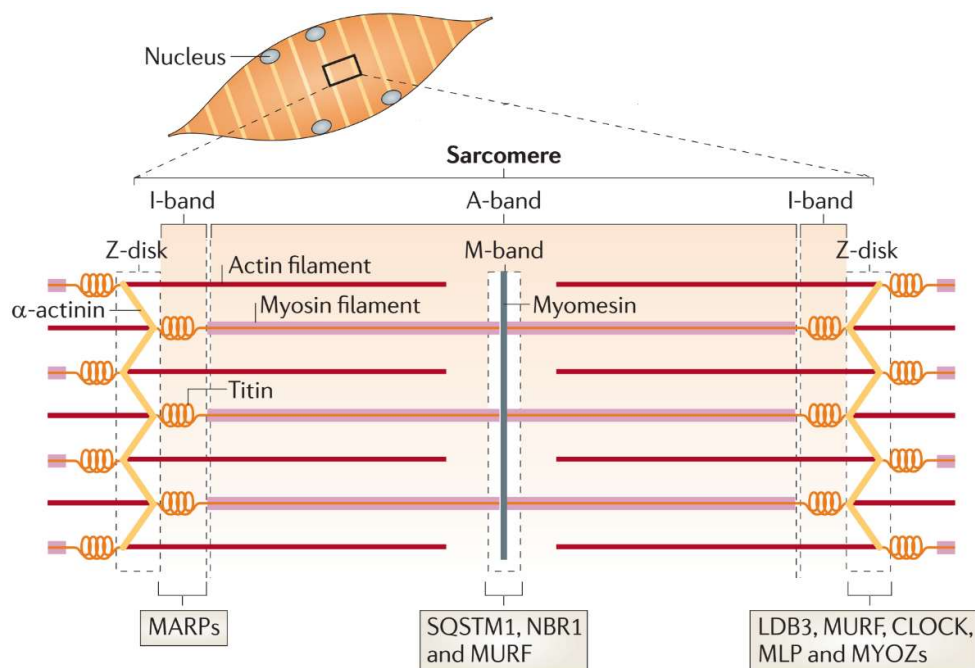


Figure 1-1 Striated muscle structure. The contractile machinery of skeletal muscle is formed by long arrays of sarcomere units. The sarcomere is constructed by interdigitating, antiparallel filaments of actin and myosin, the elastic titin filaments and the crosslinker proteins for actin, such as α actinin and myomesin. Sarcomeres contain many other accessory components, including proteins involved in transcriptional regulation and turnover control. The transcription factor CLOCK, the transcriptional cofactors muscle LIM protein (MLP), muscle ankyrin-repeat proteins (MARPs) and LIM domain-binding protein 3 (LDB3) are found at the Z-disk and/or the I-band. Multifunctional components of the protein turnover machinery include sequestosome 1 (SQSTM1), NBR1 and the muscle-upregulated RING finger proteins (MURFs). MYOZs, myozenins. [adapted from Braun, et al 2011 2].

1.1.2 Cancer Cachexia

The skeletal muscles have a high plasticity in response to changes in functional demands; resistance training induces skeletal muscle hypertrophy, which is characterized by increased protein synthesis, fiber diameter and strength^{3,4}. In contrast, conditions of disuse, immobilization, denervation, microgravity, aging and food restriction result in loss of muscle mass, known as muscle atrophy. Muscle atrophy is characterized by a decrease in the amount of protein, fiber diameter and reduction of strength²⁻⁵. The skeletal muscle atrophy is also a common phenomenon in many chronic systemic conditions such as sepsis, chronic heart failure, chronic obstructive pulmonary disease, chronic kidney disease, diabetes, AIDS and cancer^{6,7}. These conditions may be accompanied by a complex metabolic multifactorial syndrome characterized by decreased muscle mass, with or without loss of fat, named cachexia^{7,8}.

The cachectic state is particularly important in cancer, representing poor prognosis and decreased response to radio and chemotherapy treatment; more than 50% of cancer patients develop cachexia and, remarkably, approximately 30% of cancer-related deaths are estimated as a result of cachexia^{6,9}. Depending on the tumor type, site and mass, weight loss occurs in 30 – 80% of cancer patients; patients with pancreatic or gastric cancer have the highest frequency of weight loss, while patients with non-Hodgkin's lymphoma, breast cancer, acute nonlymphocytic leukemia, and sarcomas have the lowest frequency of weight loss⁹. In patients with pancreatic cancer, weight loss is an important symptom with a median weight loss of 14.2% of their pre-illness stable weight¹⁰ (**Figure 1-2**). This weight loss is progressive, increasing to a median of 24.5% at the last assessment before death (**Figure 1-2**).

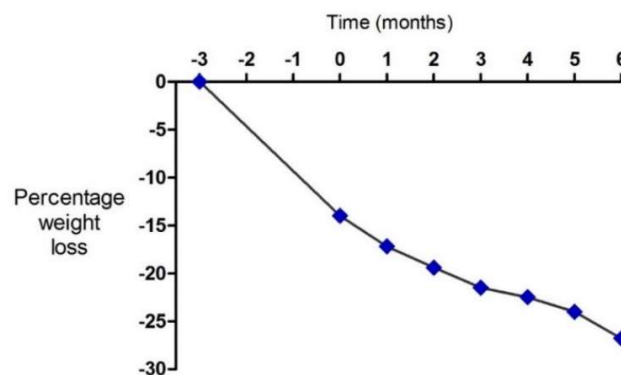


Figure 1-2. Time course of weight loss in patients with advanced pancreatic cancer (n=20). At diagnosis, 85% of patients have lost weight. [Adapted from Wigmore, et al 1997¹⁰].

1.1.3 Molecular pathways in cachexia

The molecular pathways responsible for cachexia are not completely understood, however, a number of studies have shown that cachexia is linked to raised plasma levels of pro-inflammatory cytokines such as interleukin (IL)-1 β , IL-6, tumor necrosis factor alpha (TNF) and interferon gamma (IFN); these cytokines trigger the activation of different axis such as: nuclear factor kappa-light-chain-enhancer of activated B cells (NF- κ B), Signal transducer and activator of transcription (STAT), MAP kinase family (MAPKs) and Activator protein 1 (AP-1). The signal transduction to NF- κ B and STAT transcription factors have a key role, especially in the development of cellular and molecular alterations that mainly in the regulation of genes of three main pathways: a) ubiquitin proteasome system, b) IGF1-AKT-FOXO signaling and c) autophagy-lysosome system (**Figure 1-3**); which lead to an imbalance between protein synthesis and degradation that results in loss of muscle mass and function^{11,12}.

Ubiquitin Proteasome System: Protein degradation through the ubiquitin-proteasome system is the major pathway of non-lysosomal proteolysis of intracellular proteins¹³. Proteins are targeted for degradation, by covalent modification with ubiquitin; requires the coordinated reactions of three enzymes: ubiquitin-activating enzymes (E1), ubiquitin-conjugating enzymes (E2) and the ubiquitin ligases E3 that recognizes the specific protein to be ubiquitinated¹³. The central role of ubiquitin E3 ligases in atrophy of skeletal muscle atrophy is generally due to reduced protein synthesis, increased degradation, or a relative imbalance of the two processes¹⁴. These signaling mediators are required to up regulate the expression of the key E3 ligases such as , tripartite Motif Containing 63- E3 Ubiquitin Protein Ligase, TRIM63 (AKA: MuRF1, in the **Figure 1-3**) , and F-Box Protein 32, FBXO32 (AKA: Atrogin-,1 in the **Figure 1-3**), which mediate sarcomeric breakdown and inhibition of protein synthesis^{14,15}. FBXO32 induces the ubiquitination of an eIF3f, which is part of the protein translation machinery¹⁶.

IGF1-AKT-FOXO Signaling Pathway: The protein mass within a muscle is regulated by an interplay between protein synthesis and degradation. In rodent models of cancer associated muscle wasting, both decreased synthesis and increased degradation have been described¹⁷. One of the best-characterized mechanisms for inducing protein synthesis is through IGF1 (insulin-like growth factor 1) signaling. The pathway that mediates hypertrophy

downstream of IGF1 activation is IRS1/PI3K/AKT/mTOR (**Figure 1-3**)¹⁸. AKT induces activation of protein synthesis by blocking repression of mTOR, which in turn maintains muscle mass through two distinct complexes, known as TORC1 and TORC2¹⁹. TORC1 signals to the p70S6 kinase and 4E-BP pathways, which induce ribosome formation and induce protein synthesis¹⁹.

Autophagy-lysosome system: Under atrophy conditions, autophagy is induced in addition to ubiquitin-mediated proteolysis, which also contributes to the degradation of muscle proteins that promotes muscle atrophy²⁰. In autophagy, organelles are sequestered in autophagosome vacuoles that fuse with lysosomes and become digested by lysosomal enzymes²¹. Autophagy genes and the lysosomal proteolytic system are activated in skeletal muscle during denervation and cancer and, in both cases, contribute to atrophy through the activity of FOXO (**Figure 1-3**)²². A unique finding determined that analogous to AKT, FOXO3 is negatively regulated by PGC-1 α ²³. PGC-1 α is itself down-regulated in muscles from tumor-bearing mice and other wasting conditions, and transgenic expression of PGC-1 α rescues muscle loss in part by inhibiting FOXO3 and through the production of metabolic products.

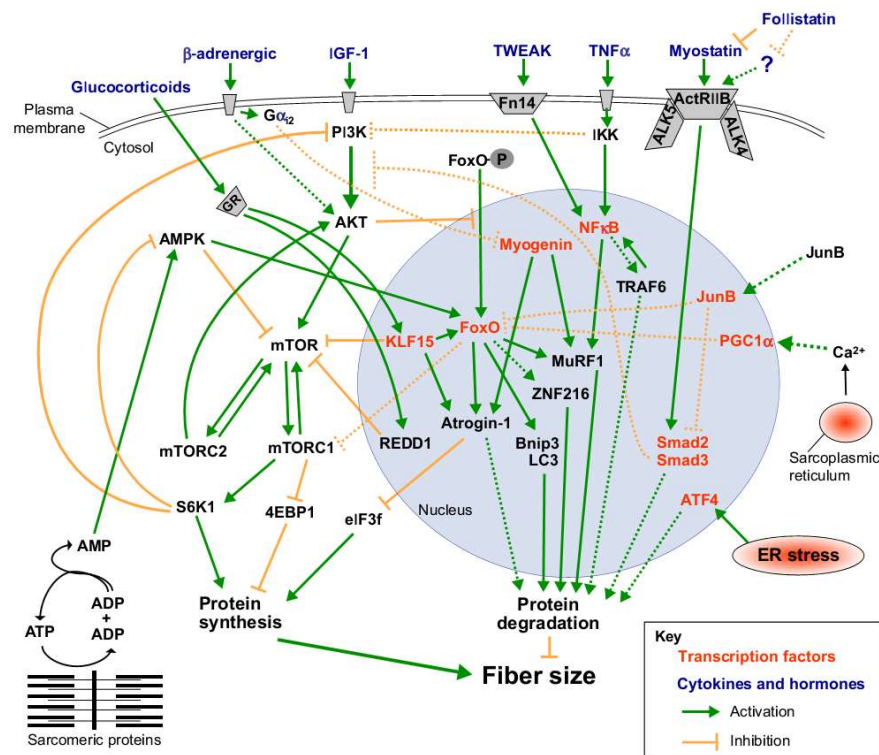


Figure. 1-3. Major pathways that control muscle fiber size. Protein synthesis and degradation are regulated by several different stimuli, which activate multiple signaling pathways, many of which

converge at common intermediates and crosstalk with one to another. Dotted lines depict pathways whose molecular mechanisms and role in adult skeletal muscle have yet to be completely defined. [adapted from Bonaldo et al, 2013¹⁵].

1.1.4. Genome wide studies

Although some pathways are characterized as responsible for the muscle wasting in cancer cachexia, there are still many unknown molecular mechanisms that are involved in gene regulation in this condition¹⁵. Currently, the availability of high-throughput technologies to acquire genome-wide data is expected to change the way we formulate and address biological questions²⁴. With nearly all genes in hand, the conventional reductionist approach in the study of cancer cachexia, studying one gene at a time can now be complemented by more global or integrative approaches that consider all genes at once. Even though reductionist approaches have pointed out many basic facts of biology, they are limited in giving us a comprehensive picture of the life of cells, tissues and organisms²⁵. Thus, it is reasonable to imagine that more integrative genome wide approaches will bring better understanding of the dynamics muscle wasting in cancer cachexia disease processes at a fundamental level. So, by integrating the information contained in the genome wide data sets, increasingly meaningful biological hypotheses can be formulated. However, it should be kept in mind that these hypotheses still need to be tested back in the context of relevant biological settings, perhaps using more refined approaches²⁵.

1.1.5 Transcriptome

Transcriptomics is the measurement of the expression of thousands of genes at once, through the quantification of the mRNA levels to create a global picture of cellular function. This study is the logical next step after sequencing a genome; the sequence tells us what the cell could possibly do, while the transcriptome tells us what the cell is doing at a specific time point.

The first transcriptomics analysis in cancer cachexia was conducted in 2001²⁶ with the development of the differential display retro transcription PCR (DDRT-PCR) for the analysis of several candidate genes (**Table 1-1**). Later, new strategies of massive analysis (high-throughput) of transcriptome have been applied, such as the microarray technology, producing larger amounts of data in terms of expression of many genes in a single experiment (**Table 1-**

1). However, the microarrays analysis used in previous publication has limitations such as: 1) semi quantitative technique due the probe saturation²⁷, 2) annotation issues associated with predefined probes²⁸ and 3) inability to comprehensively detect novel transcripts and isoforms²⁸. To our knowledge, to date, there is no study that have used the high-performance sequencing mRNA (RNA-Seq) to analyze muscle samples in cancer cachexia. Additionally, these transcriptome analyses in cancer cachexia based in microarrays platforms (**Table 1-1**) have just analyzed individual genes that are up- or down-regulated rather than the relationships between genes.

Finally, many factors determine whether a gene is on or off, and this information cannot be accessed just by a transcriptome analysis. For the comprehensive study of the mechanisms that control gene expression is necessary examine transcriptional and posttranscriptional regulation. Transcriptional regulation can be explored genome wide by adding other layers of information such as methylation (e.g. BS-seq), Transcription factors binding sites (e.g. CHIP-seq) or chromatin accessibility (e.g. ATAC-seq). On the other hand, post-transcriptional regulation mechanisms can be explored using microRNA profiles (e.g. small RNAseq) or global mapping of targets for specific RNA-binding proteins (HITS-CLIP-seq).

Model	Tumor type	Tissue	Technology	Genes	#DE Genes	Ref
Rat	Hepatocellular carcinoma	Muscle	DDRTPCR	15	1	26
Mouse	Adenocarcinome 16	Muscle	Microarray	588	9	29
Rat	Hepatocellular carcinoma	Muscle	Microarray	16392	133	3
Humans	Gastrointestinal	Muscle	Microarray	38500	83	30
Humans	Gastrointestinal	Adipose	Microarray	28869	425	31
Mouse	C26 colon adenocarcinoma	Muscle	Microarray	26766	1607	32
Humans	Pancreatic	Muscle	cDNA-AFLP	ND	183	33
Mouse	C26 colon adenocarcinoma	Hypothalamus	Microarray	21225	19	34
Mouse	C26 colon adenocarcinoma	Muscle	Microarray	28132	1907	35

Table 1-1. Transcriptome studies in cancer cachexia. DDRTPCR: Differential Display Retro Transcription PCR, cDNA-AFLP: cDNA Amplified fragment length polymorphism, ND: Not determinate. # DE genes: number of differential expressed genes.

1.1.6 MicroRNome

Almost 90% of the human genome is actively transcribed, and most of these transcripts are composed by non-coding RNAs (ncRNA). ncRNAs are important regulatory molecules

involved in diverse physiological and cellular processes³⁶. The micro RNAs (miRNAs) constitute the most studied and characterized class of small non-coding regulatory, with size ranging from 17 to 25 nucleotides^{37,38}. The miRNAs impose an additional level of post-transcriptional regulation that influence gene expression in a sequence-specific manner, where miRNAs bind complementary to a mRNA sequenced named seed region^{37,38}. This binding results in either degradation of the targeted mRNA or inhibition of translation of the targeted mRNA to its corresponding protein³⁹.

There are many signaling pathways through which miRNAs influence muscle metabolism. Regarding to the IGF-1 pathway, which control protein synthesis, miR-1, miR-206, miR-133 and miR-125b modulates the pathway by targeting IGF-1 or IGF-1 receptor (**figure 1-4**)^{40,41}. The ubiquitin proteasome system is also regulated by miRNAs. The miRNAs miR-486 and miR-17-92 down regulated PTEN and FoxO transcription factor, which direct induce the expression of a number of atrophy-inducing genes^{40,42}. Also, several studies have demonstrated that miR-23a suppresses the translation of both atrogenes, TRIM63 (AKA: MuRF1 in the **Figure 1-4**) and FBXO32 (AKA: Atrogin-1 in the **Figure 1-4**) as well as an increase in muscle mass (**Figure 1-4**)^{40,43}.

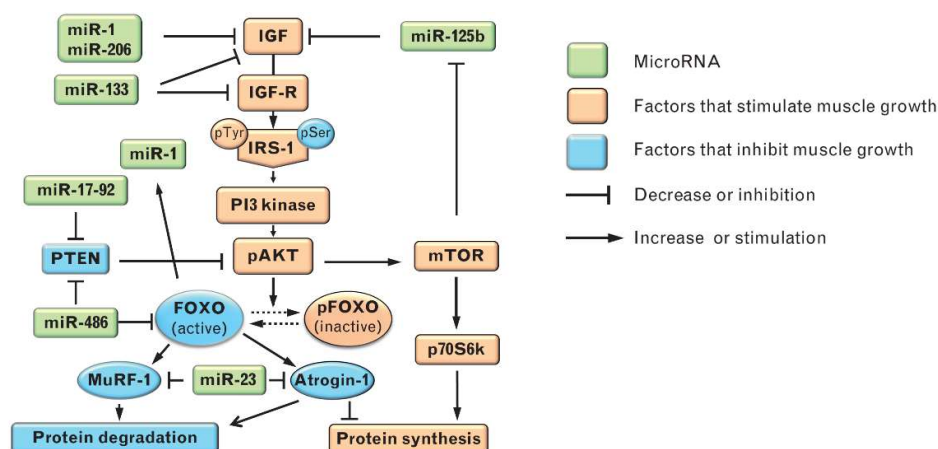


Figure 1-4. MicroRNAs in muscle atrophy. Protein synthesis and degradation are regulated by several miRNA in different key point of pathways such IGF/PI3K/Akt signaling and the Ubiquitin proteasome system [adapted from Wang, 2013⁴⁰].

While the present study was developed, genome wide analysis of miRNAs profiles was described in cancer cachexia⁴⁴. Although the study was performed in humans, mRNA and miRNA data from the same sample were not integrated to identify the main pathways related

to muscle atrophy in cancer cachexia. So, it is still needed to explore the complex gene regulatory networks in terms of miRNA and mRNA expression profiles. So, our current project will also decipher a miRNA signature for muscle atrophy in cancer cachexia, and how this signature is integrated with the transcriptome of the cell.

1.2. Question to be answered

In this chapter, we will analyze qualitatively the GRN of muscle wasting in cancer cachexia by examine genome-wide the mRNA and microRNA profiles. This data helps us to explore the major pathways and cell effectors that underlay muscle wasting in cancer cachexia and explore potential mRNA posttranscriptional regulations by microRNAs.

1.3 Characterization of Lewis Lung Cancer (LLC) tumor bearing mice

We use the LLC tumor-bearing mice model, a well-established model of cancer cachexia. As expected, all mice that received subcutaneous LLC cells injection developed cachexia (LCC group) compared to control mice injected with saline (Control group). After seven days of LLC cells injection, it was possible to locate the tumor by palpation. Fifteen days post-injection, it was possible to see the tumor site as a projection of the skin. Twenty-two days post-injection, the tumor was visually observed as a mass under the skin; the tumor mass ulcerated in some animals, causing open lesions. When surgically exposed, the tumor was solid, vascularized, roughly spherical in shape (**Figure 1-5**), measuring ~ 2 cm in diameter, and weighing ~ 3g (data not shown).

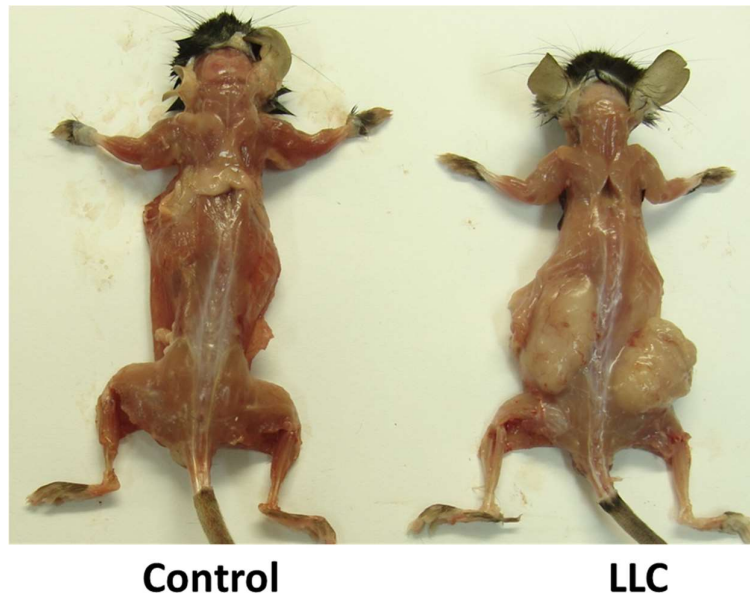


Figure 1-5. Morphological features of Lewis Lung Cancer (LLC) tumor-bearing mice. Exposed LLC tumor, twenty-two days following subcutaneous injection of 1.5×10^6 LLC cells, constituted by a spheroid mass measuring ~ 2 cm in diameter, and weighting ~ 3 g. The tumor mass is well-defined. The LLC tumor-bearing mice carcass show muscle atrophy and pallid coloration.

The LLC line is highly tumorigenic; however, we did not visually identify metastasis to the lungs or other organs. Approximately 25% of tumor-bearing-mice died within 22 days after treatment (**Figure 1-6a**). Weight loss in cancer cachexia is associated with loss of body fat and deterioration of muscle mass^{9,31,45}. Consistent with cancer cachexia syndrome, tumor-bearing mice exhibited more than 20% of weight loss 23 days after LLC cell injections compared to control injected with saline (**Figure 1-6b**). We also observed that GAS, TA, and SOL in LLC were atrophic, demonstrating that muscle atrophy occurs regardless the glycolytic or oxidative muscle phenotype **Figure 1-6c**). In addition to the deterioration of muscle mass, cancer cachexia was also confirmed by splenomegaly (**Figure 1-6d-e**), and the loss of epididymal, retroperitoneal, and visceral fat (**Figure 1-6f**); no alterations were found in the control mice. Finally, we observed no changes in heart and liver weight in both groups (**Figure 1-6d**). Taken together, these findings correlate with the metabolic changes associated with clinical cancer cachexia.

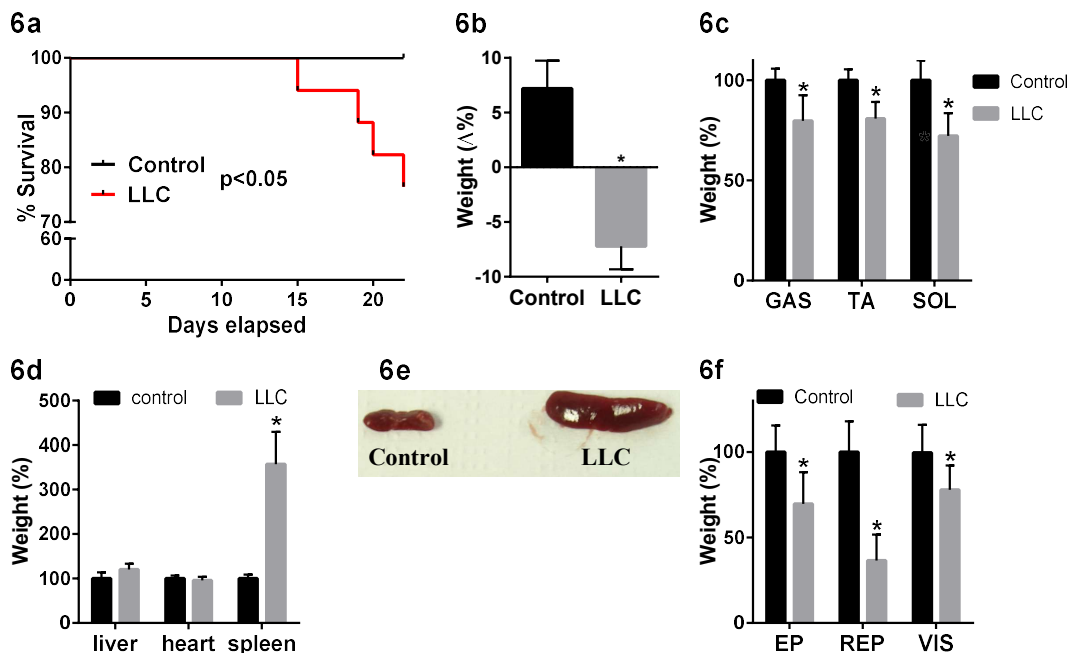


Figure 1-6. LCC tumor-induced cachexia in mice. (6a) Kaplan-Meier analysis of survival was performed in Control (PBS injected; $n = 10$) and LLC tumor-bearing mice ($n = 20$). (6b) Carcass weight loss, defined as total body weight - tumor weight, and reported as a percentage of the initial body weight of each mouse. (6c) Gastrocnemius (GAS), tibialis anterior (TA), and soleus (SOL) muscles weight. (6d) Weights of liver, heart, and spleen (6e) Image showing the splenomegaly in LLC tumor-bearing mice compared to the control. (6f) Weights of epididymal (EP), retroperitoneal (RP), and visceral (VIS) fat. The values are mean \pm SD. Statistical analysis was conducted using the two-tailed t-test. * $p < 0.05$.

Next, we evaluated molecular marks of muscle wasting in cancer cachexia by using RT-qPCR. The total RNA extracted from gastrocnemius (GAS), tibialis anterior (TA) and soleus (SOL) muscles. RNA quality was assessed using Bioanalyzer (Agilent, USA) and the RNA Integrity Ratio was higher than 9.0 for all samples (supplementary information 1). We selected three transcripts related with muscle atrophy: *Myh2*, *Myh7* and *Colla1*. Expression of *Colla1*, a component of the extracellular matrix, was repressed in LLC compared to control in GAS, TA, and SOL (Figure 1-7). Additionally, transcripts that encode for sarcomere proteins *Myh2* and *Myh7* were analyzed. The *Myh2*, predominantly expressed in fast-twitch muscles, was down-regulated in TA; whereas the *Myh7* mRNA, predominantly expressed in slow-twitch muscles, was repressed and induced, in SOL and GAS, respectively (Figure 1-7).

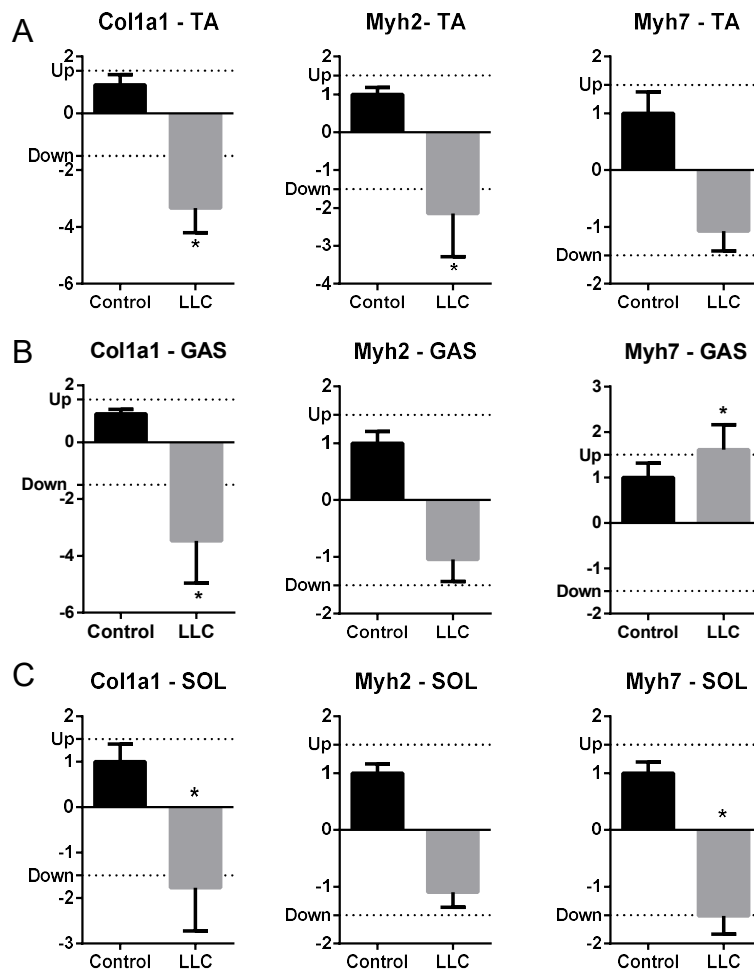


Figure 1-7. Gene expression of molecular markers of muscle atrophy in LLC tumor-bearing mice. The expression of genes that encode for sarcomere and extracellular matrix were analyzed by RT-qPCR in (A) GAS: gastrocnemius, (B) TA: tibialis anterior, and (C) Sol: soleus skeletal muscles. The expression was normalized to the reference genes: beta actin (*Actb*), TATA-binding protein (*Tbp*), and ribosomal protein L13 (*Rpl13a*). Data are expressed as Fold change (mean \pm SD; Control: n = 6; LLC: n = 13; * fold change > 1.5 and p-value < 0.05).

Gene expression analysis showed a molecular profile consistent with muscle wasting in cachectic mice gastrocnemius, tibialis anterior and soleus skeletal muscles. Considering that fast-twitch muscle fibers have greater wasting susceptibility in cancer cachexia⁴⁶, we selected TA muscle, which presents the highest percentage of fast-twitch fibers among the analyzed muscles, to conduct the subsequent experiments. Finally, TA fiber cross-sectional area (CSA; taken as an index of muscle atrophy) confirmed that cachectic mice decreased muscle CSA in 18% when compared to control mice (**Figure 1-8**).

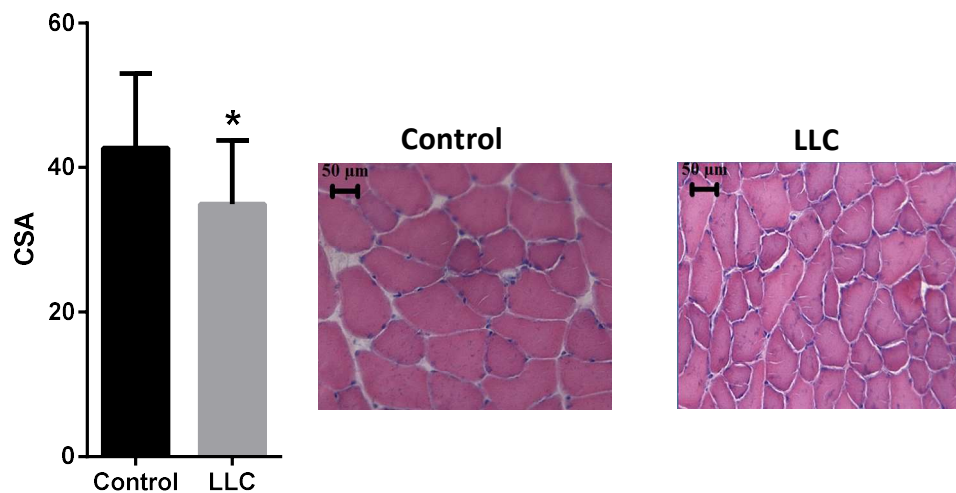


Figure 1-8. Cancer cachexia decreases cross-sectional area (CSA) of tibialis anterior (TA) muscle fibers. The CSA (μm^2) values from control (n=6) and LLC tumor-bearing (n=13) are expressed as mean \pm SD. * $p < 0.001$.

1.4 Muscle atrophy in cancer cachexia is associated with heterogeneity in transcriptome changes

We analyzed the transcriptome of fast-glycolytic tibialis anterior muscle by high-throughput sequencing in LLC and control group. Out of nearly 45,000 Refseq genes, 11,436 were expressed in skeletal muscle (mapped reads > 32 in at least one of the sequenced samples). The inspection of 11436 expressed RefSeq genes through principal component analysis (PCA), showed that gene expression data were able to LLC and control samples (**Figure 1-9a**). Moreover, the PCA uncovered a heterogeneity on transcriptome regulation in the LLC group, evidenced by the spatial dispersion of the samples in the PCA (**Figure 1-9a**). This heterogeneity in transcriptome is expected since tumor progression is a stochastic process, and each mouse develop variable cachectic state from mild to terminal phase⁴⁷. The functional implication of this heterogeneity is important, and especially determine if there is a sequence of transcriptional events that culminate in the loss of muscle mass and function during the progression of cachexia.

To examine the transcriptomic changes associated with skeletal muscle wasting in cancer cachexia, we performed differential expressed analysis over the 11436 expressed RefSeq genes. We found 1008 differentially expressed genes (DEG) ($p \leq 0.05$ and $|\text{fold change}| \geq 1.5$), of which 487 and 521 were up- and down-regulated, respectively

(Supplementary information S2). Unsupervised hierarchical clustering analysis of mRNAs expression data further confirmed a clear segregation between control and LLC samples (**Figure 1-9b**).

This analysis also showed, these 1008 DEG were grouped into four clusters (I-IV) according to their expression profile (**Figure 1-9b**). Clusters I (n=386) and II (n=101) contain genes that are up-regulated, while clusters III (n=157) and IV(n=364) includes genes that are down-regulated. Most importantly, the expression of genes from cluster II and IV their expression is homogeneous among LLC samples (**Figure 1-9c**). On the other hand, gene expression of genes on cluster I and III is variable among LLC samples, in particular the sample L1 which also showed the higher spatial dispersion in the PCA (**Figure 1-9a**).

Next, we explored the identity of the genes with variability between samples in clusters I and III. Interestingly, cluster I includes induced genes that encode proteins associated with proteolysis: Proteasome (e.g. *Trim63*, *Fbxo32*, *Ubc*, *Ubf1*, *Ubb*, *Psmd4*, *Psmd11*, *Psm7*, *Psmd2*, *Psmc2*, *Psmc4*, *Psmd8*, *Psm5*, *Psmd7*, *Fbxo31*, *Ube4a*, *Hectd1* and *Nub1*), lysosome (e.g. *Ctsl* and *Retreg1*) and a translation inhibitor (e.g. *Eif4ebp1*) (**Figure 1-9d**). Additionally, the interleukin 6 receptor (*Il6ra*), a signaling pathway activated in muscle atrophy⁴⁸⁻⁵⁰, has a range of expression variability of 5 logarithms (fold change that from 1.5 up to 32) (**Figure 1-9d**). Group III is largely composed of variable repressed genes related to extracellular matrix (e.g. *Has3*, *Col4a3*, *Cdon*, *Col15a1*, *Col22a1*, *Col9a1*, *Hmcn1*, *Cpq*, *Itm2a* and *Mmp15*) and sarcomeric proteins (e.g. *Myom3*, *Myh2*, *Myl3*, *Myoz2*, *Myh7*, *Palld*, *Lmod3*, *Synpo2* and *Myl1*) (**Figure 1-9e**). Our data show, a set of high variable induced and repressed genes across cachectic samples. This variability may explain why in some human studies, atrophy genes such as *Trim63* and *Fbxo32* have not been found as differentially expressed^{51,52}. Moreover, the data from experimental models are also difficult to transpose into findings of cachectic patients⁵³⁻⁵⁶. However, it is not possible to determine whether there is a relationship between the severity of cachexia and the degree of expression of the genes. Thus, gene expression dynamics and its relationship with survival and severity in cancer cachexia needs to be further explored.

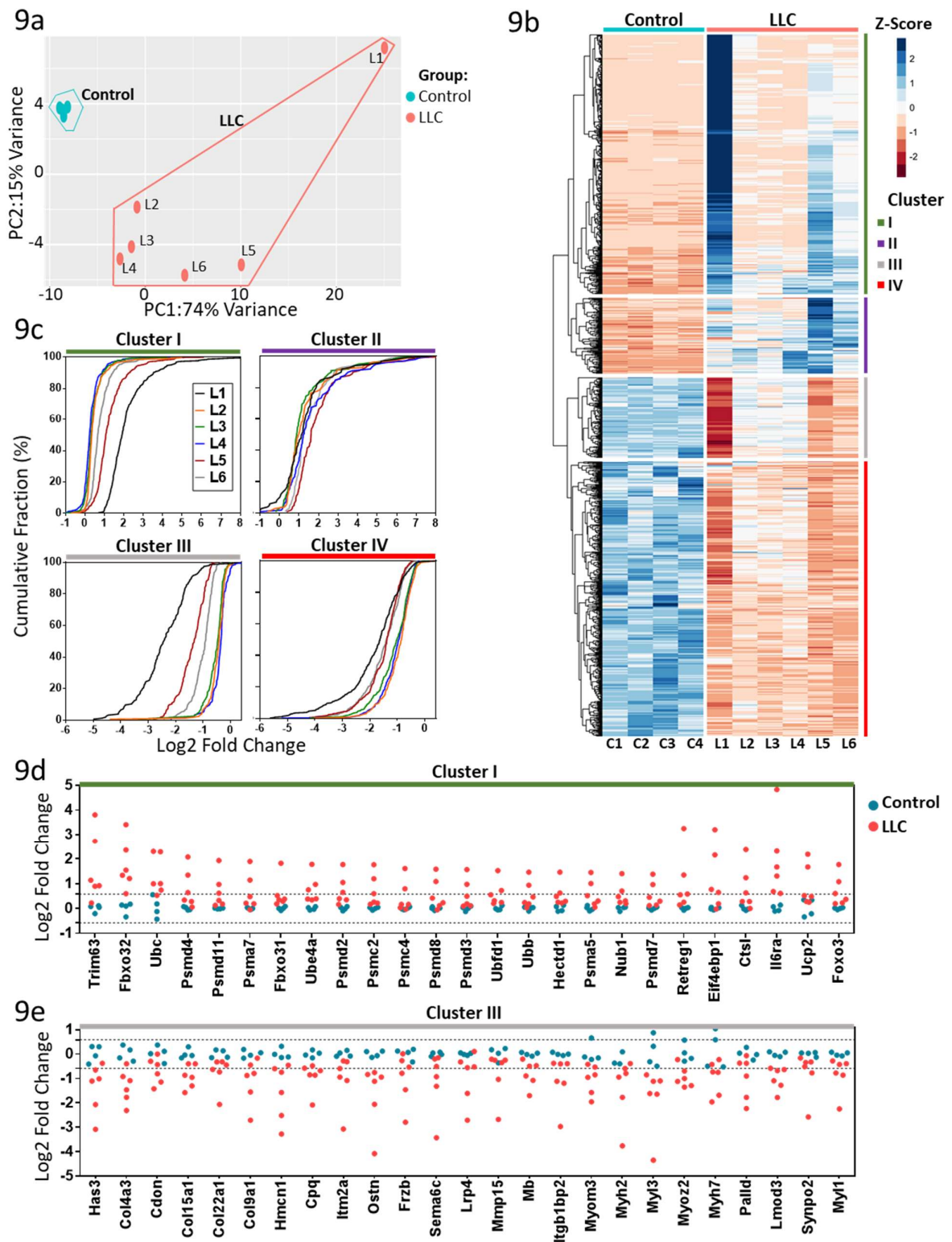


Figure 1-9. Skeletal muscle expression profiles of LLC tumor bearing mice. (a) Principal component analysis of the gene expression of control and LLC samples. The percentage of variance explained by each principal component is indicated. **(b)** Heatmap of DEG of control and LLC samples. Unsupervised hierarchical clustering analysis of gene expression patterns show clusters I (n=386), II

(n=101), III(n=157) and IV(n=364) indicated by different colors. **(c)** Cumulative frequency distribution of transcripts log₂-fold changes values for each sample of LLC group in each cluster I to IV. **(d)** Fold induction of the 25 variable proteolytic genes in cluster I for LLC tumor bearing mice (pink) and control group (light blue). **(e)** Fold repression of the 25 variable scaffold genes in cluster III for LLC tumor bearing mice (pink) and control group (light blue). Dashed lines mean the threshold for up and down regulation ($|\text{fold change}| \geq 1.5$).

1.5 Muscle atrophy in cancer cachexia is discriminate by a reduced set of genes

Considering that there is a high variability in the gene expression profile among the atrophic skeletal muscle samples of cachectic animals, we determined the minimum number of differentially expressed genes that simultaneously group cachectic samples and differentiates it from the control group. First, we used Pearson correlation values for each transcript to identify similarity across muscle samples (**Figure 1-10a**). Hierarchical grouping shows that within LLC group, sample L1 has the most different transcriptional and additionally two groups, A (samples L2, L3 and L4) and B (samples L5 and L6) were identified (**Figure 1-10a**). This analysis further confirms the homogeneity of the control samples, which generate a single control group.

Considering the transcriptome variability across LLC samples, we determined differential expression genes comparing the sub-groups A, B, or their union (sub-group AB) to evaluate the impact of the sub-grouping whit in LLC. We found changes in the number of DEG when we compared all LLC samples, or only the sub-groups (A, B, or AB), with the control samples (**Figure 1-10b**). For example, comparing sub-group B (LLC, n=2) to the control group increases in 57% the number of DEG (1582, of which 630 are up- and 952 down-regulated) while for sub-group A (LLC, n=3), was found a reduction in 56% the number of DEG (443, of which 145 are up- and 298 down-regulated) (**Figure 1-10b**). Importantly, this reduced transcriptomic profile was enough to differentiate cachectic from a control muscle (**Figure 1-10c**).

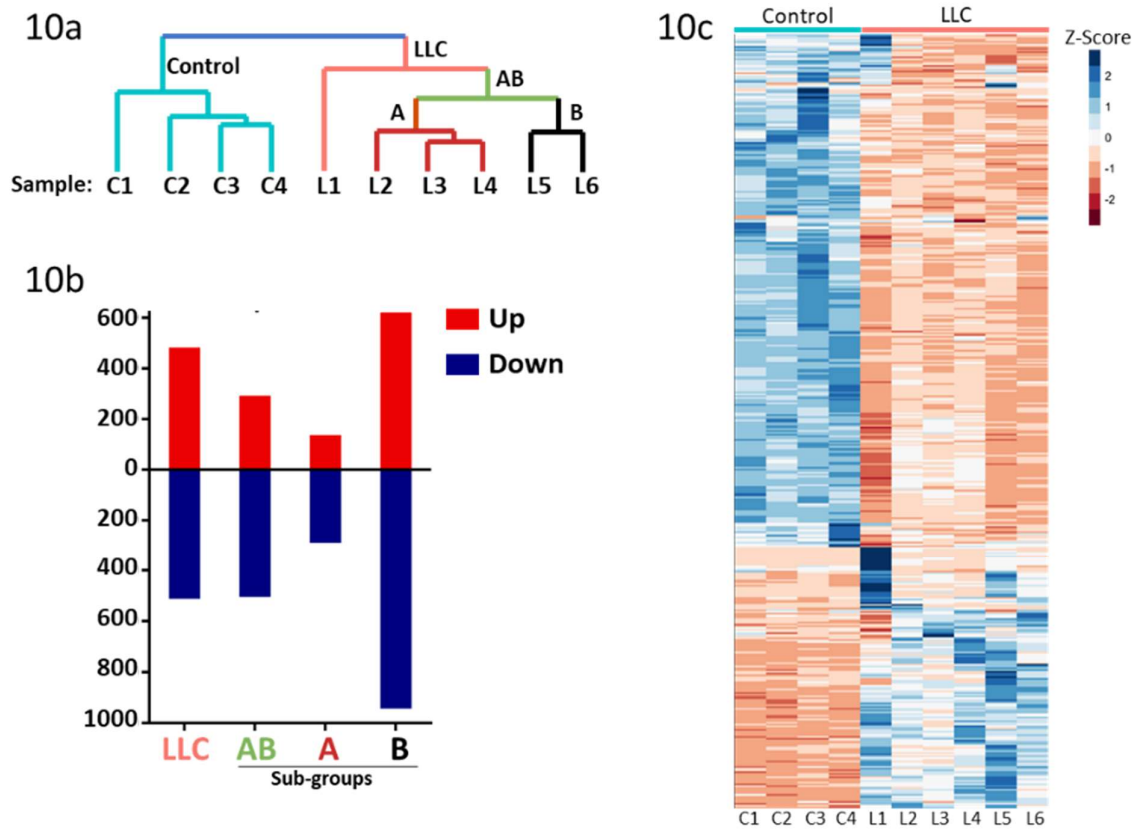


Figure 1-10. Reduced muscle expression profile of LLC tumor bearing mice. (a) Hierarchical clustering of the Pearson correlation values was performed. Colors in the dendrogram represent the different clusters: Control group (Light blue), LLC group (light pink), AB sub group (green), A sub-group (Red) and B sub-group (black). **(b)** Bar plot representing the total number of up-regulated and down-regulated genes in each consider group of samples. **(c)** Heatmap of DEG of control and A sub group samples.

1.6 Identification of regulatory pathways associated with muscle wasting in cancer cachexia

One approach to identify the most biologically relevant transcripts for the cellular phenotype is to identify those that are most abundant and their degree of regulation⁵⁷. Using a scatter plot integrating the transcript degree of regulation (Fold change- FC) and abundance (Reads Per Kilobase Million-RPKM), we identify that most abundant transcripts has subtle changes in the degree of regulation when compared to low abundant transcripts (**Figure 1-11a**). Notably, this analysis shows that the most relevant genes, based on abundance and degree of expression, are those related to the proteasomal degradation pathway: *Trim63*, *Fbxo32* and *Ubc* (with a log₂ FC: 2.2, 2.0, and 1.4, respectively), in accord with previous results⁵⁸⁻⁶³. Additionally, we identified: *Ddit4* and *Eif4ebp1* (log₂ FC: 2.4 and 1.7

respectively) which are implicated in protein synthesis during skeletal muscle atrophy but have not been studied in cancer cachexia^{18,64-66}. Also importantly, we found the antioxidant genes *Gpx3*, *Mt1* and *Mt2* (log₂ FC: 1.6, 3.1 and 4.7, respectively) which have also been described with a role in muscle repair in atrophic conditions⁶⁷⁻⁷⁰. Although the regulation of the sarcomere and the extracellular matrix genes have been strongly related to muscle function and atrophy⁷¹⁻⁷³ the transcripts most abundant and with the highest degree of regulation need to be determined.

Our analysis approach shows that the transcripts related to the sarcomere with the highest degree of regulation are: *Myl1*, *Myh1*, *Fhl1*, *Gsn*, *Myl3* and *Actc1* (log₂ FC: -0.7, -0.7, -1.7, -1.5, -1.7 and -2.0, respectively), and for extracellular matrix we found the genes: *Col3a1*, *Thbs4*, *Col6a1*, *Colla1*, *Colla2* and *Col6a2* (log₂ FC: -3.1, -1.1, -2.2, -3.1, -2.8 and -2.4, respectively). Finally, we also found low abundant genes with a high degree of regulation, these included the genes *Il6ra*, *Mmp9* and *Mmp8* (log₂ FC: 2.8, 2.0 and 4.5, respectively), which are related to activation of the IL-6 pathway and extracellular proteolysis^{48-50,74,75}.

Although the scatter plot analysis was able to identify key deregulated genes, we also perform gene set enrichment analysis to identify the over-represented gene ontology categories of differential expressed genes in muscle wasting in cancer cachexia. This analysis revealed a negative regulation in sarcomere, cell migration and extracellular matrix genes, as well as positive regulation in genes involved in proteasome complex, autophagy, IL-6 signaling, and cell differentiation (**Figure 1-11b and supplementary information S3**), these results are consistent with previous results^{3,32}. Notably, our analysis reveals some novelties such as the negative regulation of cell junctions (e.g.: gap and tight junctions), carbohydrate metabolism (e.g.: glycolytic process), cell differentiation (e.g.: axonogenesis, angiogenesis, and PDGF signaling) and positive regulation of the immune system (e.g.: neutrophil and leukocyte chemotaxis).

Considering the high transcriptome variability across LLC samples, we also asked which pathways are enriched in LLC transcriptome profile when we compared with the reduced set of genes enriched specifically in the LLC sub-group A. This analysis was possible since all deregulated genes in the A sub-group were also deregulated in LLC group. we found that cachectic animals deregulated key ontology groups to different degree, specifically those

associated with proteasome complex, autophagosome, gap junctions, and glutathione metabolic process (Figure 1-11c). These results indicate that differentially expressed genes in skeletal muscle atrophy condition are mainly involved in the reorganization of ECM, cytoskeleton, sarcomere, autophagy, cell differentiation and immune system pathways.

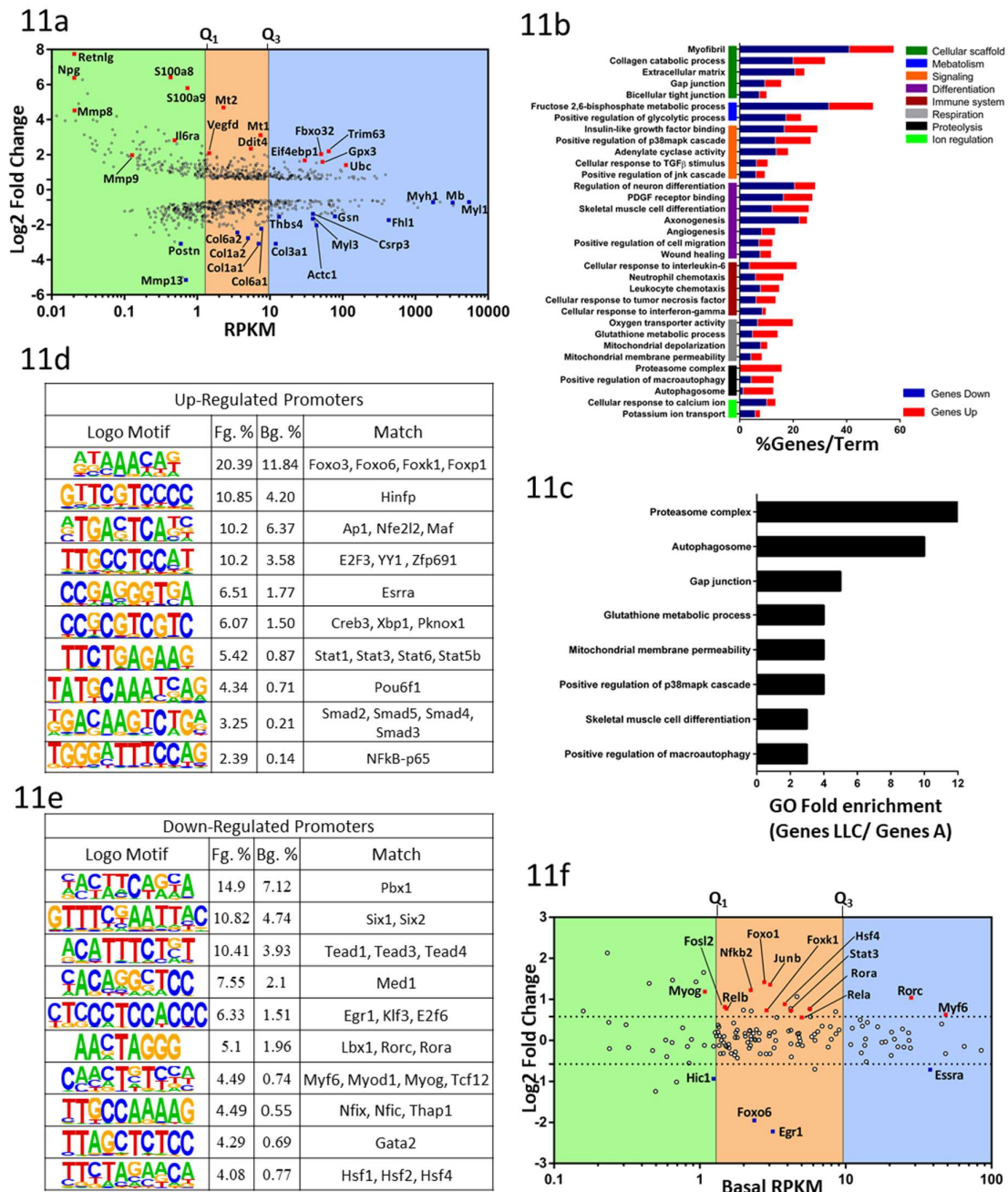


Figure 1-11. Transcriptional alterations in cancer cachexia. Scatterplot comparing abundance (RPKM, x axis) and their degree of expression (log₂ fold change, y axis). Each dot represents an expressed transcript (a) or a transcript coding for a transcription factor (f). Red and blue dots indicate up- and down-regulated transcripts, respectively. Green, orange and blue shadows represent low, medium and high abundance, defined by using quartiles (Q₁ and Q₃) (b) Gene-set enrichment

analysis of differentially expressed genes. Each vertical colored bar (y-axis) represent a major module; horizontal bars represent the percentage of genes presented in the data set compared to the total number of genes in each ontology category. Fraction of genes in each ontology category (up/down, red/blue; respectively) are shown in x-axis. **(c)** Relative gene set enrichment analysis. Each bar represents the ratio of genes in LLC and A sub-group for each ontology category. *de novo* motif analysis performed on promoters (-300 and +50 relative to TSS) of up-regulated **(d)** and down-regulated **(e)** genes. Motifs were compared to a transcription factor JASPAR database to determine the closest annotated match. Fg. %, bg. %: fraction of foreground/background sequences that contain at least one motif occurrence.

1.7 Transcriptional regulation during muscle atrophy

The transcriptional profile provides a step towards the identification of transcription factors that regulate the induction or repression of genes. To identify the transcriptional factors that potentially regulate gene expression in skeletal muscle atrophy in cancer cachexia, we performed an enrichment analysis of transcriptional motifs with the promoter sequences of the differentially expressed genes (**Figures 1-11d and e**).

Promoters of up-regulated genes revealed a motif enrichment for the Forkhead transcription factor (FoxO) (**Figure 1-11d**), these results are consistent with previously role of this transcription factor modulating the ubiquitin-proteasome and autophagy-lysosomal proteolytic activities, as well as in metabolic adaptation and myogenic differentiation⁷⁶⁻⁷⁹. Additionally, when we analyze transcript degree of expression and abundance, it is shown that only two FoxO family members, *FoxO1* and *FoxO6*, are regulated (induced and repressed, respectively) (**Figure 1-11f**). The induction of *FoxO1* are in accordance with previous data since this transcription factor binds to the promoter sequence of *Trim63* and *Fbxo32* genes^{80,81}. It has been shown that FoxO6 forms a regulatory loop with the PGC-1 α factor in the determination of oxidative metabolism⁷⁷, however the role of FoxO6 during atrophy has not been determined.

In addition, binding sites for factors within the NF- κ B and STAT families were also enriched (**Figure 1-11d**). These results are supported by our gene set enrichment analysis that shows categories that include these genes as over-represented (**Figure 1-11b**). Additionally, we observed components of these two families up-regulated, for NF- κ B (*Rela*, *RelB* and *Nfkb2*), and for STAT (*Stat3*) (**Figure 1-11f**). This finding is consistent with the signaling of the proinflammatory cytokines TNF α and IL-6, which activate NF- κ B and Stat3 respectively, to promote protein degradation and muscle atrophy^{82,83}. Finally, many studies describe

cachexia triggered by a single predominant cytokine, however our results suggest that muscle atrophy in cachexia may only be understood in the context of simultaneous presence of different cytokines.

Furthermore, we found an enrichment in the AP-1 transcription factor, as well as the up-regulation of *Junb* and *Fosl2*, proteins that compose the AP-1 heterodimer (**Figure 1-11f**). Indeed, AP-1 activates a muscle atrophy gene program in cancer cachexia and muscle denervation^{84,85}. We also found enrichment for other transcriptional factors without a change in their expression (**Figures 1-11d and f**), among these are transcription factors related to the cell cycle regulators (*E2f3*, *Yy1* and *Creb3*)^{86,87}, Unfolding protein response (*Xbp1*)⁸⁸ and the SMAD family. This last is related to activation of a program of autophagy genes and inhibition of protein synthesis mediated by the Akt/mTORC1 axis⁸⁹.

At the same time for promoters of down-regulated genes, revealed interesting motif enrichment for transcriptional factors related to myogenesis (*Myf6*, *Myod1*, *Myog*, *Tcf12*, *Pbx1*, *Ibx1*, *Nfix* and *Nfic*)⁹⁰⁻¹⁰⁰, lipid homeostasis (*Rora* and *Rorc*)¹⁰¹, glucose and energy metabolism (*Med1*)¹⁰² and muscle fiber-type specification (*Six1*, *Six2*, *Tead1*, *Tead3*, *Tead4*, *Egr1*, *Klf3*, *Hsf1*, *Hsf2* and *Hsf4*)¹⁰³⁻¹¹² (**Figure 1-11e**). However, only the transcription factors *Myf6*, *Myog*, *Rorc*, *Rora* and *Egr1* changed their expression (**Figure 1-11f**). Indeed, myogenesis impairment is a key factor in muscle regeneration and contributes to the progression of skeletal muscle atrophy in cancer cachexia (reviewed in¹¹³). Above all, an additional interest is that many of the factors identified above have not yet been studied in a context of cancer cachexia, which will allow to identify changes in the transcriptional dynamics in the regeneration program in conditions of muscular atrophy.

1.8 miRNAs associated with muscle wasting in cancer cachexia

Equally important to identification of transcription factors is the identification of post-transcriptional regulation mediated by miRNAs, which modulate mRNA stability and protein synthesis. Our experimental strategy was to evaluate miRNAs expression by high-throughput sequencing in the same samples used for transcriptome analyses (except for sample L4 of the LLC group that did not pass the quality filters). Out of 1915 mature miRNAs, 302 were expressed in skeletal muscle (mapped reads > 32 in at least one of the sequenced samples). Eighteen miRNAs were differentially expressed (FDR ≤ 0.05 and |fold change| ≥ 1.5), in

muscle wasting during cancer cachexia compared to controls (13 up and 5 down-regulated) (Supplementary information S4).

We next ask whether the 18 miRNAs differentially expressed may discriminate between LLC and control group. PCA and clustering analysis (**Figures 1-12a and b**) shows that 18 miRNAs do not provide a clear segregation as found for mRNAs (**Figures 1-9a and b**). Furthermore, 44% of differentially expressed miRNAs have low abundance and degree of expression (**Figure 1-12c**). Interestingly, these results suggest a no determining role of miRNAs in mRNA regulation since previous experimental data showed that only abundant miRNAs are capable of effectively modulates the expression of target mRNA¹¹⁴. Among the differentially expressed miRNAs only miR-29b-3p, miR-146b-5p, miR-146a-5p and miR-181c-3p have been previously studied in a skeletal muscle context¹¹⁵. Notably, miR-10b-5p is induced in muscle wasting in cancer cachexia and is one of the most abundant miRNAs in skeletal muscle (**Figure 1-12c**), and importantly their mRNA targets in skeletal muscle is unknown. Finally, the MyomiRs mir-208a, mir-208b, mir-499, miR-133a, miR-133b and miR-1 were not differentially expressed in LLC.

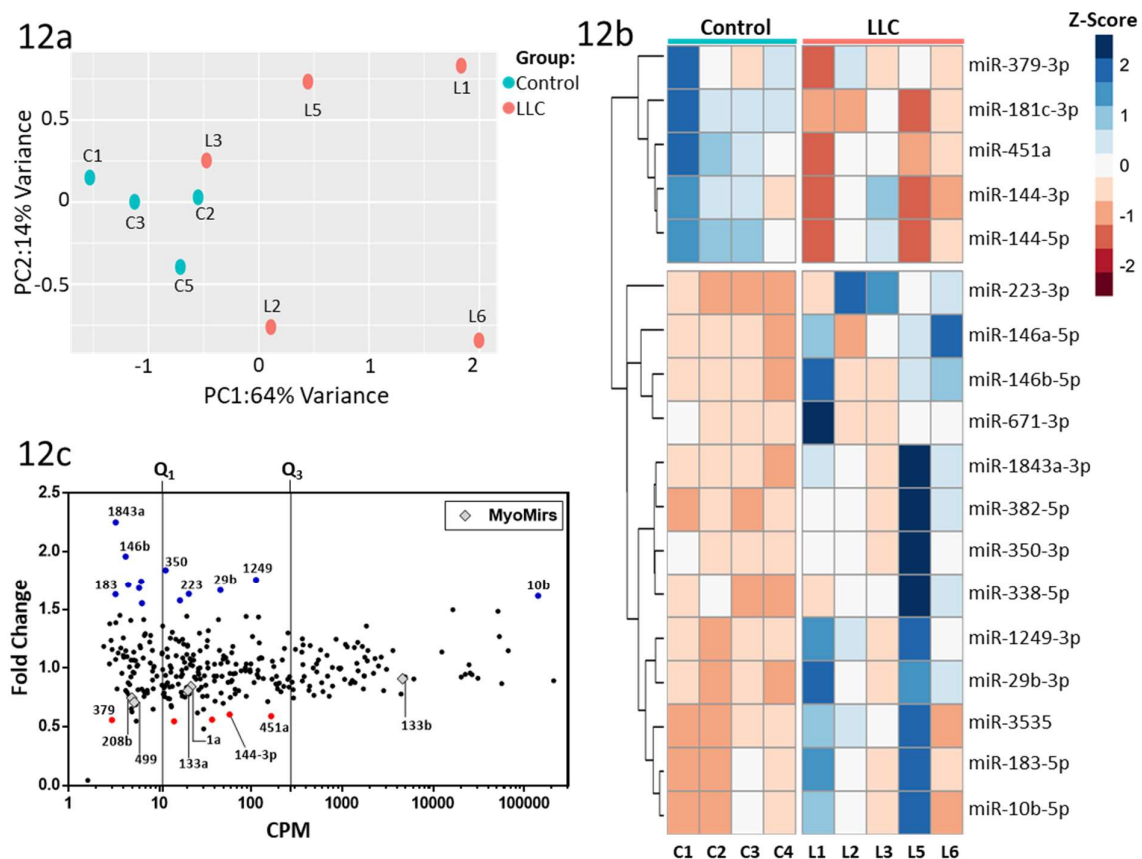


Figure 1-12. Differentially expressed miRNAs in cancer cachexia. (a) PCA of 18 differentially

expressed miRNAs in control and LLC atrophying skeletal muscle samples. The percentage of variance explained by each principal component is indicated. **(b)** Heatmap of differentially expressed miRNAs in control and LLC samples. **(c)** Scatterplot comparing abundance (Counts per million-CPM, x axis) and their degree of expression (fold change, y axis). Each dot represents a miRNA. Red and blue dots indicate up- and down-regulated miRNAs, respectively. Solid lines indicate quartiles (Q1 and Q3) representing the threshold for low, medium and high abundance.

1.9 Integrative analyses of miRNA and mRNA expression profiles identified signaling pathways enriched with predicted miRNA targets

Since miRNAs regulate gene expression by both mRNA degradation and translational repression mechanisms, and miRNA-mRNA regulatory networks are complex, we used a parallel miRNA-mRNA expression profile approach as previously described¹¹⁶ to increase the accuracy of our *in silico* mRNA target prediction used to identify potential mRNA targets of the differentially expressed miRNAs. A dataset of predicted and experimentally validated mRNAs were paired to the 18 differentially expressed miRNAs in LLC-tumor bearing mice. To avoid target multiplicity, we filtered our data using differentially expressed genes (mRNA and miRNA) identified by RNA-Seq, considering that mRNA and miRNA expression levels should be inversely correlated if one regulates the other.

We found that this network included 171 interactions between 18 miRNAs and 131 target genes (**Figure 1-13a** and Supplementary Information S5). These analyses revealed that the upregulated miRNA miR-350-3p has the higher number of targets (n=47). Interestingly, the miRNA miR-29b-3p also showed a high number of targets (n=22), including many transcripts that encode proteins related to extracellular matrix. Additionally, we found that repressed miRNAs do not overlap in mRNAs targets. Furthermore, some transcripts, such as *Map2k6*, *Ptpn3*, *Mettl21c*, *Plxdc2*, *Ppargc1b*, *Rgs5* and *Vegfa* are co-regulated by up to three upregulated miRNAs (Supplementary Table S6). These results indicate, as previously reported by our research group in cardia cachexia, a complicated combination in terms of both target multiplicity and miRNA cooperativeness¹¹⁶.

Based on the integrative miRNA-target analysis described above, we identified enriched pathways for target genes deregulated by differentially expressed miRNAs (**Figure 1-13b**). Gene set enrichment analysis revealed miRNA interactions affecting genes regulating matrix organization, cell migration, transcription factor binding, ion transport and FoxO

signaling. To elucidate the functions of these complex interactions between mRNAs and miRNAs in cancer cachexia, we construct a regulatory network displaying predicted and validated interactions between the miRNAs-target mRNAs, considering physical and pathway protein-protein interactions. We found some sub networks such as those related to extracellular matrix organization (**Figure 1-13c**), cell migration (**Figure 1-13d**), and transcription factors (**Figure 1-13e**). Extracellular matrix organization network (**Figure 1-13c**) contains a set of collagen proteins which are experimental validated target of miR-29b-3p. Furthermore, we found predicted interactions for miR-1843a-3p, miR-350-3p, miR-223-p and miR-3535 with components of the extracellular matrix such as *Col6a1*, *Timp2*, *Mmp15*, *Dcn* and *Actn2*. For Cell migration network (**Figure 1-13d**) we found key growth factors such as *Igfl*, *Bmp1*, *Pdgfra*, *Pdgfrb*, *Wnt5* and *Vegfa* their transcripts are repressed by mirR-29b-3p, miR-3535, mir-671-3p, miR14b-50, miR-146a-5p, miR-350-5p, miR-1843 and miR-1249-3p. In the case of transcription factor binding key factor in muscle metabolism and muscle atrophy such as *Foxo1*, *Egr1*, *Ppargc1b*, *Ccnd1*, *Bcl2*, *Cebpb* and *Myc* their transcripts are repressed by mirR-29b-3, miR-181c-3p, miR-379-3p, miR-451a, miR146a-5p, miR-183-5p, miR-350-3p, miR-1249-3p and miR-3535. Finally, these networks share 3 miRNAs: mir-29b-3p, mir350-3p and miR-3535, which suggests a pleiotropic effect of these miRNAs on muscle physiology.

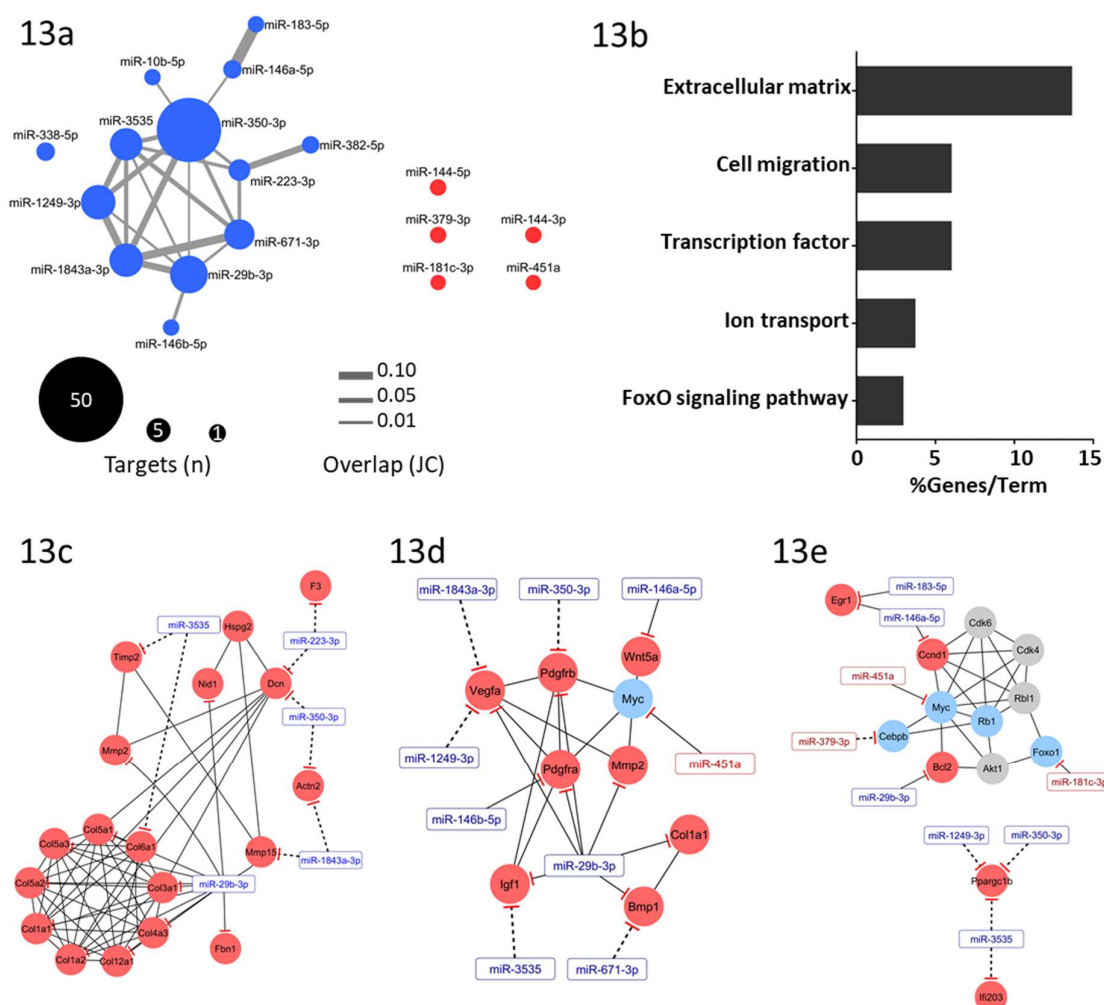


Figure 1-13. Integrative analyses of miRNA and mRNA expression. (a) miRNA-mRNA target network as red node label color. Node size represents number of targets for each miRNA, edge width denotes overlap of targets between miRNAs measured by the Jaccard coefficient (JC), Blue and red color in nodes represent up and down regulation of the miRNAs. (b) Gene-set enrichment analysis of the of the predicted and validated mRNAs regulated by microRNAs. Horizontal bars represent the percentage of genes presented in the data set compared to the total number of genes in each pathway. miRNA-mRNA regulatory network for (c) extracellular matrix organization (d) cell migration (e) Transcription factors. Networks displays predicted (dashed lines) and validated (solid lines) interactions between miRNAs (rectangle) and mRNAs (circles). Light red nodes represent down-regulation, light blue nodes represent up-regulation and genes associated with the pathway and not differentially expressed are denoted as grey nodes

1.10 Discussion

To the best of our knowledge, ours is the first study performing an integrated and simultaneous global miRNA and mRNA expression profiling in the skeletal muscle of a mice model of cancer cachexia to unravel novel regulatory networks and molecular pathways involved in muscle wasting. Our results highlight miRNA-regulated gene networks involved

in skeletal muscle wasting in cancer cachexia. Specifically, our results suggest that key ECM miRNAs and their target genes may contribute to muscle wasting in cancer cachexia.

First, we performed a genome-wide profiling of miRNA that identified 18 altered miRNAs; 13 were upregulated and 5 downregulated. Previous studies have also reported alterations of global miRNA expression in muscle atrophy in primary muscle disorders¹¹⁷, diabetes¹¹⁸, denervation¹¹⁸, dexamethasone-induced atrophy¹¹⁹, fasting¹¹⁸ and cancer cachexia¹¹⁸. The comparison of our cancer cachexia miRNA profile with these previous studies did not reveal any similar miRNA profile but instead identified a specific subset of cancer cachexia miRNAs in the LLC tumor-bearing mice. This is in line with the work by Soares et al., 2014¹¹⁸ who did not find a common signature of miRNAs in different atrophic models (starvation, denervation, diabetes, and cancer cachexia – C26 model). We also did not identify shared miRNAs with those miRNAs associated with cachectic patients with pancreatic and colorectal cancer⁴⁴. These discrepancies may be related to miRNAs “kinetic signatures” (i.e., characteristic time-course patterns to attain protein and mRNA steady-state levels, as well as the number of ribosomes per mRNA molecule after microRNA application), as proposed by Morozova et al.,¹²⁰. These authors generate kinetic signatures by creating a complete mathematical model of microRNA action, which includes all previously described miRNAs mechanisms of action by applying a rigorous mathematical analysis of dynamical behavior of the systems involving microRNA action. Thus, further studies are necessary in muscle wasting during muscle cachexia to identify a specific miRNA regulation mechanism or for selecting between several alternative suggested mechanisms.

Importantly, the miR-350 presented the highest number of target transcripts, comprising transcripts encoding proteins related to ECM such as collagens and matrix metalloproteinases. This miRNA is the only highly expressed miRNA identified in the late stage of pressure overload-induced hypertrophy and induces pathological heart hypertrophy by repressing both p38 and JNK pathways¹²¹. Also notable, we identified miR-29b-3p, which had been previously reported as involved in the regulation of myogenesis¹²². Specifically, high level of miR-29 is important for driving myogenic differentiation, and loss of miR-29 promotes transdifferentiation of myoblasts into myofibroblasts by targeting extracellular molecules including collagens^{123,124}. In fact, previous studies have demonstrated the miR-29 family as a “master fibromiRNA” regulator of the liver, lung, skin, kidney, heart, and skeletal muscles fibrosis^{125–132}. Multiple transcripts encoding standard ECM proteins such as collagens,

fibrillins and elastin have been implicated as miR-29 family direct targets^{126–130}. In C2C12 muscle cells, the stable over-expression of miR-29 down-regulates ECM and cell adhesion genes¹²³. Most recently, Galimov et al., 2016¹³³ used next generation RNA sequencing from miR-29a knockout myoblasts, identified members of the basement membrane as the most abundant miR-29a targets. This same study also showed that miR-29 can initiate muscle cell senescence leading to aging-induced atrophy by suppressing the expression of several mediators of cell proliferation and muscle growth. Furthermore, *in vivo* studies have shown that intramuscular injection of miR-29 into dystrophic limb muscles down-regulated collagen and elastin mRNA expression¹³⁰, whereas the systemic delivery of miR-29 mimics led to significant improvement of dystrophic diaphragm muscle by reducing existing fibrosis and increasing regeneration¹²⁴. Thus, the upregulation of the miRNAs miR-29b-3p in our model of cancer cachexia suggest that they may have an important role in ECM remodeling in this condition.

We have also produced a global transcriptome catalogue of muscle wasting in cancer cachexia that identified 1008 differentially expressed genes. These most highly expressed genes revealed the matrix metalloproteinase 9 (*Mmp9*), which substrates include collagen types IV, V, VII, X, XIV, elastin, fibronectin, aggrecan, fibrillin, and gelatin. *Mmp9* has a role in skeletal muscle atrophy⁷⁴, and is also significantly increased in adipose tissue turnover and fibrosis during cancer cachexia¹³⁴. It is also noteworthy that the atrogene *Fbxo32* is among the top up-regulated genes in muscle wasting in our cancer cachexia model. The *Fbxo32* is highly expressed during muscle atrophy in a range of catabolic conditions including cancer cachexia (reviewed in^{9,135}). We also identified the upregulated *Tgfb1* transcript with the highest number of potential deregulated targets. Interestingly, it has been demonstrated that TGF- β , apart from being a local growth factor, has systemic effects, in conditions such as cachexia and multiple fibrosis^{136,137}. TGF- β also decreased muscle fiber size and dramatically reduced maximum isometric force production in TGF- β -treated mice¹³⁸. According to these authors, TGF- β increase procollagen I α 2 and atrogin-1 levels in the skeletal muscle.

In addition to the induced genes, repressed genes include mRNAs encoding ECM, proteins which is consistent with muscle ECM remodeling. To further understand the possible contribution of these downregulated genes, we constructed a regulatory network displaying predicted and validated interactions of these top downregulated genes, considering physical and pathway protein-protein interactions information. This analysis also showed that the top

downregulated genes are associated with ECM remodeling, a possible a key event that likely contribute to skeletal muscle wasting in cancer cachexia. Importantly, these ECM remodeling in cancer cachexia is in agreement with recent studies that showed thickening of endomysium and downregulation of several ECM gene transcripts in muscle wasting in cancer cachexia^{139,140}.

The category analysis of the all differentially expressed genes also demonstrated the regulation of genes for extracellular matrix and cell-cell adhesion. However, this analysis showed additional pathways that were altered, including cytokine-mediated signaling pathways and immune cell chemotaxis. These results are consistent with a previous meta-analysis on gene expression signatures pertaining to different types of muscle atrophy¹⁴¹. These authors described six functional pathways that occupy central positions in the molecular network obtained by the integration of atrophy transcriptome and interaction data. Similar to our study, pathway analysis of these different types of muscle atrophy transcriptome indicated that deregulated genes in atrophy conditions are involved in cytokines signaling and ECM reorganization¹⁴¹.

To reduce the complexity of predicted miRNA-mRNA interactions identified by in silico prediction, and to increase the list of miRNAs targets likely associated with muscle wasting in cancer cachexia, we applied an integrated and simultaneous mRNA and miRNA analysis. This strategy enabled us to identify biologically relevant and experimentally validated miRNA target genes and provided a comprehensive picture of molecular networks regulated by the identified miRNAs.

Several mechanisms have been proposed to explain muscle wasting in cancer cachexia, focusing largely on muscle fibers intracellular alterations. The data obtained in our model, LLC-tumor bearing mice, described in details mRNAs and miRNAs alterations that may contribute to alterations in muscle endomysium during cancer cachexia.

To summarize, we have discovered deregulated miRNAs and their target mRNAs in cancer cachexia that modulate important biological processes in the skeletal muscle, such as cell migration, transcriptional activity and importantly, ECM organization. In addition, our data showed that 8 miRNAs, including miR-1843a-3p, miR-350-3p, miR-223-p and miR-3535 target transcripts encoding proteins related to ECM, comprising the collagens and matrix

metalloproteinases. Herein, our integrative miRNA and mRNA analysis highlight miRNA candidates to regulate genes that may contribute to muscle wasting in cancer cachexia.

1.11 Methods

LLC-tumor-bearing mice. For the LLC-tumor-bearing mice, we followed the next protocol: after 3 days of acclimation, isogenic C57BL/10 mice were randomly assigned to a non-tumor control group (n=10) or a LCC-tumor-bearing group (n=20). LLC cells were cultured in DMEM medium supplied with 10% of fetal bovine serum and 1% penicillin/streptomycin and maintained in a 5% CO₂, 37°C humidified incubator. Cells were passaged when sub-confluent and 1.5 x10⁶ cells per mouse were injected subcutaneously (7.5 x 10⁵ cells in each flank). Mice were weighed daily and then sacrificed, using *ketamine/xylazine* (100/14 mg/100g), 3 weeks following tumor implantation. Gastrocnemius (GAS), tibialis anterior (TA), and soleus (SOL) muscles were collected, weighted, and then snapped frozen in liquid nitrogen. Mice were treated in strict accordance to the guidelines of the Control of Animal Experimentation and Ethical Principles in Animal Research (CONCEA - National Council for Control of Experimental Animals), and was approved under the protocol n° 702 by the Institute of Bioscience of Botucatu Ethics Committee on Animal Use, from the Sao Paulo State University (UNESP).

Muscle fiber cross-sectional area. Muscle fiber cross-sectional area (CSA) was used to analyze the degree of muscle atrophy. Briefly, a cryostat (Leica) were used to obtain 10-µm sections of muscle, and H&E staining was performed on three sections representing the entire length of the muscle. Images were acquired by an Olympus BX51 bright field microscope and, at least, 200 individual muscle fiber CSA were determined by the Olympus Microsuite Pathology software (version 5.1). Results from all muscle fiber CSA for each animal were average prior to the statistical analysis.

Total RNA isolation. RNA extraction was performed using TRIZOL reagent (Thermo Scientific, USA), according the manufacturer's instructions. The RNA was quantitated by spectrophotometry using the equipment NanoVue (GE Healthcare Life Sciences, USA). RNA Integrity was ensured by obtaining a RNA Integrity Number - RIN > 8 with Agilent 2100 Bioanalyzer (Agilent Technologies, Germany). RNA samples were treated with DNA Free Kit (Thermo Scientific, USA) to remove genomic DNA contamination.

Gene expression analysis by RT-qPCR. The RT-qPCR experiments were carried out in accordance to the “Minimum information for Publication of Quantitative Real-Time PCR Experiment” guidelines 18. Reverse transcription of mRNA was performed using the High Capacity kit RNA-to-cDNA Master Mix (Life Technologies, USA) following the manufacturer's guidelines. For each reaction, 4 μ L of Master Mix were added to 1 μ g of total RNA and the final volume adjusted to 20 μ L with nuclease-free water. The mixture was incubated under the following conditions: 25 ° C for 5 min., 42 ° C for 30 min; followed by inactivation of the reverse transcriptase at 85 ° C for 5 min. Quantitative Polymerase Chain Reaction (qPCR) was performed as follow: For each reaction, 5 μ L of RT reaction were amplified with 1 μ L GoTaq ® qPCR Master Mix (Promega, USA), 1 μ L of primers 10 mM (Supplementary Table S1) in a final volume of 20 μ L completed with nuclease-free water. Thermocycling was performed in a QuantStudio™ 12K Flex Real-Time PCR System (Thermo Fisher, USA) using the following conditions: GoTaq Hot Start Polymerase activation, 2 min at 95 °C; followed by 40 cycles of 15 secs at 95 °C; and 1 min, at 60 °C. Finally, a dissociation curve experiment was performed in the range of 60-95 °C to confirm the presence of a single amplicon. Relative gene expression were evaluated by using the comparative quantification method ¹⁴². All relative quantifications were assessed by using REST software 2009 v 2.0.13 with the pair-wise fixed randomization test with 10,000 permutations ¹⁴³ and PCR efficiencies were calculated by linear regression of fluorescence increasing in the exponential phase using the software LinRegPCR v 11.1¹⁴⁴. The changes in gene expression were considered statistically significant when fold change (FC) ≥ 1.5 and p-values ≤ 0.05 .

Preparation and processing of mRNA-Seq libraries. The RNA-Seq was conducted in a HiSeq 2000 Sequencing System Platform (Illumina, USA) using the services of the Laboratory of Animal Biotechnology, School of Agriculture Luiz de Queiroz (ESALQ, USP). RNA libraries were created from TA RNA four controls and six LLC tumor bearing mice. The protocol followed the manufacturer's instructions (available at: <http://goo.gl/hyslD>). In summary, sequencing protocol included the preparation of the transcriptome analysis of RNA (5 mg total RNA), followed by fragmentation and purification of the messenger RNA. The next step was the amplification for the construction of cDNA libraries: hybridization and binding of adapters, reverse transcription, cDNA purification, and finally, amplification and quantification of the

amplified cDNA. This cDNA was diluted and used to generate clusters (amplification of specific fragments), and subsequently sequenced. Constructed libraries were 100 bp paired-end sequenced. Sequencing was performed on ten RNA samples in each lane of the flow cell, following manufacturer's instructions. Each lane produced ~ 600 million raw paired reads. The data output in fastq file format contained sequence information, including the sequencing quality (Phred quality score). Average Phred scores of ≥ 20 per position were used for alignment.

Preparation and processing of miRNA-Seq libraries Total RNA (typically 5 μ g) from each sample were run on denaturing polyacrylamide-urea gels. Approximately 17-25 nucleotide RNAs were excised from the gel, ligated to sequencing adaptors on both ends, and reverse-transcribed. The resulting cDNA library were PCR-amplified for 15 cycles and gel-purified on 6% acrylamide gel. The gel-purified amplicon quality and quantity was analyzed on a 6% acrylamide gel relative to oligonucleotides of known concentration and size. After obtaining a ~92-bp DNA band on 6% PAGE gels, the PCR products were ethanol precipitated and purified using Spin-X filter columns. Finally, miRNA libraries were 50 bp paired-end sequenced by an Illumina HiSeq2000 instrument (Illumina, USA). Sequencing was performed on ten RNA samples in one lane of the flow cell, following manufacturer's instructions.

Read Alignment and differential gene expression. Paired-end reads for mRNA were mapped to the mm10 genome using TopHat2¹⁴⁵. Single-end reads for miRNA were mapped to the miRBase version 21 using Bowtie^{146,147}. Counts for RefSeq genes were obtained using HTSeq¹⁴⁸ and DESeq2 (version 1.4)¹⁴⁹ was used to normalize expression counts. The changes in gene expression were considered statistically significant when $|\text{fold change}| (\text{FC}) \geq 1.5$ and $p\text{-values} \leq 0.05$.

Motif Analyses. Pscan was used to detect DNA motifs overrepresented in each class between nucleotides -300 and +50 relative to the TSS. Significance was tested against CpG-content-matched promoters as background. A binding site was considered significantly overrepresented with a p value < 0.01 .

miRNA target prediction. Candidate miRNA-RNA targets relationships was predicted by at least one or more of the following target prediction algorithms (union set) extracted from: mirDB¹⁵⁰, TargetScan 5.1 (conservation and non-conservation sites)¹⁵¹, DIANA-microT¹⁵²,

PicTar (4-way, and 5-way)¹⁵³. Additionally, we used validated targets deposited in miRTarBase¹⁵⁴. We will construct a miRNA target–dysregulated network using candidate miRNA–target relationships and filtered to mapping only differentially expressed genes derived from mRNA-Seq.

Gene Ontology (GO) Enrichment Analysis. GO enrichment was performed using the BiNGO Cytoscape plugin¹⁵⁵, using a hypergeometric test with a Benjamini and Hochberg False Discovery Rate correction. A p-value cut-off of 0.05 will be used to identify enriched processes. Additionally ClueGO will be used to group and analyze the GO and KEGG enrichments¹⁵⁶. Networks was visualized and analyzed using Cytoscape¹⁵⁷.

Interaction Network The interacting genes/proteins graphs were generated by the STRING database (<http://string-db.org/>), which also detect functional interactions among the corresponding genes.

“If you are faced by a difficulty or a controversy in science, an ounce of algebra is worth a ton of verbal argument”

J. B. S. Haldane

2

Integrated regulation of mRNA transcription and degradation decodes TNF signaling during inflammatory muscle-atrophy

2.1 Introduction

In general, chronic systemic inflammation in cachexia is driven by proinflammatory cytokines such as interleukin (IL)-1 β , IL-6, leukemia inhibitory factor (LIF), tumor necrosis factor alpha (TNF) and interferon gamma (IFN)¹⁵⁸⁻¹⁶¹. TNF in particular has been found elevated in the circulation of cachectic patients and it showed induce cachexia in mice models^{162,163}. The gene expression in cachexia triggered by TNF are mediated by a group of transcription factors, such as NF- κ B, AP-1 and interferon-regulatory factors. Among those, NF- κ B is a key factor critically involved in the activation of a gene expression program related to muscle atrophy¹⁶⁰. Several data suggest that the NF- κ B activation impairs skeletal muscle myogenesis by the down regulation of Myod1 and Pax7, and also promotes atrophy by the breakdown of myofibrillar proteins mediated through the induction of Murf1, a ubiquitin E3 ligases^{73,160,164}. However, the depletion of the Murf1 gene, does not fully protect mice against muscle wasting, suggesting that NF- κ B also triggers atrophy by activating other pathways.

Until now, a mechanism has been described that explain the down regulation of Myod1 by TNF α -dependent muscle wasting in cachexia¹⁶⁵. This mechanism involves the activation of the NF- κ B pathway, which in turn drives the transcription of the iNOS gene¹⁶⁵⁻¹⁶⁷. In addition, the iNOS mRNA 3' untranslated region (3'UTR) contains a classical destabilizing sequence, the AU-rich element (ARE), which when bound to the stabilizing RNA-binding protein HuR, it increases the mRNA stability and rapid export to translation in cytoplasm^{165,168}. These two events, increased transcription via NF- κ B and increased mRNA stability via the RNA-binding protein HuR, consequently induce iNOS protein synthesis, which through its enzymatic activity leads to the production and release of Nitric oxide (NO) gas. NO react with superoxide (O₂⁻) to form peroxynitrite (ONOO⁻), which ultimately mediate both Myod1 mRNA decay and muscle atrophy¹⁶⁵ (**Figure 2-1**).

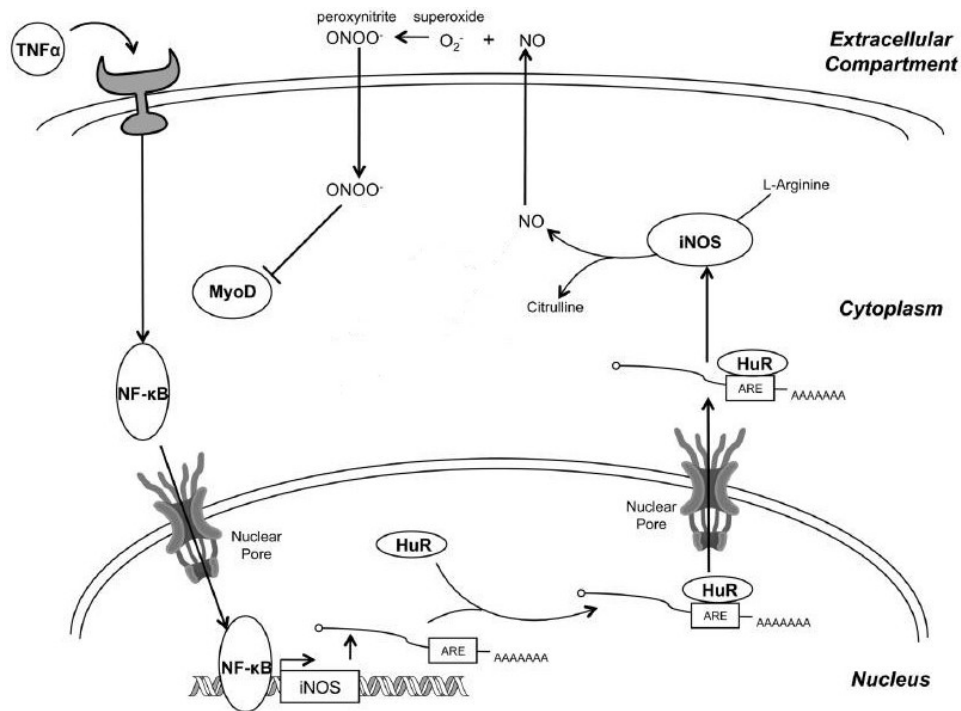


Figure 2-1. The mechanism of iNOS-induced muscle wasting in cachexia. TNF α activate NF- κ B that enhances the transcription of the iNOS mRNA. Then the transcript binds to HuR protein by ARE motif. This results in an increase in iNOS mRNA levels, and consequently in an enhanced translation of the iNOS protein. iNOS activity leads to the production and release of NO that react with O $_2^-$ to form ONOO $^-$, which ultimately mediate both MyoD mRNA decay and muscle atrophy. Adapted from 169.

Although a mechanism for the down regulation of MyoD has been proposed, it is still unclear which other mechanism affect the expression of genes genome-wide. Moreover, the majority of genome-wide studies have only measured the steady-state mRNA levels that do not distinguish between the control of mRNA synthesis vs. the control of mRNA decay genes^{165,170,171}. Nevertheless, in recent years, new next generation sequencing technologies^{172,173}, have dramatically changed our knowledge on gene expression and revealed that cellular gene expression is controlled by a dynamic regulation of mRNA abundance, which are chiefly governed by the rates of nuclear mRNA synthesis, processing, and cytoplasmic mRNA degradation¹⁷⁴⁻¹⁷⁶. Several genome-wide studies, measuring separately the contribution of mRNA degradation and transcription, have established the importance of both process in gene expression¹⁷⁷⁻¹⁸⁰. This data suggest that complex dynamic mRNA profiles can be regulated at each stage of RNA metabolism by the tuned interplay among rates of RNA synthesis, processing and degradation (**Figure 2-2**).

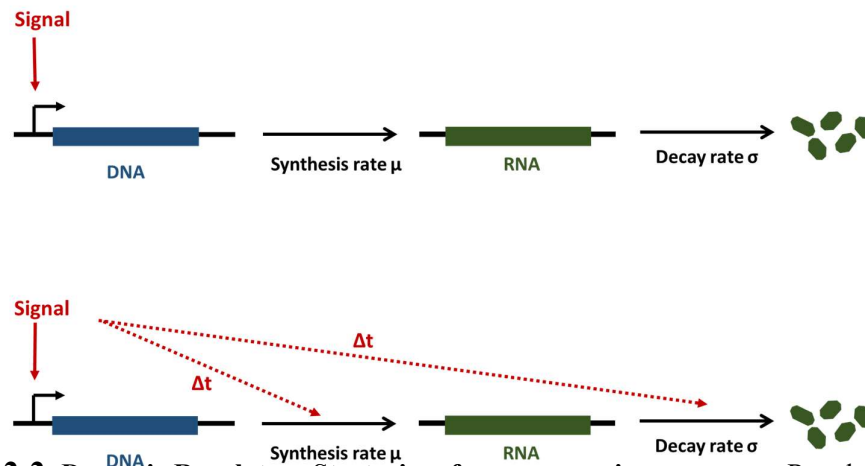


Figure 2-2. Dynamic Regulatory Strategies of gene expression programs. Regulatory Strategies of gene expression programs. Top: simple regulatory strategy shaped only by transcription rates. Bottom: dynamic regulatory strategy shaped by the interplay among transcription, processing and degradation rates.

These findings highlight the importance of RNA dynamics strategies to regulate gene expression programs during a dynamic response. Thus, given these new evidences and technologies in the knowledge of gene expression regulation and coupled with the lack of a compressive mechanism controlling gene expression in cachexia triggered by TNF, a genome-wide approach exploring the contribution of transcription and mRNA degradation, is essential in order strike regulatory events and interactions related to skeletal muscle wasting.

2.2 Question to be answered

In cancer cachexia the regulation of mRNA levels in response to TNF signaling is a fundamental process; however, the mechanisms that control and shape this gene expression program are still poorly understood. Here we propose to study in a mechanistic way, using experimental, on a genome-wide level, and mathematical modeling approaches, the effect of TNF signaling on RNA metabolic events that regulate gene expression programs. This knowledge will help to shed light on how the interplay between TNF signaling and RNA metabolism leads to gene expression program related to muscle atrophy in cancer cachexia. The project also has a methodological goal, which consists of setting up a full experimental and analytical workflow to profile dynamic gene expression and dynamic data on RNA metabolism in muscle wasting.

2.3 TNF stimulation induces skeletal muscle cell atrophy

As muscle atrophy and proteolysis are hallmarks in cachexia state, we measured these both parameters in C2C12 skeletal muscle cell treated with TNF. TNF caused a reduction, 30% less than non-treated cells, in the diameter of the C2C12 myotubes (**Figure 2-3a and 2-3b**). Consistent with these results, we observed the same results in the protein content (**Figure 2-3c**).

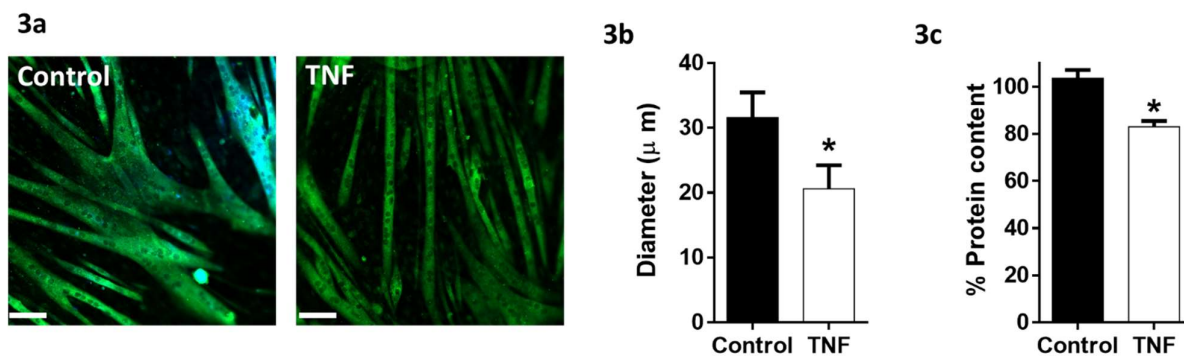


Figure 3. TNF induce skeletal muscle atrophy. C2C12 myoblasts were differentiated into myotubes for 7 days and subsequently switched to growth medium containing TNF (10 ng/ml) or growth medium (Control). (a) Representative field of myosin immunofluorescence at 20h post treatment. Magnification 40X, scale bars: all panels 20 μm. (b) fiber diameter was measured from ten randomly selected field. (c) Whole extract cells were prepared, and total protein quantified. *p-value <0.05.

2.4 Dynamic response of cytoplasmic mRNA.

Subcellular localization of RNAs determine their function in cellular physiology. For instance, changes in temporal concentrations of cytoplasmic mRNA (cytoRNA) determines protein production. Nevertheless, gene expression profiles usually have used whole cell extracted RNA, but the inclusion of nuclear RNA misrepresent the mRNA profile; therefore, the exclusion of the nuclear fraction can provide more reliable differentially expressed genes. Here, we performed RNA-seq analysis of biochemically fractionated chromatin-associated, and cytoplasmic RNA, which has been used previously to study gene expression dynamics^{181–184}. Purity of the cell fractions was confirmed by western blotting detection of key cellular compartments markers (Cytoplasm: b-tubulin, Nucleoplasm: SNRP70, and Chromatin: histone H3) (**Figure 2-4a**).

Out of approximately 11,356 expressed cytoplasmic RNA transcripts, we filtered the genes with absolute value of log₂ fold change ≥ 1 ($p < 0.05$) which yielded that TNF significantly affected the expression of a total of 784 genes, with gene induction

predominating (528 genes, 67%) over gene repression (256 genes, 33%). By examining the maximum fold change over time in the differentially expressed genes, we found that out of the 528 induced genes, 108 genes (20.45%) were induced by at least 5-fold (**Figure 2-4b**). On the other hand, gene repression is not as strong as the induction; and only 22 genes (8.59%) were repressed above the same cut-off used for induction (**Figure 2-4c**). Also, by inspecting the basal transcriptional level, genes that were induced have a lower basal level than genes were repressed (**Figure 2-4d**). Moreover, for both gene induction and repression, there is a correlation between the basal level and the strength of the fold-change (**Figure 2-4e**). In fact, as in immune cells, TNF induced genes encoding immune response genes in muscle cells, which were off before stimulation and exhibited strongly induction (>10-fold).

Dynamic gene expression was assessed by k-means clustering of cytoplasmic RNA expression data. Differential expressed genes were grouped in twelve classes, A to L, (**Figure 2-4f**). Examining the different classes, two characteristics are evident. Firstly, a sequential order of gene expression, for both induction and gene repression, which is characterized according to the time to reach the maximum or minimum fold-change expression (**Figure 2-4g**). Thus, these classes could be categorized as early- (classes A and B), intermediate- (C to E and H to K) and late- responding genes (F, G and L). Interestingly, early response genes (less than 60 min) are only restricted to induced genes, and represent only a reduced set of genes. Nevertheless, despite being a small set, 23 of the 49 genes are related to gene expression regulation: transcription factors (e.g., *Fos*, *Junb*, *Irf1*, *Myc* and *Klf6*), transcriptional coregulators (e.g., *Nfkb1a*, *Nfkbiz*, *Id3* and *Gadd45b*), and RNA-binding proteins (*Zfp36* [Ttp], *Zc3h12a*, *Mex3b* and *Ccn1l*). Secondly, our long timescale allows to unveil six gene expression profile strategies: transiently induced (classes A to D), induction until saturation (classes E and F), constantly induced (class G), transiently repressed (classes H and J), repressed (classes I and K) and repressed preceded by transient induction (class L and some genes of classes A and B e.g., *Fos*, *Id3* and *Timp3*).

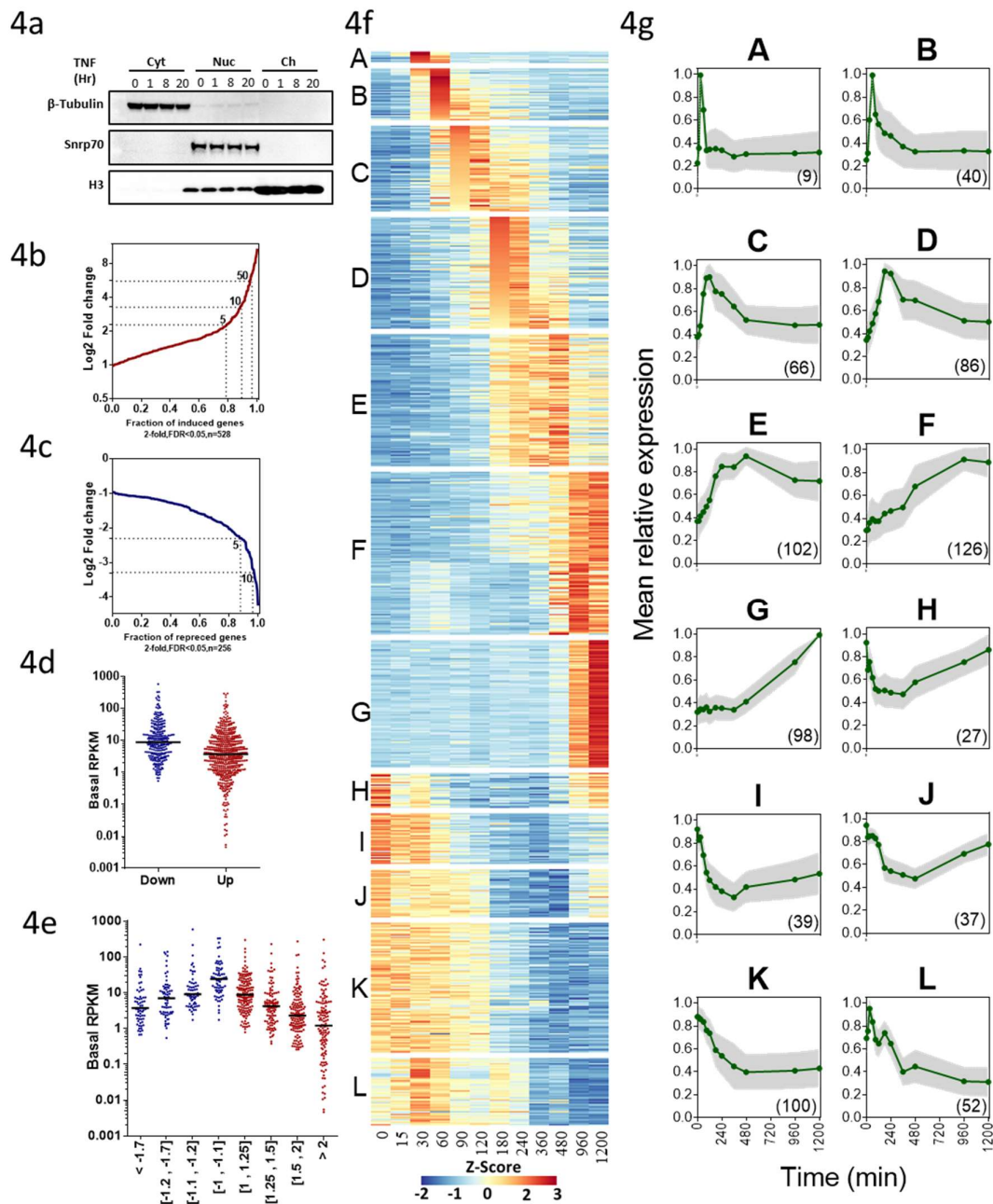


Figure 2-4. Features of TNF-induced dynamic gene expression profiles. (a) Immunoblot analysis of cell fractionation from a representative experiment, in which the segregation of cytoplasmic (beta-tubulin), nucleoplasmic (SNRP70), and chromatin-associated (histone H3) is shown in four samples taken from a stimulation time-course (0h, 1h, 8h, and 20h). Cumulative frequency distribution of maximum gene expression fold change values over the TNF stimulation is shown for (b) induced genes and (c) repressed genes. The dashed lines represent 5-, 10-, and 50-fold change thresholds. (d) Scatter plot of basal abundance for the differentially expressed genes, shown as RPKMs, for induced (red) and repressed (blue) genes, and median RPKMs designated as solid black-line. (e) Induced and repressed genes were grouped according to the strength of the fold-change, with distribution of basal RPKMs shown for each bin and median RPKMs designated as solid black-line. (f) Heatmap of time course RNAseq of cytoplasmic polyA RNA reveals 12 temporal clusters across 12-time points (g) Temporal profiles averaged across two distinct biological replicates, the size of expression of each cluster is indicated in parentheses. Grey shadows indicate standard deviation.

2.5 Integration of temporal mRNA degradation and transcription rates reveal the dynamics of gene expression in response to TNF.

A key cellular response during TNF signaling is the regulation of gene expression which directs and coordinates signal-specific cellular activities. An important aspect of the regulation of gene expression refers to the control of temporal concentration profiles of RNAs, through mainly transcriptional and post-transcriptional mechanisms which control RNAs synthesis and decay, respectively.

2.5.1 mRNA degradation rates correlate with the temporal ordering of gene expression clusters.

To directly investigate the role of post-transcriptional control in the regulation of the dynamic gene expression, we evaluated basal (unstimulated) mRNA degradation rates in C2C12 muscle cells by measuring mRNA abundance changes using RNAseq, after blocking transcription with actinomycin D (ActD), and collecting the samples after 0, 10, 50, 110, 230 and 360 min. The abundance of each mRNA was plotted over time and fitted to a first-order exponential decay curve allowing the determination of a half-life and confidence interval (**Figure 2-5a**). We could generate reliable half-lives for more than 6738 mRNAs. The median half-life of these transcripts was ~229 min, with 80% of the transcripts decaying with half-lives ranging from 100 min to 547 min (**Figure 2-5b**). Overall, we found that the half-lives that we calculated fits within the reported range for mRNAs decay in C2C12 cells previously investigated¹⁸⁵ For example, in our analysis, *Myod1* mRNA presented a half-life of ~60 min, which is consistent with the ~90 min half-life previously reported¹⁸⁶; and *col16a1* mRNA had a half-life of ~317 min, which is also similar to that described in a previous report¹⁸⁵

We tested whether basal mRNA half-life correlates with the temporal ordering of expression clusters (**Figure 2-5c**). Interestingly, we found a strong correlation between a sequential order of gene expression and basal half-life. In addition, it was evident that induction, compared to gene repression, has a lower half-life. Specifically, classes A through C presented the lowest half-lives, and thus are the classes that fall into the category of early expression genes.

Given that the estimation of half-lives is challenging since each of the existing methods have disadvantages, we confirmed the above results using metabolic labeling with 4-

thiouridine (4sU) to estimate mRNA half-lives. We also compared mRNA half-lives obtained by metabolic labeling using 4sU with blocking transcription using ActD (**Figure 2-5e**). Likewise, basal RNA half-lives, estimated using metabolic labeling, correlates with temporal ordering of gene expression (**Figure 2-5d**). Together, these results support the idea that mRNA degradation rates are an important determinant that controls the temporal patterns of the TNF-induced muscle atrophy gene expression program.

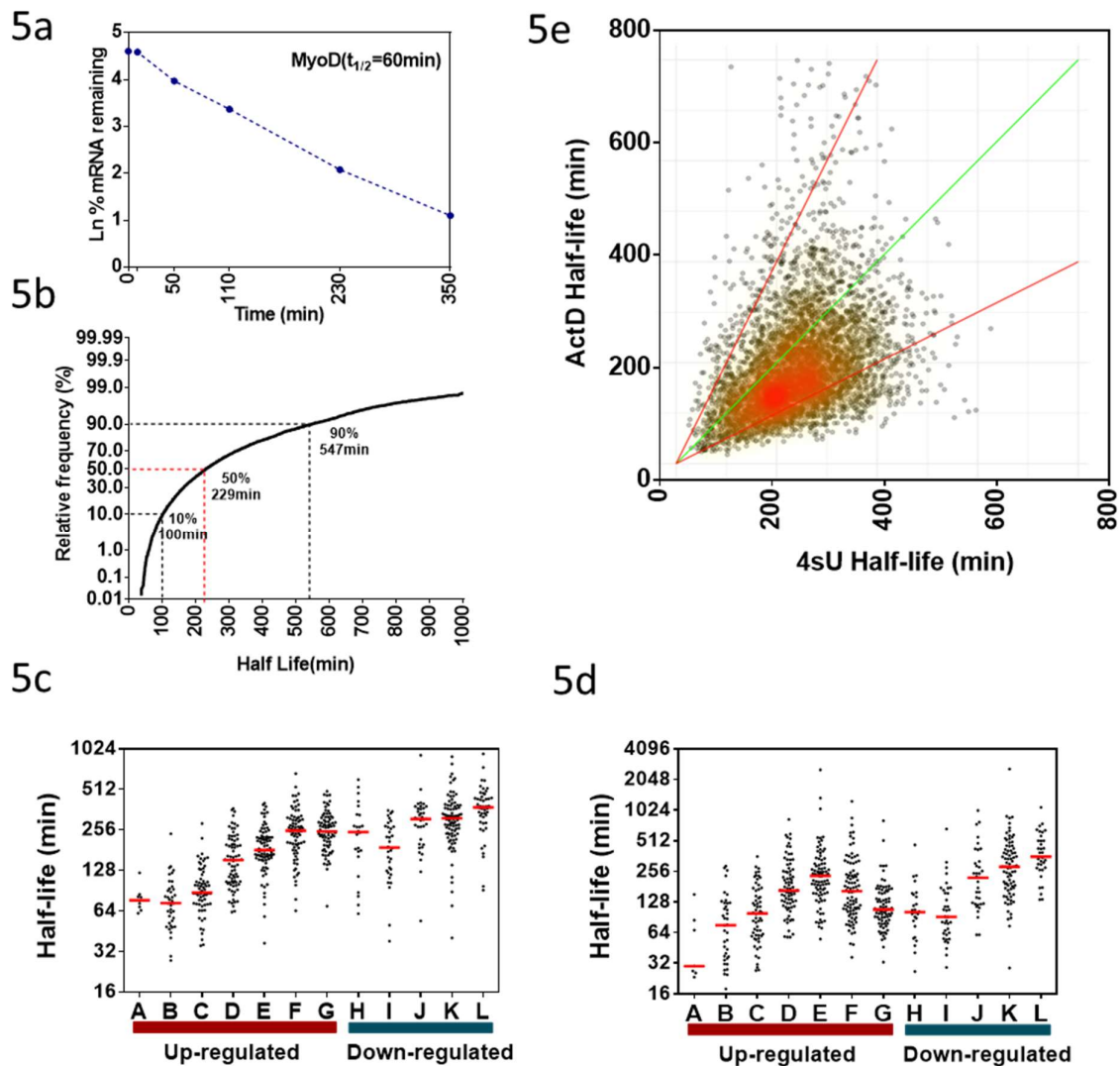


Figure 2-5. Analysis of mRNA degradation rates in skeletal muscle cells. (a) Example of mRNA decay curve. Half-lives were derived from the slope of log-linear regression of the percentage RNA remained. (b) Distribution of mRNA half-lives. The 10th-percentile and 90th-percentile values (indicated by black dotted lines). The median value (229 min) is indicated by a red line. Scatter plot of the half-life of all genes estimated using ActD (c) or 4sU (d) in each of 12 gene clusters (x axis) with similar temporal profile. (e) Heatscatterplot comparison of mRNA half-lives obtained by ActD treatment and 4sU RNA labeling, half-lives (min) determined by 2 h ActD treatment and 60 min of 4sU labeling. Green line means equal half-life and red lines means 2-fold up or down difference in half-lives.

2.5.2 Changes in transcription rates correlates with cytoRNA expression levels.

Transcriptional control is the most basic and intuitively important step in gene expression, and mainly its relevance is due to many factors such as: 1) being the first step in gene expression, 2) involves changes in synthesis that finely tune the amount of RNA being produced, 3) a variety of mechanisms can control transcription rates, and 4) transcriptional control is the most effective and efficient in the use of cell resources.

Given the relevance of transcriptional control in the regulation of the dynamic gene expression, we analyze changes in transcription using RNA-seq analysis of biochemically fractionated chromatin-associated transcripts (caRNA) from unstimulated and stimulated C2C12 skeletal muscle cells. Evaluation of the mapped reading for the caRNA-seq shows that these were broadly distributed throughout all the body of the gene, i.e. they are distributed equally in both introns and exons; whereas in cytoRNA-seq, the majority of the readings are distributed exclusively in exons (**Figure 2-6a and 2-6b**). These results provide strong evidence for the use of caRNA to quantify nascent RNA, and consequently, to calculate transcription rates using gene expression temporal data.

Kinetics profiles of the caRNA for the differential expressed genes were visualized using the same clusters previously used for cytoRNA (**Figure 2-6c**). Interestingly, caRNA profiles follow the same temporal profile of gene expression not only for induced genes, as previously reported^{175,183,184,187,188}, but also for gene repression (**Figure 2-6d**). This finding suggests that reduction in transcription rates play an important role in gene repression. In addition, changes in transcript levels were in early times for caRNA profiles resulting in a temporary delay in the cytoRNA profiles (**Figure 2-6d**). This time-lag is apparently attributed by the delay generated by RNA processing and exporting to the cytoplasm.

Our results, as well as previous work^{175,187,188}, support the hypothesis that changes in cytoplasmic RNA levels can be explained mostly by transcriptional mechanisms. To test this hypothesis for each gene, we use the statistical cross-correlation analysis, which return an index of similarity of two-time series profiles as a function of the shift of one relative to the other. Overall, the analysis showed that 85% of the genes present high correlation (greater than 0.6) between caRNA and cytoRNA temporal profiles (**Figure 2-6e**).

Finally, besides the correlation of the two temporal profiles, it is known that if the changes in the abundance of cytoRNA are of greater magnitude than the changes in caRNA, there is an indicative of RNA stability regulation. Comparing the frequency distribution of the maximum fold change over time revealed a shift towards a greater magnitude for the caRNA (Figure 2-6f). Consequently, by combining the above results, transcription seems to be a dominant regulator of kinetic cytoRNA concentrations.

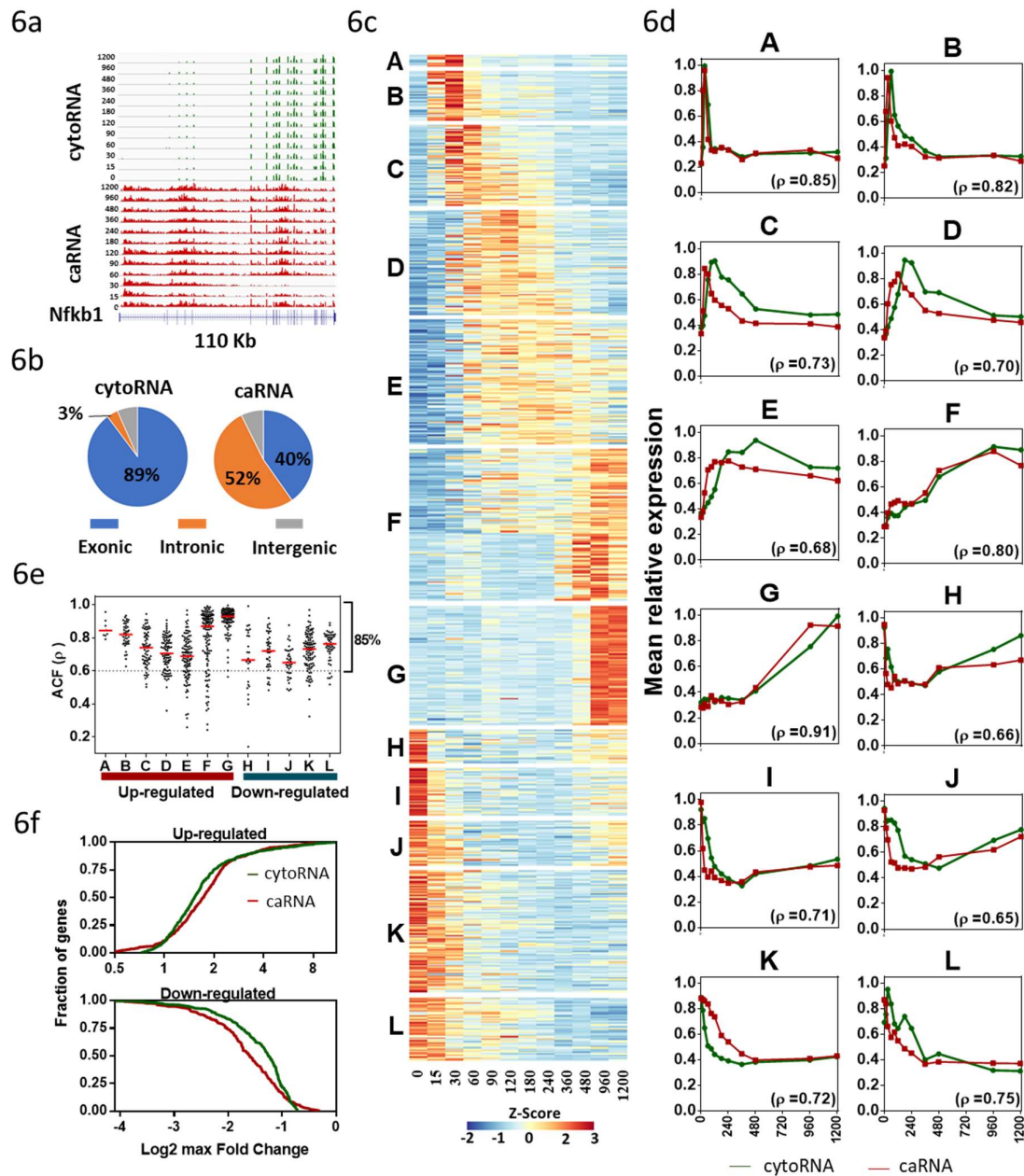


Figure 2-6. Kinetic analysis of transcription during the response of skeletal muscle cells to TNF. (a) Distribution of RNA-Seq reads mapping to the Nfkb1 locus in libraries prepared from cytoRNA and caRNA. The time point is indicated at the left. Exon (blue bars) and intron (blue line) locations are shown at the bottom, and the transcription direction is indicated by the bent arrows. (b) Following

Cell Fractionation into cytoRNA and caRNA, pie charts distribution of reads in gene body in exons and introns. (c) Heatmap of expression values across time of caRNA profiles. Genes were grouped in the same clusters and same order as the cytoRNA heatmap on Figure 4f, also same standardization (z-score) and scale color was used (red, high expression; white, mean expression; blue, low expression). (d) Line graphs of the temporal expression averages per cluster of cytoRNA (red) and caRNA (green) for each temporal cluster. Pearson correlation coefficient (ρ). (e) Scatter plot of the time lagged analysis showing the autocorrelation function coefficient (ACF) between caRNA and cytoRNA temporal profiles of all genes in each of 12 clusters (x-axis). (f) maximum fold change amplitude is greater in caRNA. Cumulative distribution plots, for up and down regulated genes, of the maximum log₂ fold change for caRNA (red) and cytoRNA (green); data represent the average from two independent datasets.

2.6 Coupling transcription and degradation dynamic through a mathematical model

Gene regulation is a complex multifaceted process involving a dynamic interplay between the synthesis and the degradation of gene products. Complexity lies in the fact that these processes operate in a non-linear manner, which makes virtually impossible to study, through traditional statistical analysis such as above used, their functional properties and capture for each gene the degree of cooperation between synthesis and degradation control. Nevertheless, the inter-disciplinary field of systems biology offers an ample range of quantitative tools to study the molecular interacting systems at different levels of granularity. Systems biology-inspired modeling approaches have been increasingly used to account for mechanistic details of the molecular biology process. Therefore, a mathematical model of transcriptome-wide regulation to quantitatively delineate control mechanisms is essential.

2.6.1 Model accurately describes dynamic changes in gene expression

Using the data generated for more than 60 years in the field of molecular biology, we can abstract the basic principles of the processes of gene expression regulation (**Figure 2-7a**). This abstraction can be formulated mathematical by two coupled linear differential equations, as previously described¹⁸⁷ (**Figure 2-7b**). Briefly, in the formulation, M is the cytoRNA concentration, P is the caRNA concentration, dM/dt and dP/dt are their rates of change with respect to time t respectively, β denotes transcription rate, α_1 is conversion rate and α_2 is degradation rate (**Figure 2-7b**). This model considers the following assumptions:

- Transcription and degradation rates (β and α_2) can abruptly shift to new values in response to TNF stimulation. In our model transcription and degradation rates follow a time-dependent function (impulse model function, see methods for more details).
- Exporting rate (α_1) to be a rapid rate (5 min on average), it is considered that it is not susceptible to changes in time after TNF-stimulation.
- Nuclear degradation of the caRNA was considered negligible and had no major impact on cytoplasmic RNA concentrations.

Under the above mathematical framework, we use direct measurements of nascent RNA levels (dP/dt , as caRNA) and RNA levels (dM/dt , as cytoRNA) to parameterize the kinetic model that recapitulate the expression behavior of co-regulated clusters of genes. After optimization of the model, we compare the model fitted values for caRNA and cytoRNA to the experimental data and calculate the error (root-mean-square deviation, RMSD). Out of 784 differential expressed genes, we got 634 genes (81%) that were considered fitted to the model, RMSD less than 0.15 for both caRNA and cytoRNA (**Figure 2-7c**). Moreover, when the profiles of the simulated data are compared visually with the experimental data, a great correlation is observed (**Figure 2-7d**). On the other hand, temporal resolution of our experimental data allows precise quantification of levels of caRNA, cytoRNA and transcription rates, but we cannot measure degradation in a comparably resolution, therefore we validate the nominal value of the basal degradation rate for each gene with the previously obtained experimental data. Interestingly, this analysis showed that the half-lives estimated by the model also capture the correlation with the temporal ordering of expression clusters (**Figure 2-7e**).

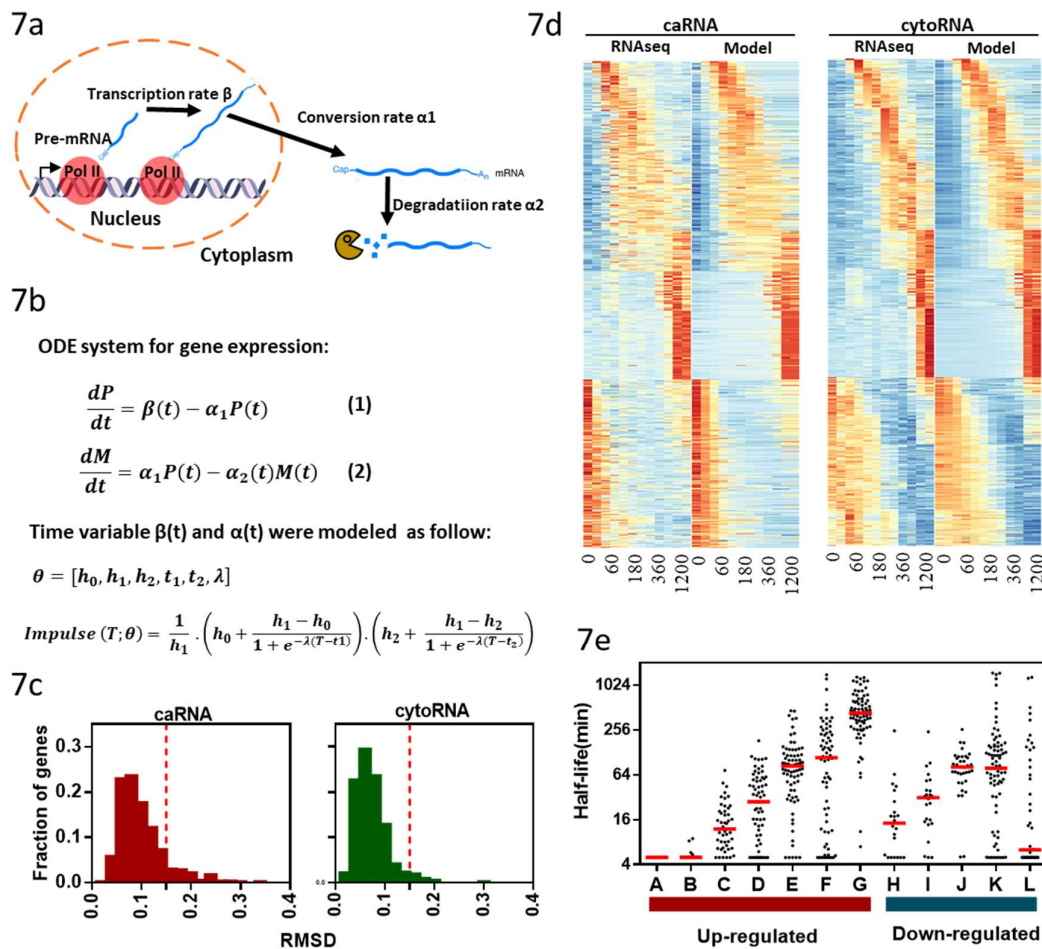


Figure 2-7. Mathematical model delineates regulation of mRNA synthesis and degradation. (a). Schematic abstraction and (b) mathematical formulation of gene expression regulation (see the text for details). (c) Histogram of root mean square error (RMSE) for caRNA (red) and cytoRNA (green), red dashed lines represent the threshold (RMSE < 0.15) of well fitted modeled profiles compared to the experimental data. (d) Comparative heatmaps of expression profiles across time between experimental data (RNA-seq) and the fitted data (Model). 634 genes (81%) were grouped in the same clusters and same order as the previous heatmaps on Figure 4f and Figure 6c, as well as the same standardization and scale color. (e). Scatter plot of the basal half-life (unstimulated) of all genes estimated in the parametrization of the model. X-axis represents the 12 temporal clusters as previously defined. Note that the same rank of basal half-lives is recover using the model, and the experimental data (4sU and ActD).

2.6.2 Synthesis control dominates but degradation control is critical for some genes

So far, the mathematical formulation applied describes most of the genes profiles accurately therefore the next step is quantitatively analysis of transcription and degradations rates. In this manner, we systematically studied dynamic RNA regulation examining how regulatory steps are coordinated for each gene. Genes were clustered into the same 12

temporal expression profiles used above (**Figure 2-4f**), but we consider changes in the rate of degradation as a higher hierarchical level (**Figure 2-8a**). Notably, for most genes (80.6%), transcriptional control is found to be dominant over the control in degradation in both induction and repression of gene expression (**Figure 2-8b**), but for the remaining group of genes (19.6%), changes in degradation rates cooperatively coordinated with transcription in the configuration of the dynamics of RNA concentrations during TNF stimulation.

Interestingly, changes in degradation rates were more common in late response gene (**Figure 2-8b**); probably, this is related to the substantial modifications degradation rates dependent on the increased concentrations of RNA binding factors (e.g., miRNAs, RNA binding proteins), which require time to be synthesized. In addition, our results show that none of the RNA profiles is fully dependent on post-transcriptional regulation; therefore, concerted regulation in the regulation dynamics in degradation and transcription rates implies that their actions may have a synergistic or antagonistic effect on the temporal concentrations of RNA. Thus, to discriminate the effects mentioned above, we use the results of the mathematical model and explore the relationship between stability and expression (**Figure 2-8c**), which showed the following 4 strategies:

- Destabilization of transiently induced genes: Those in classes B, C and L, a set of genes the transcription increases for a short period of time, but after it returns to its basal level, the rate of degradation is increased by destabilizing the cytoRNA, decreasing it to levels lower than basal (e.g., Id3; **Figure 2-8d**).

- Stabilization of constantly induced genes: For a group of genes of late induction (class F and G), the transcription increases to a point of saturation where it reaches a new steady state, however, reducing the rate of degradation the cytoRNA increasing its concentration and surpasses the new steady state imposed by the transcription rate (eg, Ikbke, **Figure 2-8d**).

- Destabilization of repressed genes: In this strategy, some late repressed genes (class K and L), the rate of transcription decreases at the same time as the rate of degradation increases (eg, Lix1, **Figure 2-8d**), this synergistic action makes it possible to rapidly decrease cytoRNA levels of stable genes.

- Stabilization of transiently repressed genes: Among this strategy are genes from classes H to J (**Figure 2-8d**), transcription decreases rapidly and therefore cytoRNA levels, but after

a time the rate of degradation is reduced, stabilizing the cytoRNA and diminishing the effect of repression imposed by decreasing transcription (e.g., Mpp2, **Figure 2-8d**).

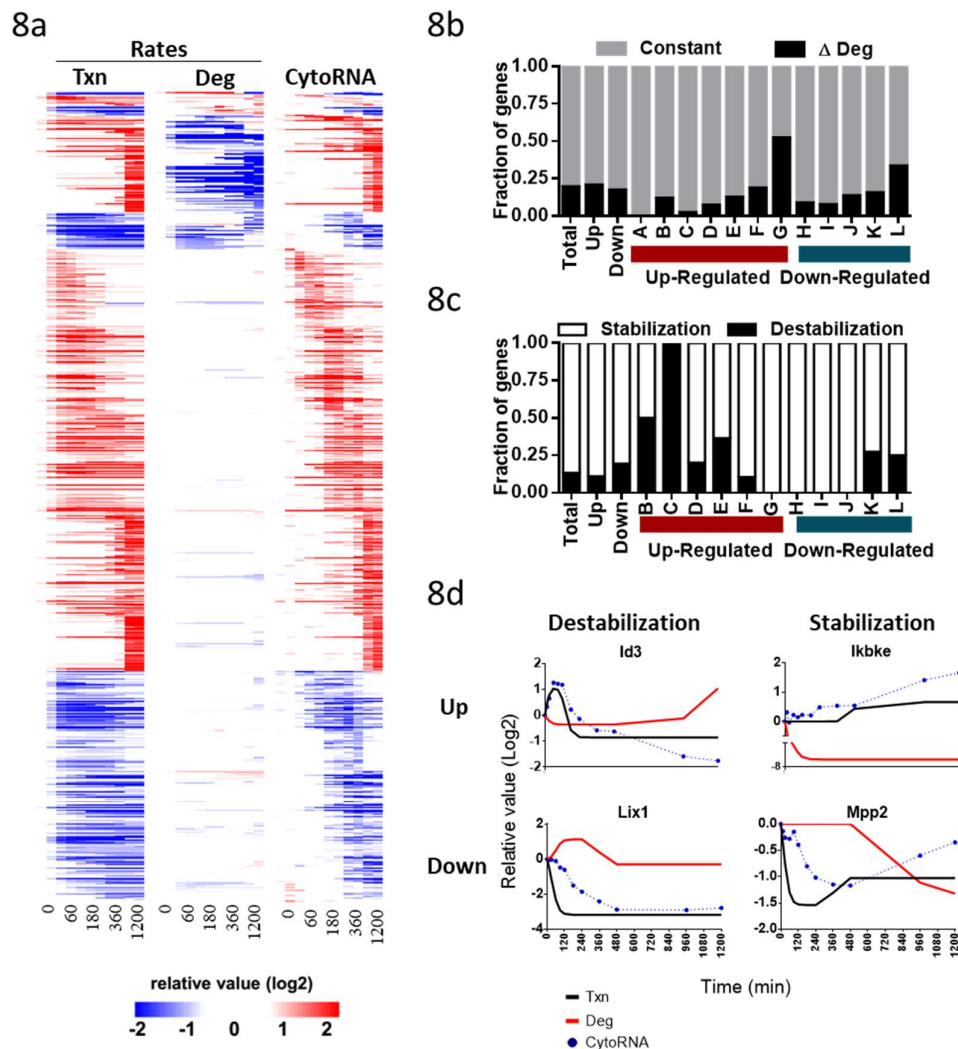


Figure 2-8. Transcription control dominates, but degradation control relaxes transcriptional constraints. (a) Time-dependent changes in rate parameters governing transcription (left), and degradation (middle) as inferred by gene regulation modelling. Genes were clustered into the same 12 temporal expression profiles used before, but changes in the rate of degradation (constant, variable) as a higher hierarchical level. Rates and cytoRNA values are relative to unstimulated cells, and presented as log2. (b) Fraction of genes with dynamic (black) or constant degradation (grey) in each temporal cluster. (c) Fraction of genes with dynamic degradation that showed an increase (destabilization, black) or decrease (stabilization, white) in the rate of degradation in each temporal cluster. (d) Example genes for which degradation rates change over time. Kinetic parameters (relative to rate at t0): transcription (black curve), degradation (red curve), experimental cytoRNA abundance (blue dots).

2.7 Molecular Regulatory Mechanisms of cytoRNA levels.

Extensive studies of signal transduction in the TNF pathway have shown that its cellular effect depends on the activation of a set of activated transcription factors across two major axes. The first axis, and the most studied, comprises the activation of the transcription factor NF- κ B which translocate to the nucleus and mediates the activation of a large set of genes (Figure 9a). Signaling by TNF results not only in the activation of NF- κ B but also signaling via mitogen activated protein kinase axis (MAPK), which is divided into three sub-axes, which include extracellular signal-regulated kinase (ERK), c-Jun N-terminal kinase (JNK), and p38. Furthermore, the activation of MAPK and its subsequent signaling activates transcriptional factors such as AP1, ATF2 and ELK1 (**Figure 2-9a**). Our results show that most dynamic levels of cytoRNA are dependent on temporal changes in transcription rate. To explore some of the molecular mechanisms governing dynamic gene expression, we dissected the transcription network of TNF signaling using mutation models for NF- κ B, and pharmacological inhibition of MAPK.

2.7.1. Transcriptional control is dependent of RelA transcription factor

As TNF induced muscle atrophy depends on the activation of the NF- κ B transcription factor⁸³ and transcriptional control were the dominant mechanism in the regulation of both gene induction and repression, therefore we test the hypothesis that NF- κ B transcription factor modify transcriptional rates during TNF response. NF- κ B is a heterodimer whose most abundant form is the RELA/NFKB1 complex (p65/p50), thereby we use a myoblast cell line in which the NF- κ B subunit RELA, which contains a transcription activation domain, has been homozygous knocked out (REAL-KO) using CRSIPR/Cas9 technology (**Figure 2-9b**). Alternatively, we used C2C12 which contains a stably expressing a mutant form of the I κ B α (gene name: *Nfkb1a*) inhibitor in which the serine at positions 32 and 36 are changed to alanine (Supplementary information S7). During TNF stimulation this dominant negative mutation, named super repressor (SR), makes I κ B α insensitive to phosphorylation and following proteasome degradation, thereby inhibiting translocation to the nucleus of the transcription factor NF- κ B (**Figure 2-9c**).

We observed that the inhibition of NF- κ B transcription factor in myotubes subjected to TNF reduces the amplitude of change of the cytoRNA temporal expression profiles of both

induced and repressed genes (**Figure 2-9d**). Additionally, when we analyzed the cumulative frequency distribution of maximum fold change gene expression, it is evident that the SR mutant, compared to RELA-KO, presents a greater inhibition in the induction and repression of gene expression (**Figure 2-9e**). This greater effect of the SR mutant is explained by the fact that the mutation is upstream the NF- κ B heterodimer; therefore, the SR mutation can inhibit not only the heterodimer RELA/NFKB1 but alternative heterodimers such as REL/NFKB1 and RELB/NFKB1. A deeply analysis of the maximum fold change in the SR mutant, revealed that 223 genes (43%) of the induced genes has a decrease of more than two times in its expression, on the other hand the number of repressed genes with the same degree of decrease was 49 (20%) (**Figure 2-9f**).

These results clearly suggest that most of the induced genes depend on the activity of the transcription factor NF- κ B, and unexpectedly we found that a small fraction of repressed genes is also dependent. However, other sets of experiments, such as RELA-ChIP-seq, are needed to determine if the dependence is a direct effect of NF- κ B on the gene promoter. This is especially important in repressed genes for which no effect has been reported for Nf- κ B as a transcriptional repressor.

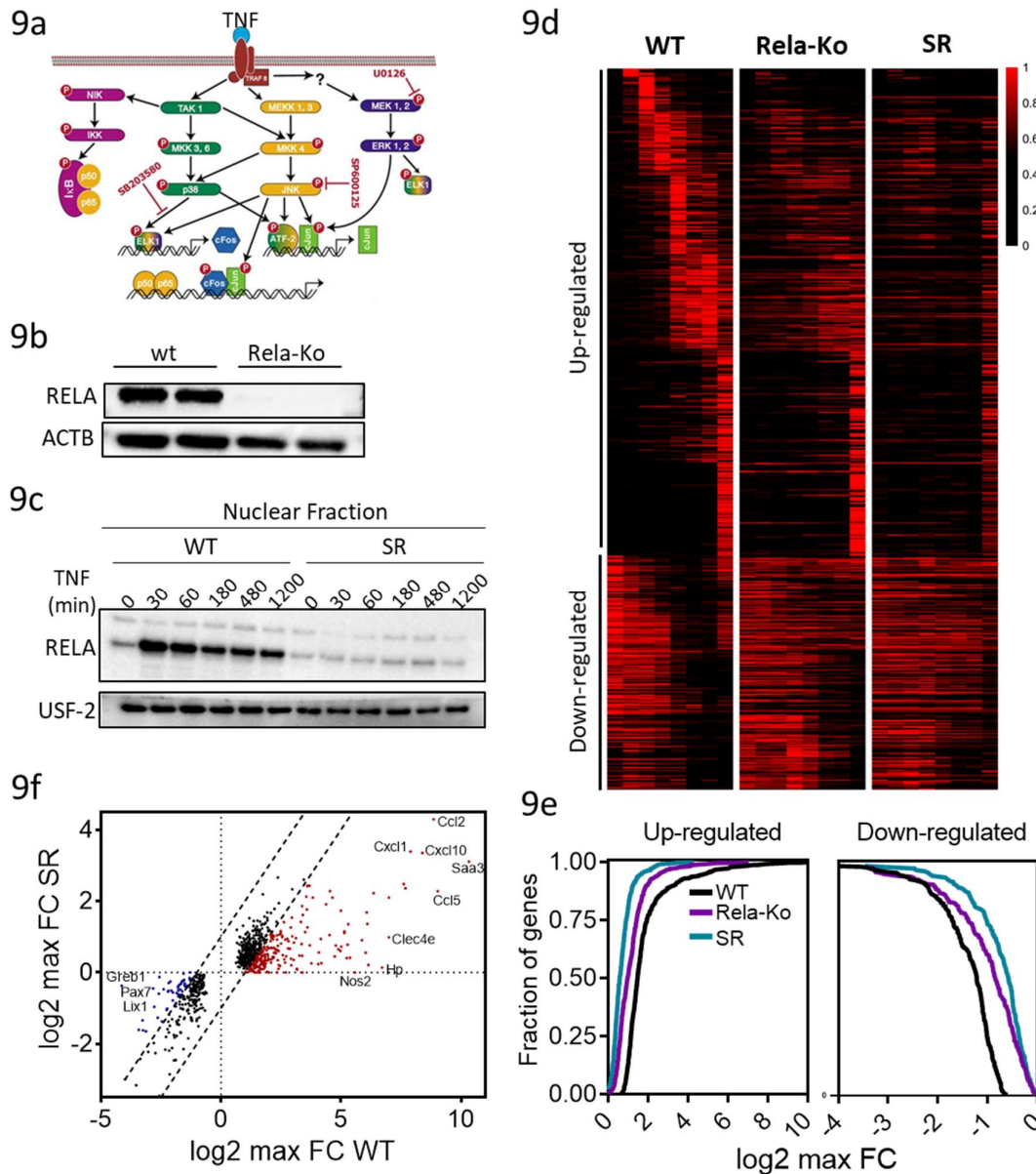


Figure 2-9. Analysis of NF-κB dependent genes. (a) TNF signaling with the two major axes activated, NF-κB and MAPK. Complex wired and functional interaction between these axes determine the activation of transcription factor network (e.g., NF-κB, ATF-2, AP-1 and ELK1) which determine the physiological outcome of TNF response (adapted from¹⁸⁹). (b) Validation of RELA knockout (RELA-Ko) cell lines using immunoblot analysis of cell lysates of wild-type (WT) and RELA-Ko, probed with RELA antibody and with an anti-actin antibody as a loading control. (c) Inhibition, after TNF stimulation, of nuclear translocation of NF-κB by the super-repressor forms of IκBα (SR) was validated using immunoblot analysis of nuclear extracts of WT and SR, probed against RELA antibody and with an anti USF-2 antibody as nuclear loading control. (d) Heatmap of expression values across time of WT, RELA-Ko and SR. Same genes were grouped in the same clusters and same order as the cytoRNA heatmap on Figure 4f. Standardization from 0 to 1 was performed using the ratio of maximum expression value across the three genotypes. Scale color mean: red: high expression, black: low expression. (e) Cumulative distribution plots, for up- and down-regulated genes, of the maximum log₂ fold change for WT (black), RELA-KO (purple) and SR (blue); data represent the average from two independent datasets. (f) Scatter plot showing the maximum log₂-fold change after TNF

stimulation of RNA transcript levels between WT (x axis) and SR (y axis), averaged from two biological replicates. Each dot represents an expressed gene. Dashed black lines means 2-fold up or down difference. Red and blue dots indicate induced and repressed genes, respectively, with a substantial reduction in their expression in the SR mutant (NF- κ B dependent genes).

2.7.2 Transcriptional control dependent of MAPK.

The activation of MAPK and NF κ B are the two major axes in the regulation of gene expression in TNF signaling. MAPKs control gene expression through cascades of phosphorylation that targets: Transcription factors, co-regulatory and chromatin proteins. Despite the importance of MAPKs, their study in skeletal muscle, as well as in other cell types, has been neglected.

To examine the role of MAPKs in modifying transcription rates, we used pharmacological inhibition with SB203580 (p38 inhibitor), SP600125 (JNK inhibitor) and U0126 (ERK inhibitor) as a strategy (**Figure 2-9a**). We use a combined inhibition of all MAPKs as strategy to reduce cross-reactive activation of targets. Moreover, an alternative methodology using CRIPSR/Cas9 knockout is unfeasible given two factors: First, MAPKs are essential genes for many cellular functions including metabolism, cell division and differentiation. Second, there is a methodological complexity due to the occurrence of multiple gene products (i.e. ERK1 and ERK2; JNK1, JNK2, and JNK3; p38 α , p38 β , p38 γ , and p38 δ).

We evaluated the phosphorylation of transcriptional factor ATF-2 and c-Jun, which are direct targets of p-38 and JNK, respectively. For ERK we evaluated its own phosphorylation, since the inhibitor U0126 acts on MEK1/2 which is the kinase upstream of ERK. Data in Figure 10 shows that after 30 minutes with TNF stimulation the p-38 pathway is activated, whereas for JNK and ERK, despite being active, TNF increases its activation. Additionally, it is found that ERK inhibition requires 20 μ M of U0126, whereas for the inhibition of p-38 and JNK, require between 50 and 70 μ M respectively (**Figure 2-10**).

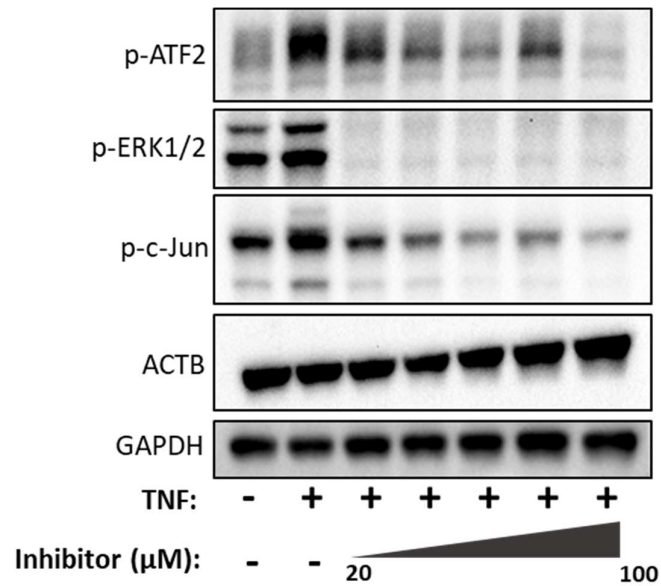


Figure 2-10. Pharmacological inhibition of MAPKs after TNF stimulation. Cells TNF stimulated for 10 min and in presence of a cocktail of MAPK inhibitors (SB203580: p38 inhibitor, SP600125: JNK inhibitor, and U0126: ERK inhibitor) with an increased concentration. Immunoblotted against phosphorylated version of ATF-2 and c-Jun were used to check p-38 and JNK inhibition respectively and ERK1/2 phosphorylation inhibition was checked directly. Antibodies anti ACTB and GAPDH were used as a loading control.

2.8 Discussion

The ability to continuously respond to changing input signals from the environment is a hallmark of all living systems. A main component of this response is achieved through complex molecular circuits, consisting of multiple intertwined feedback loops and non-linear interactions, that compute a quantitative level of each type of RNA at each time. Living cells control RNA levels by tightly regulating the processes for their production, by transcription, maturation (processing and transport), compartmentalization and degradation, which together encompass the dynamic RNA life cycle. However, their immense complexity limited available research that describe, analyze and predict their behavior.

In this work, we use RNA-seq of RNA from different cell compartment (caRNA and cytoRNA) coupled with basal degradation rates (half-lives) measurements (ActD and 4sU labeling) and computational modeling to study RNA regulation in skeletal muscle atrophy induced by TNF. Leveraging the massively parallel sequencing technology for accurate temporal measurement of RNA concentrations at a high temporal resolution on a genome-scale. The data and the computational approach allows to decompose RNA concentrations

into the separate contributions of RNA transcription and degradation, and estimate changes in degradation rates over time.

We discover key principles of temporal RNA regulation in skeletal muscle cell atrophy. Genome-wide analysis shows that the variation in basal degradation rates between genes, rather than over time, determines the temporal order of expression. In agreement to recent works, we find that changes in transcription rate highly correlate with changes in RNA level and that dynamic changes in degradation rates have minimal effect on most RNA profiles, but that they do play a unique role in genes where transcription impose a constrain when reach a new steady state. Thus, stabilization of cytoRNA is the most frequent change, which implies amplification in the induction of up-regulated genes while on the other hand diminishes the effect of gene repression in down regulated genes.

Deciphering the molecular mechanisms that control the dynamic RNA life cycle is a highly difficult task. However, our approach points out to a transcriptional mechanism as mainly responsible for almost all the temporal changes in cytoRNA. Between all the myriad molecules that could control transcription the most studied are the transcription factors. Specifically, we found that the NF-kB transcription factor is responsible for 63% of the gene expression profiles, including gene repression.

Our approach provides a new and effective tool to simultaneously study several key cellular regulatory processes and model their interactions with each other, generating a complementary view to any RNA expression analysis, and deepening our understanding of the RNA regulatory mechanisms in skeletal muscle atrophy.

2.9 Methods

Cell culture. The mouse immortalized myoblast cell line C2C12 (ATCC® CRL-1772™), was used as *in vitro* model. Cells was grown at 37°C and 5% CO₂ in Dulbecco's modified Eagle's medium (DMEM) (Life Technologies, USA) supplemented with 10% calf serum (Omega scientific, USA). Muscle differentiation to myotubes will be induced for 6 days by switching to serum-deprived media (DM). TNF (10 ng / mL) was added in differentiated myotubes to induce muscle wasting, and samples was taken at 0, 15, 30, 60, 90, 120, 180, 240, 360, 489, 960 and 1200 min. Platinum-E (Plat-E) was used as retroviral packaging cell line. Plat-E cells were grown at 37°C and 5% CO₂ in Dulbecco's modified Eagle's medium

(DMEM) (Life Technologies, USA) supplemented with 10% calf serum (Omega scientific, USA) and containing blasticidin (10 µg/ml) and puromycin (1 µg/ml). Hek293 cell line was used as lentiviral cell line, cells was grown at 37°C and 5% CO₂ in Dulbecco's modified Eagle's medium (DMEM) (Life Technologies, USA) supplemented with 10% calf serum (Omega scientific, USA).

Generation of RelA Knockout cell line. gRNA sequence to the first exon of RelA were designed with the Cas9 design target tool (<http://crispr.mit.edu>) and inserted into the Cas9-containing lentiCRISPR v2 vector¹⁹⁰. To generate lentiviruses with the LentiCRISPR v2 with RelA gRNA plasmid, HEK293 cells were plated in 10cm dishes 24h prior transfection. For virus production, 5 µg of pVSV-G, 7.5µg of pMDL-RRE and 7.5µg of pRSV-REV was transfected with 10µg of the LentiCRISPR v2 with RelA gRNA plasmid using Polyethylenimine. Lentivirus-containing supernatant was harvested 48h after the transfection, filtered through a 0.45 µm membrane (Milipore Steriflip HV/PVDF) and used jointly with 8 µg/mL polybrene to infect C2C12 cells. Cells were refreshed with DMEM 18h after infection and subsequently recovered for 24h. Afterward, cells were selected with 1µg/mL puromycin for 1 week.

Stable expression of IκBαSR cell line. Plat-E at 80% confluence in 10cm dishes was transfected with 20µg of pLXSN-IKBA-SR using polyethylenimine (Sigma Aldrich, USA). Retroviral supernatant was harvested 48 h and 96h after transfection and filtered through a 0.45 µm syringe filter (Millipore).C2C12 cells were infected with diluted viral supernatant plus 8 µg/mL polybrene (Sigma Aldrich, USA). Drug selection was conducted using 1 mg/mL Geneticin (Sigma Aldrich, USA) for 12 days; uninfected controls were obliterated after 4 days of selection.

Immunofluorescence staining. Myoblast were culture in gelatin (2%) glass slide for five days in DM and treated with TNF (10 ng/mL) for 1200 min. cells were fixed with 4% paraformaldehyde for 30 minutes. The cells were permeabilized with 0.2% Triton X-100 for 10 minutes at room temperature. Cells were treated with 5% horse serum and 2% bovine serum albumin for 30 minutes and then incubated with a mouse Anti- Skeletal Myosin (M7523,1:600, Sigma, USA) for 12 h at 4 ° C. After washing in PBS, samples will be incubated with a secondary antibody (TRITC, 1:1000, Sigma, USA) for 1 hour at room temperature and subsequently assembled with Vecta Shield-DAPI (Vector laboratories, USA).

Nuclear Extract Preparation. nuclear extracts were prepared as described¹⁹¹. Briefly, 2×10^6 C2C12 cells were washed with cold PBS, scraped, and suspended in 100 μ l of hypotonic lysis buffer (10 mM HEPES (pH 7.9), 10 mM KCl, 1.5 mM MgCl₂, 0.1 mM EDTA, 0.1 mM EGTA, 1 mM dithiothreitol, 0.5 mM phenylmethylsulfonyl fluoride, 2.0 μ g/ml leupeptin, 2.0 μ g/ml aprotinin, 0.5 mg/ml benzamidine) for 10 min. The cells were then lysed with 3.25 μ l of 10% IPEGAL, the homogenates were centrifuged, and the supernatants containing the cytoplasmic extracts were stored frozen at -80 °C. The nuclear pellets were resuspended in 25 μ l of ice-cold high salt nuclear extraction buffer (20 mM HEPES (pH 7.9), 420 mM NaCl, 1 mM EDTA, 1 mM EGTA, 25% glycerol, 1 mM dithiothreitol, 0.5 mM phenylmethylsulfonyl fluoride, 2.0 μ g/ml leupeptin, 2.0 μ g/ml aprotinin, 0.5 mg/ml benzamidine). After 30 min of intermittent mixing the extracts were centrifuged, and the supernatants containing the nuclear extracts were collected. The protein content was measured using BioRad protein assay reagent. If the extracts were not used immediately, they were stored at -80 °C.

Immunoblot. Samples was separated by SDS-PAGE and the separated proteins transferred to Hybond ECL nitrocellulose membranes (Amersham, UK). The membranes will be blocked with 5% skimmed milk diluted in TBS-Tween for 1 hour and then incubated overnight at 4°C with primary antibody according to the manufacturer's specifications. Secondary antibodies conjugated with horseradich peroxidase (HRP) and ECL chemiluminescent detection (Amersham, UK) system was used for visualization and quantification of the bands by densitometry. The values will be normalized by the values obtained reference genes.

RNA fractionation and extraction. Different transcripts were obtained, through biochemical fractionation of cell in cytoplasmic, nucleoplasmic and chromatin, from unstimulated and TNF (10 ng / mL) stimulated skeletal muscle cells. Subcellular fractions were prepared as described¹⁸³, with minor changes. The cell lysis buffer contained 0.15% NP-40, and the sucrose cushion not contain detergent. The nuclear lysis buffer contains 3M Urea. Fraction purity was confirmed by immunoblot analysis of anti-SNRP70 (Nucleoplasmic fraction: ab51266, Abcam,), anti- β -tubulin (Cytoplasmic fraction: T8328, Sigma), and anti-histone H3 (Chromatin fraction: ab39655, Abcam,). Trizo LS will be added to the chromatin and cytoplasmic. cytoRNA was purified by using Direct-zol RNA MiniPrep (Zymo research, USA). caRNA was isolated by using choroform followed by further purification with Direct-zol RNA MicroPrep (Zymo research, USA). The experiment was performed in parallel for two biological replicates.

RNA-Seq. Strand-specific libraries were generated from 500 ng total RNA (labeled and unlabeled), 200 ng caRNA or 2000 ng cytoRNA, 2000. KAPA Stranded mRNA-Seq Kit (Roche) was used for Total and cyto RNA. KAPA Stranded RNA-Seq Kit with RiboErase (Roche) was used for caRNA. cDNA libraries were single-end sequenced (50bp) on an Illumina HiSeq 4000. Reads were aligned to the mouse genome (NCBI39/mm10) with STAR v2.5¹⁹² and allowed one alignment with up to two mismatches per read. Read counts values were gotten using featureCounts version 1.4.4¹⁹³, in the case of total and cytoRNA we use exon as feature option, on the other hand for caRNA we use gene as feature option and allowing overlapping. A gene was included in the analysis if it met all of the following criteria: the maximum count reached 32 at any time point, the gene has a relative expression at least 2-fold, and significantly different from the basal (FDR < 0.05) as determined by R package DESeq. Genome tracks were generated by using the bam2wig.py (<https://github.com/MikeAxtell/bam2wig>), and visualization was made using IGV V2.4¹⁹⁴. Standardization (subtracted the mean and divided by s.d.) of the data normalized counts of a gene, separately per time series, was used to generate the heatmaps and clustering using k-means (with random initialization, and using Euclidian distance). To determine the impact of a mutation, the maximal normalized count in any samples was set at 1 for each gene.

RNA half-life measurement after transcriptional inhibition. C2C12 myotubes were treated with actinomycin D (Sigma, USA) at a final concentration of 8 µg/ml to inhibit transcription. Cells were then harvested at 0, 10, 50, 110, 230 and 350 min for total RNA isolation using Direct-zol RNA MiniPrep (Zymo research, USA). Cells, was spiked-in with ERCC RNA controls (Ambion, USA) before the isolation of total RNA. DESeq was used to calculate ERCC spike-in RNA size factors, which were then applied to normalize for library size changes in each replicate. Degradation rate of mRNA was estimated using linear regression of log-transformed normalized counts versus time. Given the wide range in degradation rates and the dynamic range of RNAseq, for some genes time points were removed sequentially from the time course till the lower confidence limit for slope was maximized. A transcript was considered to have reliable half-life measurement if 1) the data had a good fit to the linear regression ($R > 0.7$) and 2) the 95% confidence interval for half-life is less than two times the half-life.

RNA half-life measurements by 4-Thiouridine (4sU). RNA half-life measurements by 4sU labeling was carried out essentially as described previously¹⁸⁸. Briefly, C2C12 cells

were incubated with 500 μ M 4sU (Sigma, USA) for 60 min or 90 min. Then cells were collected and RNA was extracted with TRIzol reagent (Thermo Fisher Scientific, USA) according to the manufacturer's instructions. Biotinylation reaction was done with 100 μ g total RNA in labeling buffer (10 mM Tris pH 7.4, 1 mM EDTA) and 0.2 mg/ml EZ-Link Biotin-HPDP in dimethylformamide (Thermo Fisher Scientific, USA) for 2 h at 25 °C. Unbound Biotin-HPDP was removed by chloroform/isoamylalcohol (24:1) extraction using Phase Lock Gel Heavy tubes (Eppendorf, Germany). RNA was precipitated at 20,000g for 20 min with a 1:10 volume of 5 M NaCl and an equal volume of isopropanol. The pellet was washed with an equal volume of 75% ethanol and precipitated again at 20,000g for 10 min. The pellet was resuspended in 100 μ l RNase-free water. Biotinylated RNA was captured using Dynabeads MyOne Streptavidin T1 beads (Invitrogen). Biotinylated RNA was incubated with 100 μ l Dynabeads with rotation for 15 min at 25 °C. Beads were magnetically fixed and washed with 1 \times Dynabeads washing buffer. Flow-through was collected for unlabeled preexisting RNA recovery. 4sU-RNA was eluted with 200 μ l of freshly prepared 100 mM dithiothreitol (DTT). Unlabeled and 4sU-RNA was recovered from eluates and washing using chloroform/isoamylalcohol (24:1) extraction. As shown in **Figure 2-11**. Libraries and RNAseq for total, label and unlabeled RNA were performed as describe above. Data normalization, 4sU labeling bias estimation and accurate RNA half-lives estimations were accessed as described in the Supplemental Experimental Procedures of Miller et al. (2011)¹⁷⁷, using the R package DTA¹⁹⁵.

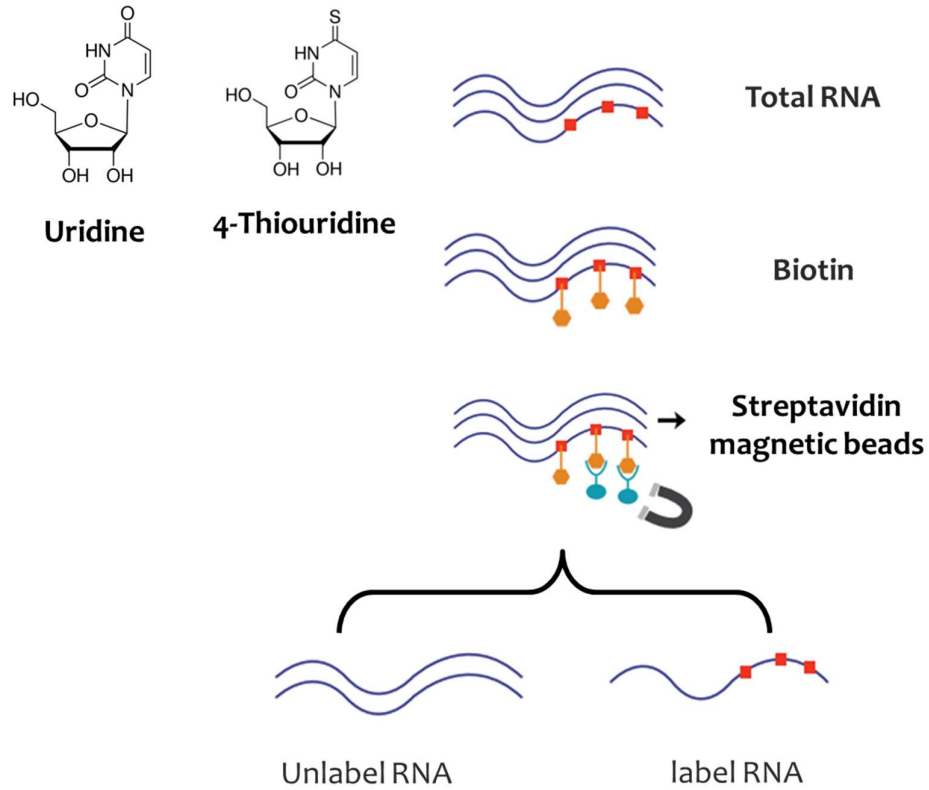


Figure 2-11. Metabolic labeling of RNA with 4-thiouridine (4sU). 4sU, a naturally occurring uridine derivative, is added to the medium where the cell will incorporate to the new transcribed RNA. Purification is made using streptavidin magnetic beads. Total RNA extract is biotinylated by covalently linking biotin (orange) to 4sU, followed by binding to Streptavidin coated magnetic beads (light blue). Biotinylated (4sU labeled) RNA is magnetically isolated, whereas unlabeled RNA is washed out. Finally, cleaving the biotin-4sU disulfide bond releases the labeled RNA from the beads. Adapted from ¹⁸⁸.

Mathematical model. We use two coupled ordinary equations formulation of dynamic RNA life cycle that has been previously described¹⁸⁷:

$$\frac{dP}{dt} = \beta(t) - \alpha_1 P(t) \quad (1)$$

$$\frac{dM}{dt} = \alpha_1 P(t) - \alpha_2(t) M(t) \quad (2)$$

With a steady state solution (ss):

$$P_{ss} \frac{\beta}{\alpha_1}, M_{ss} = \frac{\beta}{\alpha_2} \Rightarrow \frac{P_{ss}}{M_{ss}} = \frac{\alpha_2}{\alpha_1} = \frac{t_{1/2}^P}{t_{1/2}^M} \quad (3)$$

$P(t)$, $M(t)$ are the caRNA and cytoRNA concentrations at time t , α_1 is the export rate (from nuclear to cytoplasm), $\alpha_2(t)$ is the time-dependent cytoRNA degradation rate, and $\beta(t)$ is the

transcription rate. Note that the system can easily be solved analytically for fixed (independent of time) α_1 , α_2 , β . An analytic solution can be written as:

$$P(t) = \left(P_0 - \frac{\beta}{\alpha}\right) e^{-\alpha_1 t} + \frac{\beta}{\alpha_1} \quad (4)$$

$$M(t) = \left(M_0 - \frac{\alpha_1 P_0 - \beta}{\alpha_2 - \alpha_1} - \frac{\beta}{\alpha_2}\right) e^{-\alpha_2 t} + \frac{\alpha_1 P_0 - \beta}{\alpha_2 - \alpha_1} e^{-\alpha_1 t} + \frac{\beta}{\alpha_2} \quad (5)$$

The absolute values of caRNA and cytoRNA concentrations need to be normalized respect to the RNA mass in each compartment, however it is inexactly an introduce a bias. But relative abundances (fold change) respect to time zero or unstimulated, its practical and avoid the bias of RNA mass normalization. The system at this time was at a steady state, we can formulate the equation as follow:

$$\beta(0) = \alpha_1(0)P(0) \quad (6)$$

$$\frac{P(0)}{M(0)} = \frac{\alpha_2(0)}{\alpha_1(0)} \quad (7)$$

In terms of the transformed fold change variables the equations 1 and 2 become,

$$\hat{P} = \frac{P}{P(0)}, \quad \hat{M} = \frac{M}{M(0)}, \quad \hat{\alpha} = \frac{\alpha}{\alpha(0)}, \quad \hat{\beta} = \frac{\beta}{\beta(0)} \quad (8)$$

$$\frac{d\hat{P}(t)}{dt} = \alpha_1(0) [\hat{\beta}(t) - \hat{\alpha}_1 \hat{P}(t)] \quad (9)$$

$$\frac{d\hat{M}(t)}{dt} = \alpha_2(0) [\hat{\alpha}_1 \hat{P}(t) - \hat{\alpha}_2 \hat{M}(t)] \quad (10)$$

We assume that transcription rate and degradation (β and α_2) are temporally varying rates, and we define it with the impulse model¹⁹⁶, a 6-parameter double-sigmoid function (**Figure 2-12**):

$$\theta = [h_0, h_1, h_2, t_1, t_2, \lambda]$$

$$rate(t; \theta) = \frac{1}{h_1} \left(h_0 + (h_1 - h_0) \frac{1}{1 + e^{-\lambda(t-t_1)}} \right) \left(h_2 + (h_1 - h_2) \frac{1}{1 + e^{-\lambda(t-t_2)}} \right)$$

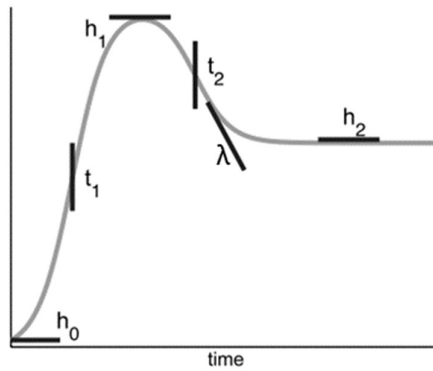


Figure 2-12. The six parameters of the impulse model. Taken from ¹⁹⁶

Fitting the model to the data. To perform the optimization of the ODE models we use the global optimization algorithm of Differential Evolution as implemented by the function `NMinimize`, with the following settings: Search Points (Population size) = 500, Scaling Factor = 0.9, Cross Probability = 0.5. Furthermore, the best parameter setting returned by the Differential Evolution algorithm is further used to perform local optimization using the Quasi Newton method.

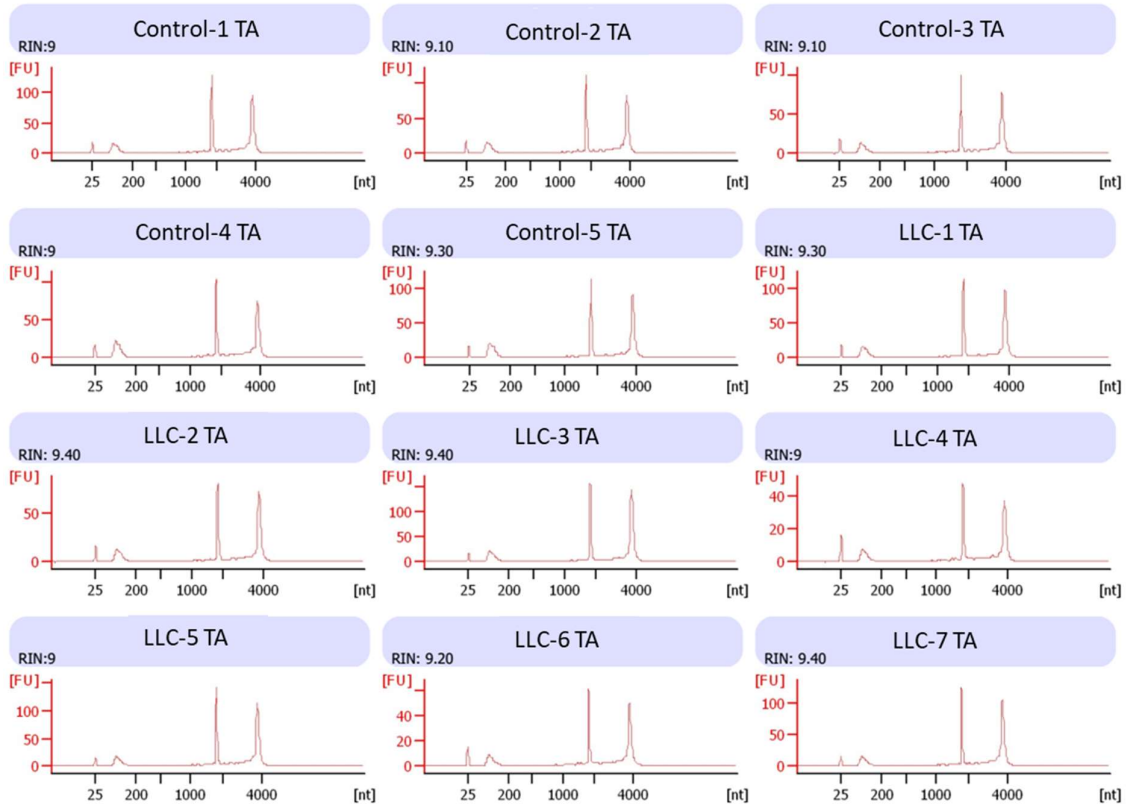
"A picture is worth a thousand words"

proverb



Supplementary information

Supplementary information S1



Supplementary Information S1 RNA integrity of tibialis anterior muscle (TA). The RNA integrity was verified by using capillary electrophoresis using the Bioanalyzer 2100 before RNA sequencing (mRNA and miRNA). All the samples presented a RNA integrity number (RIN) > 9.

Supplementary information S2 mRNAs differentially expressed in cancer cachexia

(available at: <https://goo.gl/48Vk01>)

Supplementary information 3. Gene set enrichment analysis of genes differentially expressed in cancer cancer cachexia.

GO	Fold Enrichment	% Associated Genes
GO:0001525~angiogenesis	2.119864745	13.30
GO:0005161~platelet-derived growth factor receptor binding	3.906990521	27.27
GO:0005776~autophagosome	1.876368722	12.66
GO:0016239~positive regulation of macroautophagy	2.844042143	12.77
GO:0030335~positive regulation of cell migration	2.133031607	12.31
GO:0042060~wound healing	2.306226481	11.81
GO:0031012~extracellular matrix	3.617118715	24.28
GO:0030574~collagen catabolic process	5.087675389	32.00
GO:0005921~gap junction	4.257913639	15.63
GO:0005923~bicellular tight junction	1.764874349	10.10
GO:0071354~cellular response to interleukin-6	3.964422381	21.43
GO:0030593~neutrophil chemotaxis	4.441621371	16.47
GO:0030595~leukocyte chemotaxis	7.268107698	14.86
GO:0071356~cellular response to tumor necrosis factor	2.543837694	14.19
GO:0071346~cellular response to interferon-gamma	2.725540387	9.86
GO:0071277~cellular response to calcium ion	2.725540387	13.46
GO:0006813~potassium ion transport	2.370035119	7.69
GO:0006003~fructose 2,6-bisphosphate metabolic process	5.451080774	50.00
GO:0045821~positive regulation of glycolytic process	4.360864619	23.08
GO:0046902~regulation of mitochondrial membrane permeability	4.360864619	8.33
GO:0051901~positive regulation of mitochondrial depolarization	4.845405132	10.4
GO:0030016~myofibril	2.530417248	57.73
GO:0035914~skeletal muscle cell differentiation	3.074968642	25.91
GO:0045666~positive regulation of neuron differentiation	2.133031607	28.32
GO:0007409~axonogenesis	1.998729617	25.25
GO:0005344~oxygen transporter activity	5.46978673	19.99
GO:0006749~glutathione metabolic process	2.127251034	14.29

GO:000502~proteasome complex	1.99633328	15.79
GO:0002020~protease binding	2.500473934	13.56
GO:0010466~negative regulation of peptidase activity	4.193139057	8.10
GO:0004175~endopeptidase activity	1.769636883	7.68
GO:0006508~proteolysis	1.422021071	7.02
GO:0005520~insulin-like growth factor binding	4.786063389	29.17
GO:0071560~cellular response to transforming growth factor beta stimulus	2.087647956	10.55
GO:0004016~adenylate cyclase activity	5.46978673	18.18
GO:0046330~positive regulation of JNK cascade	2.31960884	9.48
GO:1900745~positive regulation of p38MAPK cascade	3.634053849	26.67

Supplementary information S4 Differentially expressed miRNAs in tibialis anterior muscle in cancer cachexia, ranked by a combination of p-value < 0.05 and fold change ≥ 1.5 .

<i>Direction of Fold Change</i>	<i>microRNA</i>	<i>miRBase ID</i>	<i>Fold Change</i>	<i>log2 Fold Change</i>	<i>P-value</i>	<i>Chromosome</i>	<i>Start</i>	<i>End</i>	<i>Strand</i>
			<i>(cachectic mice vs. non-cachectic controls)</i>						
<i>Up</i>	mmu-miR-1843a-3p	MI0004155	2,33	1,22	0,002	chr12	80391613	80391677	-
	mmu-miR-146b-5p	MI0004665	2,02	1,02	0,003	chr19	46342762	46342870	+
	mmu-miR-350-3p	MI0000640	1,91	0,93	0,003	chr1	176772325	176772423	-
	mmu-miR-1249-3p	MI0004132	1,81	0,86	0,000	chr15	84951526	84951623	-
	mmu-miR-338-5p	MI0000619	1,79	0,84	0,015	chr11	120014765	120014862	-
	mmu-miR-3535	MI0026036	1,76	0,82	0,026	chr1	86351981	86352127	-
	mmu-miR-146a-5p	MI0000170	1,73	0,79	0,009	chr11	43374397	43374461	-
	mmu-miR-29b-3p	MI0000143	1,72	0,78	0,000	chr6	31063023	31063093	-
	mmu-miR-10b-5p	MI0000221	1,67	0,74	0,001	chr2	74726070	74726137	+
	mmu-miR-223-3p	MI0000703	1,66	0,73	0,001	chrX	96242817	96242926	+
	mmu-miR-671-3p	MI0004133	1,62	0,70	0,007	chr5	24592114	24592211	+
	mmu-miR-183-5p	MI0000225	1.81	0.85	0,006	chr6	30169668	30169737	-
mmu-miR-382-5p	MI0000799	1.71	0.77	0,008	chr12	109733771	109733846	+	
<i>Down</i>	mmu-miR-379-5p	MI0000796	0,66	-0,60	0,020	chr12	109709060	109709125	+
	mmu-miR-144-3p	MI0000168	0,62	-0,70	0,001	chr11	78073005	78073070	+
	mmu-miR-451a	MI0001730	0,60	-0,73	0,000	chr11	78073170	78073241	+
	mmu-miR-144-5p	MI0000168	0,57	-0,81	0,001	chr11	78073005	78073070	+
	mmu-miR-181c-3p	MI0000724	0,56	-0,84	0,004	chr8	84178873	84178961	-

Supplementary information S5. Number of targets mRNAs per differentially expressed microRNAs in cancer cachexia.

miRNA	Predicted	Validated	Total
miR-10b-5p	0	2	2
miR-1249-3p	19	0	19
miR-144-3p	0	2	2
miR-144-5p	0	2	2
miR-146a-5p	0	4	4
miR-146b-5p	0	2	2
miR-181c-3p	0	1	1
miR-183-5p	0	2	2
miR-1843a-3p	18	0	18
miR-223-3p	7	0	7
miR-29b-3p	0	22	22
miR-338-5p	0	4	4
miR-350-3p	47	0	47
miR-3535	17	0	17
miR-379-3p	2	0	2
miR-382-5p	3	0	3
miR-451a	1	0	1
miR-671-3p	15	0	15

Supplementary information S6. mRNAs co-deregulated by 3 or more miRNAs in cancer cachexia (mRNA downregulated; miRNA upregulated).

mRNA	miRNA (n)	List of miRNAs
Map2k6	4	miR-223-3p, miR-350-3p, miR-3535, miR-671-3p
Ptpn3	4	miR-1249-3p, miR-1843a-3p, miR-350-3p, miR-3535
Mettl21c	3	miR-1843a-3p, miR-350-3p, miR-671-3p
Plxdc2	3	miR-1249-3p, miR-1843a-3p, miR-350-3p
Ppargc1b	3	miR-1249-3p, miR-350-3p, miR-3535
Rgs5	3	miR-1843a-3p, miR-3535, miR-671-3p
Vegfa	3	miR-1249-3p, miR-1843a-3p, miR-29b-3p*

c

Supplementary information S7

Nfkbia-SR

1	ATG	TTT	CAG	CCA	GCT	GGG	CAC	GGC	CAG	GAC	TGG	GCC	ATG	GAG	GGC	45
1	Met	Phe	Gln	Pro	Ala	Gly	His	Gly	Gln	Asp	Trp	Ala	Met	Glu	Gly	15
46	CCG	CGG	GAT	GGC	CTC	AAG	AAG	GAG	CGC	TTG	GTG	GAC	GAT	CGC	CAC	90
16	Pro	Arg	Asp	Gly	Leu	Lys	Lys	Glu	Arg	Leu	Val	Asp	Asp	Arg	His	30
91	GAC	GCA	GGT	CTA	GAC	GCC	ATG	AAG	GAC	GAG	GAG	TAC	GAG	CAA	ATG	135
31	Asp	Ala	Gly	Leu	Asp	Ala	Met	Lys	Asp	Glu	Glu	Tyr	Glu	Gln	Met	45
136	GTG	AAG	GAG	CTG	CGG	GAG	ATC	CGC	CTG	CAG	CCG	CAG	GAG	GCG	CCG	180
46	Val	Lys	Glu	Leu	Arg	Glu	Ile	Arg	Leu	Gln	Pro	Gln	Glu	Ala	Pro	60

Nfkbia-Wt

1	ATG	TTT	CAG	CCA	GCT	GGG	CAC	GGC	CAG	GAC	TGG	GCC	ATG	GAG	GGC	45
1	Met	Phe	Gln	Pro	Ala	Gly	His	Gly	Gln	Asp	Trp	Ala	Met	Glu	Gly	15
46	CCG	CGG	GAT	GGC	CTC	AAG	AAG	GAG	CGC	TTG	GTG	GAC	GAT	CGC	CAC	90
16	Pro	Arg	Asp	Gly	Leu	Lys	Lys	Glu	Arg	Leu	Val	Asp	Asp	Arg	His	30
91	GAC	AGC	GGC	CTG	GAC	TCC	ATG	AAG	GAC	GAG	GAG	TAC	GAG	CAA	ATG	135
31	Asp	Ser	Gly	Leu	Asp	Ser	Met	Lys	Asp	Glu	Glu	Tyr	Glu	Gln	Met	45
136	GTG	AAG	GAG	CTG	CGG	GAG	ATC	CGC	CTG	CAG	CCG	CAG	GAG	GCG	CCG	180
46	Val	Lys	Glu	Leu	Arg	Glu	Ile	Arg	Leu	Gln	Pro	Gln	Glu	Ala	Pro	60

Supplementary Information S8. Nucleotide and aminoacidic sequence of the *Nfkbia* gene and their encoded protein I κ B α . For the Wild type (WT) genotype and the mutant (SR). Colored boxes show the point mutation in the SR genotype that lead to the change of the serine to alanine.

“I received the fundamentals of my education in school, but that was not enough. My real education, the superstructure, the details, the true architecture, I got out of the public library”

Isaac Asimov

B

Bibliography

Bibliography

1. Miyazaki, M. & Esser, K. a. Cellular mechanisms regulating protein synthesis and skeletal muscle hypertrophy in animals. *J. Appl. Physiol.* **106**, 1367–73 (2009).
2. Braun, T. & Gautel, M. Transcriptional mechanisms regulating skeletal muscle differentiation, growth and homeostasis. *Nat. Rev. Mol. Cell Biol.* **12**, 349–61 (2011).
3. Lecker, S. H. *et al.* Multiple types of skeletal muscle atrophy involve a common program of changes in gene expression. *FASEB J.* **18**, 39–51 (2004).
4. Glass, D. J. Skeletal muscle hypertrophy and atrophy signaling pathways. *Int. J. Biochem. Cell Biol.* **37**, 1974–84 (2005).
5. Kandarian, S. C. & Jackman, R. W. Intracellular signaling during skeletal muscle atrophy. *Muscle Nerve* **33**, 155–65 (2006).
6. Tisdale, M. J. Cachexia in cancer patients. *Nat. Rev. cancer* **3**, 883–9 (2002).
7. Morley, J. E., Thomas, D. R. & Wilson, M. G. Cachexia: pathophysiology and clinical relevance. *Am. J. Clin. Nutr.* **83**, 735–43 (2006).
8. Donohoe, C. L., Ryan, A. M. & Reynolds, J. V. Cancer cachexia: mechanisms and clinical implications. *Gastroenterol. Res. Pract.* **2011**, 601434 (2011).
9. Tisdale, M. J. Mechanisms of cancer cachexia. *Physiol. Rev.* **89**, 381–410 (2009).
10. Wigmore, S. J., Plester, C. E., Richardson, R. a & Fearon, K. C. Changes in nutritional status associated with unresectable pancreatic cancer. *Br. J. Cancer* **75**, 106–9 (1997).
11. Banerjee, A. & Guttridge, D. C. Mechanisms for maintaining muscle. *Curr. Opin. Support. Palliat. Care* **6**, 451–6 (2012).
12. Tan, B. H. L. *et al.* P-selectin genotype is associated with the development of cancer cachexia. *EMBO Mol. Med.* **4**, 462–71 (2012).
13. Shaid, S., Brandts, C. H., Serve, H. & Dikic, I. Ubiquitination and selective autophagy. *Cell Death Differ.* **20**, 21–30 (2013).
14. Cao, P. R., Kim, H. J. & Lecker, S. H. Ubiquitin-protein ligases in muscle wasting. *Int. J. Biochem. Cell Biol.* **37**, 2088–97 (2005).
15. Bonaldo, P. & Sandri, M. Cellular and molecular mechanisms of muscle atrophy. *Dis. Model. Mech.* **6**, 25–39 (2013).
16. Csibi, A., Leibovitch, M. P., Cornille, K., Tintignac, L. a & Leibovitch, S. a. MAFbx/Atrogin-1 controls the activity of the initiation factor eIF3-f in skeletal muscle atrophy by targeting multiple C-terminal lysines. *J. Biol. Chem.* **284**, 4413–21 (2009).
17. Samuels, S. E. *et al.* Higher skeletal muscle protein synthesis and lower breakdown after chemotherapy in cachectic mice. *Am. J. Physiol. Regul. Integr. Comp. Physiol.* **281**, R133-9 (2001).
18. Rommel, C. *et al.* Mediation of IGF-1-induced skeletal myotube hypertrophy by

- PI(3)K/Akt/mTOR and PI(3)K/Akt/GSK3 pathways. *Nat. Cell Biol.* **3**, 1009–13 (2001).
19. Bentzinger, C. F. *et al.* Skeletal muscle-specific ablation of raptor, but not of rictor, causes metabolic changes and results in muscle dystrophy. *Cell Metab.* **8**, 411–24 (2008).
 20. Mammucari, C. *et al.* FoxO3 controls autophagy in skeletal muscle in vivo. *Cell Metab.* **6**, 458–71 (2007).
 21. Lum, J. J., DeBerardinis, R. J. & Thompson, C. B. Autophagy in metazoans: cell survival in the land of plenty. *Nat. Rev. Mol. Cell Biol.* **6**, 439–48 (2005).
 22. Zhao, J. *et al.* FoxO3 coordinately activates protein degradation by the autophagic/lysosomal and proteasomal pathways in atrophying muscle cells. *Cell Metab.* **6**, 472–83 (2007).
 23. Sandri, M. *et al.* PGC-1 α protects skeletal muscle from atrophy by suppressing FoxO3 action and atrophy-specific gene transcription. *Proc. Natl. Acad. Sci. U. S. A.* **103**, 16260–5 (2006).
 24. Khalil, A. S. & Collins, J. J. Synthetic biology: applications come of age. *Nat. Rev. Genet.* **11**, 367–79 (2010).
 25. Barabási, A.-L., Gulbahce, N. & Loscalzo, J. Network medicine: a network-based approach to human disease. *Nat. Rev. Genet.* **12**, 56–68 (2011).
 26. Deval, C. *et al.* Identification of cathepsin L as a differentially expressed message associated with skeletal muscle wasting. *Biochem. J.* **360**, 143–50 (2001).
 27. Pozhitkov, A. E., Boube, I., Brouwer, M. H. & Noble, P. a. Beyond Affymetrix arrays: expanding the set of known hybridization isotherms and observing pre-wash signal intensities. *Nucleic Acids Res.* **38**, e28 (2010).
 28. Allison, D. B., Cui, X., Page, G. P. & Sabripour, M. Microarray data analysis: from disarray to consolidation and consensus. *Nat. Rev. Genet.* **7**, 55–65 (2006).
 29. Monitto, C. L. *et al.* Differential gene expression in a murine model of cancer cachexia. *Am. J. Physiol. Endocrinol. Metab.* **281**, E289-97 (2001).
 30. Stephens, N. a *et al.* Using transcriptomics to identify and validate novel biomarkers of human skeletal muscle cancer cachexia. *Genome Med.* **2**, 1 (2010).
 31. Dahlman, I. *et al.* Adipose tissue pathways involved in weight loss of cancer cachexia. *Br. J. Cancer* **102**, 1541–8 (2010).
 32. Bonetto, A. *et al.* STAT3 activation in skeletal muscle links muscle wasting and the acute phase response in cancer cachexia. *PLoS One* **6**, e22538 (2011).
 33. Skorokhod, A., Bachmann, J., Giese, N. a, Martignoni, M. E. & Krakowski-Roosen, H. Real-time imaging cDNA-AFLP transcript profiling of pancreatic cancer patients: Egr-1 as a potential key regulator of muscle cachexia. *BMC Cancer* **12**, 265 (2012).
 34. Dwarkasing, J. T. *et al.* Hypothalamic food intake regulation in a cancer-cachectic mouse model. *J. Cachexia. Sarcopenia Muscle* (2013). doi:10.1007/s13539-013-0121-y
 35. Cornwell, E. W., Mirbod, A., Wu, C.-L., Kandarian, S. C. & Jackman, R. W. C26 cancer-

- induced muscle wasting is IKK β -dependent and NF-kappaB-independent. *PLoS One* **9**, e87776 (2014).
36. Esteller, M. Non-coding RNAs in human disease. *Nat. Rev. Genet.* **12**, 861–74 (2011).
 37. Wilczynska, A. & Bushell, M. The complexity of miRNA-mediated repression. *Cell Death Differ.* **22**, 22–33 (2015).
 38. Hausser, J. & Zavolan, M. Identification and consequences of miRNA-target interactions—beyond repression of gene expression. *Nat. Rev. Genet.* **15**, 599–612 (2014).
 39. Bartel, D. P., Lee, R. & Feinbaum, R. MicroRNAs : Genomics , Biogenesis , Mechanism , and Function Genomics : The miRNA Genes. **116**, 281–297 (2004).
 40. Wang, X. H. MicroRNA in myogenesis and muscle atrophy. *Curr. Opin. Clin. Nutr. Metab. Care* **16**, 258–66 (2013).
 41. McCarthy, J. J., Esser, K. A., Peterson, C. a & Dupont-Versteegden, E. E. Evidence of MyomiR network regulation of beta-myosin heavy chain gene expression during skeletal muscle atrophy. *Physiol. Genomics* **39**, 219–26 (2009).
 42. Xu, J. *et al.* Transcription factor FoxO1, the dominant mediator of muscle wasting in chronic kidney disease, is inhibited by microRNA-486. *Kidney Int.* **82**, 401–11 (2012).
 43. Wada, S. *et al.* Translational suppression of atrophic regulators by microRNA-23a integrates resistance to skeletal muscle atrophy. *J. Biol. Chem.* **286**, 38456–65 (2011).
 44. Narasimhan, A. *et al.* Small RNAome profiling from human skeletal muscle: novel miRNAs and their targets associated with cancer cachexia. *J. Cachexia. Sarcopenia Muscle* (2017). doi:10.1002/jcsm.12168
 45. Fearon, K. *et al.* Definition and classification of cancer cachexia: an international consensus. *Lancet Oncol.* **12**, 489–95 (2011).
 46. Schiaffino, S. & Reggiani, C. Fiber types in mammalian skeletal muscles. *Physiol. Rev.* **91**, 1447–531 (2011).
 47. Matsuyama, T. *et al.* Tumor inoculation site affects the development of cancer cachexia and muscle wasting. *Int. J. Cancer* **137**, 2558–2565 (2015).
 48. Pettersen, K. *et al.* Cancer cachexia associates with a systemic autophagy-inducing activity mimicked by cancer cell-derived IL-6 trans-signaling. *Sci. Rep.* **7**, 1–16 (2017).
 49. Guo, D., Wang, C., Wang, Q., Qiao, Z. & Tang, H. Pantoprazole blocks the JAK2/STAT3 pathway to alleviate skeletal muscle wasting in cancer cachexia by inhibiting inflammatory response. *Oncotarget* **8**, 39640–39648 (2017).
 50. Bonetto, A. *et al.* JAK/STAT3 pathway inhibition blocks skeletal muscle wasting downstream of IL-6 and in experimental cancer cachexia. *Am. J. Physiol. Endocrinol. Metab.* **303**, E410-21 (2012).
 51. Bonetto, A. *et al.* Early changes of muscle insulin-like growth factor-1 and myostatin gene expression in gastric cancer patients. *Muscle Nerve* **48**, 387–392 (2013).

52. D'Orlando, C. *et al.* Gastric cancer does not affect the expression of atrophy-related genes in human skeletal muscle. *Muscle Nerve* **39**, 1–22 (2013).
53. DeBoer, M. D. Animal models of anorexia and cachexia. *Expert Opin. Drug Discov.* **4**, 1145–1155 (2009).
54. Bennani-Baiti, N. & Walsh, D. Animal models of the cancer anorexia-cachexia syndrome. *Support. Care Cancer* **19**, 1451–1463 (2011).
55. Ballarò, R., Costelli, P. & Penna, F. Animal models for cancer cachexia. *Curr. Opin. Support. Palliat. Care* **10**, 281–287 (2016).
56. Penna, F., Busquets, S. & Argilés, J. M. Experimental cancer cachexia: Evolving strategies for getting closer to the human scenario. *Semin. Cell Dev. Biol.* **54**, 20–27 (2016).
57. Li, J. J., Bickel, P. J. & Biggin, M. D. System wide analyses have underestimated protein abundances and the importance of transcription in mammals. *PeerJ* **2**, e270 (2014).
58. Gomes, M. D., Lecker, S. H., Jagoe, R. T., Navon, A. & Goldberg, A. L. Atrogin-1, a muscle-specific F-box protein highly expressed during muscle atrophy. *Proc. Natl. Acad. Sci. U. S. A.* **98**, 14440–5 (2001).
59. Bodine, S. C. *et al.* Identification of ubiquitin ligases required for skeletal Muscle Atrophy. *Science (80-.).* **294**, 1704–1708 (2001).
60. Bodine, S. C. & Baehr, L. M. Skeletal muscle atrophy and the E3 ubiquitin ligases MuRF1 and MAFbx/atrogin-1. *AJP Endocrinol. Metab.* **307**, E469–E484 (2014).
61. Wang, Z., Liu, P., Inuzuka, H. & Wei, W. Roles of F-box proteins in cancer. *Nat. Rev. Cancer* **14**, 233–247 (2014).
62. Sukari, A., Muqbil, I., Mohammad, R. M., Philip, P. A. & Azmi, A. S. F-BOX proteins in cancer cachexia and muscle wasting: Emerging regulators and therapeutic opportunities. *Semin. Cancer Biol.* **36**, 95–104 (2016).
63. Li, Y.-P. *et al.* TNF-alpha increases ubiquitin-conjugating activity in skeletal muscle by up-regulating UbcH2/E220k. *FASEB J.* **17**, 1048–1057 (2003).
64. Gordon, B. S., Steiner, J. L., Lang, C. H., Jefferson, L. S. & Kimball, S. R. Reduced REDD1 expression contributes to activation of mTORC1 following electrically induced muscle contraction. *AJP Endocrinol. Metab.* **307**, E703–E711 (2014).
65. Gordon, B. S. *et al.* Loss of REDD1 augments the rate of the overload-induced increase in muscle mass. *Am. J. Physiol. - Regul. Integr. Comp. Physiol.* **311**, R545–R557 (2016).
66. Bodine, S. C. *et al.* Akt/mTOR pathway is a crucial regulator of skeletal muscle hypertrophy and can prevent muscle atrophy in vivo. *Nat. Cell Biol.* **3**, 1014–1019 (2001).
67. Sullivan-Gunn, M. J. & Lewandowski, P. A. Elevated hydrogen peroxide and decreased catalase and glutathione peroxidase protection are associated with aging sarcopenia. *BMC Geriatr.* **13**, 1–9 (2013).
68. Nuoc, T. N. *et al.* The analysis of antioxidant expression during muscle atrophy induced by

- hindlimb suspension in mice. *J. Physiol. Sci.* **67**, 121–129 (2017).
69. Deruisseau, L. R. *et al.* Muscle contractile dysfunction and oxidative injury are observed in the soleus muscle of metallothionein deficient mice following acute spinal cord injury. *FASEB J.* **23**, 1795–1802 (2009).
 70. Summermatter, S. *et al.* Blockade of Metallothioneins 1 and 2 Increases Skeletal Muscle Mass and Strength. *Mol. Cell. Biol.* **37**, 1–11 (2017).
 71. COPENHAVER, W. M., MOORE, D. H. & RUSKA, H. Electron microscopic and histochemical observations of muscle degeneration after tourniquet. *J. Biophys. Biochem. Cytol.* **2**, 755–64 (1956).
 72. Pellegrino, C. & Franzini, C. AN ELECTRON MICROSCOPE STUDY OF DENERVATION ATROPHY IN RED AND WHITE SKELETAL MUSCLE FIBERS. *J. Cell Biol.* **17**, 327–49 (1963).
 73. He, W. A. *et al.* NF- κ B-mediated Pax7 dysregulation in the muscle microenvironment promotes cancer cachexia. *J. Clin. Invest.* **123**, 4821–4835 (2013).
 74. Liu, X., Lee, D. J., Skittone, L. K., Natsuhara, K. & Kim, H. T. Role of gelatinases in disuse-induced skeletal muscle atrophy. *Muscle and Nerve* **41**, 174–178 (2010).
 75. Mehan, R. S., Greybeck, B. J., Emmons, K., Byrnes, W. C. & Allen, D. L. Matrix metalloproteinase-9 deficiency results in decreased fiber cross-sectional area and alters fiber type distribution in mouse hindlimb skeletal muscle. *Cells. Tissues. Organs* **194**, 510–20 (2011).
 76. Chen, C.-C. *et al.* FoxOs inhibit mTORC1 and activate Akt by inducing the expression of Sestrin3 and Rictor. *Dev. Cell* **18**, 592–604 (2010).
 77. Chung, S. Y. *et al.* FoxO6 and PGC-1 α form a regulatory loop in myogenic cells. *Biosci. Rep.* **33**, 485–497 (2013).
 78. Kamei, Y. *et al.* Skeletal muscle FOXO1 (FKHR) transgenic mice have less skeletal muscle mass, down-regulated Type I (slow twitch/red muscle) fiber genes, and impaired glycemic control. *J. Biol. Chem.* **279**, 41114–23 (2004).
 79. Mammucari, C. *et al.* FoxO3 Controls Autophagy in Skeletal Muscle In Vivo. *Cell Metab.* **6**, 458–471 (2007).
 80. Sandri, M. *et al.* Foxo transcription factors induce the atrophy-related ubiquitin ligase atrogin-1 and cause skeletal muscle atrophy. *Cell* **117**, 399–412 (2004).
 81. Kamei, Y. *et al.* Skeletal muscle FOXO1 (FKHR) transgenic mice have less skeletal muscle mass, down-regulated type I (slow twitch/red muscle) fiber genes, and impaired glycemic control. *J. Biol. Chem.* **279**, 41114–41123 (2004).
 82. Haddad, F., Zaldivar, F., Cooper, D. M. & Adams, G. R. IL-6-induced skeletal muscle atrophy. *J. Appl. Physiol.* **98**, 911–7 (2005).
 83. Cai, D. *et al.* IKK β /NF- κ B activation causes severe muscle wasting in mice. *Cell* **119**,

- 285–98 (2004).
84. Moore-Carrasco, R. *et al.* The AP-1/CJUN signaling cascade is involved in muscle differentiation: Implications in muscle wasting during cancer cachexia. *FEBS Lett.* **580**, 691–696 (2006).
 85. Choi, M.-C. *et al.* A direct HDAC4-MAP kinase crosstalk activates muscle atrophy program. *Mol. Cell* **47**, 122–32 (2012).
 86. Gill, R. M. & Hamel, P. A. Subcellular compartmentalization of E2F family members is required for maintenance of the postmitotic state in terminally differentiated muscle. *J. Cell Biol.* **148**, 1187–201 (2000).
 87. Sun, K., Lu, L., Wang, H. & Sun, H. Genome-wide profiling of YY1 binding sites during skeletal myogenesis. *Genomics Data* **2**, 89–91 (2014).
 88. Xiong, G. *et al.* The PERK arm of the unfolded protein response regulates satellite cell-mediated skeletal muscle regeneration. *Elife* **6**, 1–27 (2017).
 89. Sartori, R. *et al.* Smad2 and 3 transcription factors control muscle mass in adulthood. *Am. J. Physiol. Cell Physiol.* **296**, C1248-57 (2009).
 90. Wang, H. *et al.* NF- κ B-YY1-miR-29 Regulatory Circuitry in Skeletal Myogenesis and Rhabdomyosarcoma. *Cancer Cell* **14**, 369–381 (2008).
 91. Guttridge, D. C. NF-kappa B-Induced Loss of MyoD Messenger RNA: Possible Role in Muscle Decay and Cachexia. *Science (80-.).* **289**, 2363–2366 (2000).
 92. MacPherson, P. C. D., Wang, X. & Goldman, D. Myogenin regulates denervation-dependent muscle atrophy in mouse soleus muscle. *J. Cell. Biochem.* **112**, 2149–2159 (2011).
 93. Moresi, V. *et al.* Myogenin and class II HDACs control neurogenic muscle atrophy by inducing E3 ubiquitin ligases. *Cell* **143**, 35–45 (2010).
 94. Hu, J. S., Olson, E. N. & Kingston, R. E. HEB, a helix-loop-helix protein related to E2A and ITF2 that can modulate the DNA-binding ability of myogenic regulatory factors. *Mol. Cell Biol.* **12**, 1031–1042 (1992).
 95. Parker, M. H., Perry, R. L. S., Fauteux, M. C., Berkes, C. A. & Rudnicki, M. A. MyoD Synergizes with the E-Protein HEB To Induce Myogenic Differentiation. *Mol. Cell Biol.* **26**, 5771–5783 (2006).
 96. Berkes, C. A. *et al.* Pbx marks genes for activation by MyoD indicating a role for a homeodomain protein in establishing myogenic potential. *Mol. Cell* **14**, 465–477 (2004).
 97. Dell’Orso, S. *et al.* The Histone Variant MacroH2A1.2 Is Necessary for the Activation of Muscle Enhancers and Recruitment of the Transcription Factor Pbx1. *Cell Rep.* **14**, 1156–1168 (2016).
 98. Watanabe, S., Kondo, S., Hayasaka, M. & Hanaoka, K. Functional analysis of homeodomain-containing transcription factor Lbx1 in satellite cells of mouse skeletal muscle. *J. Cell Sci.* **120**, 4178–87 (2007).

99. Rossi, G. *et al.* Nfix Regulates Temporal Progression of Muscle Regeneration through Modulation of Myostatin Expression. *Cell Rep.* **14**, 2238–2249 (2016).
100. Rossi, G. *et al.* Silencing Nfix rescues muscular dystrophy by delaying muscle regeneration. *Nat. Commun.* **8**, 1–12 (2017).
101. Raichur, S. *et al.* Identification and validation of the pathways and functions regulated by the orphan nuclear receptor, ROR alpha1, in skeletal muscle. *Nucleic Acids Res.* **38**, 4296–312 (2010).
102. Chen, W., Zhang, X., Birsoy, K. & Roeder, R. G. A muscle-specific knockout implicates nuclear receptor coactivator MED1 in the regulation of glucose and energy metabolism. *Proc. Natl. Acad. Sci. U. S. A.* **107**, 10196–201 (2010).
103. Grifone, R. *et al.* Six1 and Eya1 expression can reprogram adult muscle from the slow-twitch phenotype into the fast-twitch phenotype. *Mol. Cell. Biol.* **24**, 6253–6267 (2004).
104. Relaix, F. *et al.* Six Homeoproteins Directly Activate Myod Expression in the Gene Regulatory Networks That Control Early Myogenesis. *PLoS Genet.* **9**, (2013).
105. Southard, S., Kim, J. R., Low, S. H., Tsika, R. W. & Lepper, C. Myofiber-specific TEAD1 overexpression drives satellite cell hyperplasia and counters pathological effects of dystrophin deficiency. *Elife* **5**, 1–28 (2016).
106. Tsika, R. W. *et al.* Overexpression of TEAD-1 in transgenic mouse striated muscles produces a slower skeletal muscle contractile phenotype. *J. Biol. Chem.* **283**, 36154–36167 (2008).
107. Huraskin, D. *et al.* Wnt/ β -catenin signaling via Axin2 is required for myogenesis and, together with YAP/Taz and Tead1, active in IIA/IIx muscle fibers. *Development* **143**, 3128–3142 (2016).
108. Pardo, P. S., Mohamed, J. S., Lopez, M. A. & Boriek, A. M. Induction of Sirt1 by mechanical stretch of skeletal muscle through the early response factor EGR1 triggers an antioxidative response. *J. Biol. Chem.* **286**, 2559–2566 (2011).
109. Himeda, C. L., Ranish, J. A., Pearson, R. C. M., Crossley, M. & Hauschka, S. D. KLF3 Regulates Muscle-Specific Gene Expression and Synergizes with Serum Response Factor on KLF Binding Sites. *Mol. Cell. Biol.* **30**, 3430–3443 (2010).
110. Pierce, A. *et al.* A Novel mouse model of enhanced proteostasis: Full-length human heat shock factor 1 transgenic mice. *Biochem. Biophys. Res. Commun.* **402**, 59–65 (2010).
111. Etard, C. *et al.* Loss of function of myosin chaperones triggers Hsf1-mediated transcriptional response in skeletal muscle cells. *Genome Biol.* **16**, 1–20 (2015).
112. Yokoyama, S. *et al.* Heat shock transcription factor 1-associated expression of slow myosin heavy chain in mouse soleus muscle in response to unloading with or without reloading. *Acta Physiol.* **217**, 325–337 (2016).
113. Talbert, E. E. & Guttridge, D. C. Impaired regeneration: A role for the muscle microenvironment in cancer cachexia. *Semin. Cell Dev. Biol.* **54**, 82–91 (2016).
114. Krützfeldt, J. *et al.* Silencing of microRNAs in vivo with ‘antagomirs’. *Nature* **438**, 685–9

- (2005).
115. Li, J. *et al.* MiR-29b contributes to multiple types of muscle atrophy. *Nat. Commun.* **8**, 1–15 (2017).
 116. Moraes, L. N. *et al.* Integration of miRNA and mRNA expression profiles reveals microRNA-regulated networks during muscle wasting in cardiac cachexia. *Sci. Rep.* **7**, 6998 (2017).
 117. Eisenberg, I. *et al.* Distinctive patterns of microRNA expression in primary muscular disorders. *Proc. Natl. Acad. Sci. U. S. A.* **104**, 17016–21 (2007).
 118. Soares, R. J. *et al.* Involvement of microRNAs in the regulation of muscle wasting during catabolic conditions. *J. Biol. Chem.* **289**, 21909–25 (2014).
 119. Shen, H. *et al.* Identification of microRNAs involved in dexamethasone-induced muscle atrophy. *Mol. Cell. Biochem.* **381**, 105–13 (2013).
 120. Morozova, N. *et al.* Kinetic signatures of microRNA modes of action. *RNA* **18**, 1635–55 (2012).
 121. Ge, Y. *et al.* MicroRNA-350 induces pathological heart hypertrophy by repressing both p38 and JNK pathways. *Biochim. Biophys. Acta - Mol. Basis Dis.* **1832**, 1–10 (2013).
 122. Zhou, L. *et al.* A novel target of microRNA-29, Ring1 and YY1-binding protein (Rybp), negatively regulates skeletal myogenesis. *J. Biol. Chem.* **287**, 25255–25265 (2012).
 123. Zhou, L. *et al.* Inhibition of miR-29 by TGF-beta-Smad3 signaling through dual mechanisms promotes transdifferentiation of mouse myoblasts into myofibroblasts. *PLoS One* **7**, e33766 (2012).
 124. Wang, L. *et al.* Loss of miR-29 in Myoblasts Contributes to Dystrophic Muscle Pathogenesis. *Mol. Ther.* **20**, 1222–1233 (2012).
 125. Jiang, X., Tsitsiou, E., Herrick, S. E. & Lindsay, M. A. MicroRNAs and the regulation of fibrosis. *FEBS J.* **277**, 2015–21 (2010).
 126. van Rooij, E. *et al.* Dysregulation of microRNAs after myocardial infarction reveals a role of miR-29 in cardiac fibrosis. *Proc. Natl. Acad. Sci. U. S. A.* **105**, 13027–32 (2008).
 127. Maurer, B. *et al.* MicroRNA-29, a key regulator of collagen expression in systemic sclerosis. *Arthritis Rheum.* **62**, 1733–43 (2010).
 128. Cushing, L. *et al.* miR-29 is a major regulator of genes associated with pulmonary fibrosis. *Am. J. Respir. Cell Mol. Biol.* **45**, 287–294 (2011).
 129. Roderburg, C. *et al.* Micro-RNA profiling reveals a role for miR-29 in human and murine liver fibrosis. *Hepatology* **53**, 209–18 (2011).
 130. Cacchiarelli, D. *et al.* MicroRNAs involved in molecular circuitries relevant for the Duchenne muscular dystrophy pathogenesis are controlled by the dystrophin/nNOS pathway. *Cell Metab.* **12**, 341–51 (2010).
 131. Wang, B. *et al.* Suppression of microRNA-29 expression by TGF- β 1 promotes collagen expression and renal fibrosis. *J. Am. Soc. Nephrol.* **23**, 252–65 (2012).

132. O'Reilly, S. MicroRNAs in fibrosis: opportunities and challenges. *Arthritis Res. Ther.* **18**, 11 (2016).
133. Galimov, A. *et al.* microRNA-29a in adult muscle stem cells controls skeletal muscle regeneration during injury and exercise downstream of fibroblast growth factor-2. *Stem Cells* n/a-n/a (2016). doi:10.1002/stem.2281
134. Franco, F. de O. *et al.* Cancer cachexia differentially regulates visceral adipose tissue turnover. *J. Endocrinol.* **232**, 493–500 (2017).
135. Braun, T. & Gautel, M. Transcriptional mechanisms regulating skeletal muscle differentiation, growth and homeostasis. *Nat. Rev. Mol. Cell Biol.* **12**, 349–61 (2011).
136. Zugmaier, G. *et al.* Transforming growth factor β 1 induces cachexia and systemic fibrosis without an antitumor effect in nude mice. *Cancer Res.* **51**, 3590–3594 (1991).
137. Tsai, V. W. W. *et al.* Anorexia/cachexia of chronic diseases: a role for the TGF- β family cytokine MIC-1/GDF15. *J. Cachexia. Sarcopenia Muscle* **3**, 239–43 (2012).
138. Mendias, C. L. *et al.* Transforming growth factor-beta induces skeletal muscle atrophy and fibrosis through the induction of atrogen-1 and scleraxis. *Muscle Nerve* **45**, 55–59 (2012).
139. Devine, R. D., Bicer, S., Reiser, P. J., Velten, M. & Wold, L. E. Metalloproteinase expression is altered in cardiac and skeletal muscle in cancer cachexia. *Am. J. Physiol. - Hear. Circ. Physiol.* **309**, H685–H691 (2015).
140. Judge, S. M. *et al.* Genome-wide identification of FoxO-dependent gene networks in skeletal muscle during C26 cancer cachexia. *BMC Cancer* **14**, 997 (2014).
141. Calura, E. *et al.* Meta-analysis of expression signatures of muscle atrophy: gene interaction networks in early and late stages. *BMC Genomics* **9**, 630 (2008).
142. Pfaffl, M. W. A new mathematical model for relative quantification in real-time RT-PCR. *Nucleic Acids Res.* **29**, e45 (2001).
143. Pfaffl, M. W., Horgan, G. W. & Dempfle, L. Relative expression software tool (REST) for group-wise comparison and statistical analysis of relative expression results in real-time PCR. *Nucleic Acids Res.* **30**, e36 (2002).
144. Ruijter, J. M. *et al.* Amplification efficiency: linking baseline and bias in the analysis of quantitative PCR data. *Nucleic Acids Res.* **37**, e45 (2009).
145. Kim, D. *et al.* TopHat2: accurate alignment of transcriptomes in the presence of insertions, deletions and gene fusions. *Genome Biol.* **14**, R36 (2013).
146. Langmead, B., Trapnell, C., Pop, M. & Salzberg, S. Ultrafast and memory-efficient alignment of short DNA sequences to the human genome. *Genome Biol.* **10**, R25 (2009).
147. Langmead, B. & Salzberg, S. L. Fast gapped-read alignment with Bowtie 2. *Nat. Methods* **9**, 357–359 (2012).
148. Anders, S., Pyl, P. T. & Huber, W. HTSeq-A Python framework to work with high-throughput sequencing data. *Bioinformatics* **31**, 166–169 (2015).

149. Love, M. I., Huber, W. & Anders, S. Moderated estimation of fold change and dispersion for RNA-seq data with DESeq2. *Genome Biol.* **15**, 550 (2014).
150. Wang, X. miRDB: a microRNA target prediction and functional annotation database with a wiki interface. *RNA* **14**, 1012–7 (2008).
151. Garcia, D. M. *et al.* Weak seed-pairing stability and high target-site abundance decrease the proficiency of lsy-6 and other microRNAs. *Nat. Struct. Mol. Biol.* **18**, 1139–46 (2011).
152. Maragkakis, M. *et al.* DIANA-microT web server: elucidating microRNA functions through target prediction. *Nucleic Acids Res.* **37**, W273–6 (2009).
153. Krek, A. *et al.* Combinatorial microRNA target predictions. *Nat. Genet.* **37**, 495–500 (2005).
154. Hsu, S.-D. *et al.* miRTarBase: a database curates experimentally validated microRNA-target interactions. *Nucleic Acids Res.* **39**, D163–9 (2011).
155. Maere, S., Heymans, K. & Kuiper, M. BiNGO: a Cytoscape plugin to assess overrepresentation of gene ontology categories in biological networks. *Bioinformatics* **21**, 3448–9 (2005).
156. Bindea, G. *et al.* ClueGO: a Cytoscape plug-in to decipher functionally grouped gene ontology and pathway annotation networks. *Bioinformatics* **25**, 1091–3 (2009).
157. Cline, M. S. *et al.* Integration of biological networks and gene expression data using Cytoscape. *Nat. Protoc.* **2**, 2366–82 (2007).
158. Gelin, J. *et al.* Role of endogenous tumor necrosis factor alpha and interleukin 1 for experimental tumor growth and the development of cancer cachexia. *Cancer Res* **51**, 415–421 (1991).
159. Cahlin, C. *et al.* Experimental cancer cachexia: the role of host-derived cytokines interleukin (IL)-6, IL-12, interferon-gamma, and tumor necrosis factor alpha evaluated in gene knockout, tumor-bearing mice on C57 Bl background and eicosanoid-dependent cachexia. *Cancer Res.* **60**, 5488–93 (2000).
160. Guttridge, D. C. NF-kappa B-Induced Loss of MyoD mRNA: possible role in muscle cecay and cachexia. *Science (80-)*. **289**, 2363–2366 (2000).
161. Seto, D. N., Kandarian, S. C. & Jackman, R. W. A Key Role for Leukemia Inhibitory Factor in C26 Cancer Cachexia. *J. Biol. Chem.* **290**, 19976–19986 (2015).
162. Darling, G., Fraker, D. L., Jensen, J. C., Gorschboth, C. M. & Norton, J. A. Cachectic effects of recombinant human tumor necrosis factor in rats. *Cancer Res.* **50**, 4008–4013 (1990).
163. Balkwill, F. *et al.* Evidence for Tumour Necrosis Factor/Cachectin Production in Cancer. *Lancet* **330**, 1229–1232 (1987).
164. Li, Y.-P. *et al.* TNF-alpha acts via p38 MAPK to stimulate expression of the ubiquitin ligase atrogin1/MAFbx in skeletal muscle. *FASEB J.* **19**, 362–70 (2005).
165. Di Marco, S. *et al.* NF-kappa B-mediated MyoD decay during muscle wasting requires nitric oxide synthase mRNA stabilization, HuR protein, and nitric oxide release. *Mol. Cell. Biol.* **25**, 6533–45 (2005).

166. Williams, G., Brown, T., Becker, L., Prager, M. & Giroir, B. P. Cytokine-induced expression of nitric oxide synthase in C2C12 skeletal muscle myocytes. *Am. J. Physiol.* **267**, R1020-5 (1994).
167. Buck, M. & Chojkier, M. Muscle wasting and dedifferentiation induced by oxidative stress in a murine model of cachexia is prevented by inhibitors of nitric oxide synthesis and antioxidants. *EMBO J.* **15**, 1753–65 (1996).
168. Rodriguez-Pascual, F. *et al.* Complex contribution of the 3'-untranslated region to the expressional regulation of the human inducible nitric-oxide synthase gene: Involvement of the RNA-binding protein HuR. *J. Biol. Chem.* **275**, 26040–26049 (2000).
169. Hall, D. T., Ma, J. F., Marco, S. Di & Gallouzi, I.-E. Inducible nitric oxide synthase (iNOS) in muscle wasting syndrome, sarcopenia, and cachexia. *Aging (Albany, NY)*. **3**, 702–15 (2011).
170. Bhatnagar, S. *et al.* Tumor necrosis factor- α regulates distinct molecular pathways and gene networks in cultured skeletal muscle cells. *PLoS One* **5**, e13262 (2010).
171. Meyer, S. U. *et al.* Tumor necrosis factor alpha and insulin-like growth factor 1 induced modifications of the gene expression kinetics of differentiating skeletal muscle cells. *PLoS One* **10**, 1–36 (2015).
172. Core, L. J., Waterfall, J. J. & Lis, J. T. Nascent RNA sequencing reveals widespread pausing and divergent initiation at human promoters. *Science (80-.)*. **322**, 1845–1848 (2008).
173. Licatalosi, D. D. *et al.* HITS-CLIP yields genome-wide insights into brain alternative RNA processing. *Nature* **456**, 464–9 (2008).
174. Licatalosi, D. D. & Darnell, R. B. RNA processing and its regulation: global insights into biological networks. *Nat. Rev. Genet.* **11**, 75–87 (2010).
175. Rabani, M. *et al.* High-resolution sequencing and modeling identifies distinct dynamic RNA regulatory strategies. *Cell* **159**, 1698–1710 (2014).
176. Eser, P. *et al.* Determinants of RNA metabolism in the *Schizosaccharomyces pombe* genome. *Mol. Syst. Biol.* **12**, 857 (2016).
177. Miller, C. *et al.* Dynamic transcriptome analysis measures rates of mRNA synthesis and decay in yeast. *Mol. Syst. Biol.* **7**, 458 (2011).
178. García-Martínez, J., Aranda, A. & Pérez-Ortín, J. E. Genomic run-on evaluates transcription rates for all yeast genes and identifies gene regulatory mechanisms. *Mol. Cell* **15**, 303–313 (2004).
179. Grigull, J. *et al.* Genome-Wide Analysis of mRNA Stability Using Transcription Inhibitors and Microarrays Reveals Posttranscriptional Control of Ribosome Biogenesis Factors Genome-Wide Analysis of mRNA Stability Using Transcription Inhibitors and Microarrays Reveals Posttran. *Mol. Cell. Biol.* **24**, 5534–5547 (2004).
180. Wang, Y. *et al.* Precision and functional specificity in mRNA decay. *Proc. Natl. Acad. Sci. U. S. A.* **99**, 5860–5865 (2002).

181. Wuarin, J. & Schibler, U. Physical isolation of nascent RNA chains transcribed by RNA polymerase II: evidence for cotranscriptional splicing. *Mol Cell Biol* **14**, 7219–7225 (1994).
182. Pandya-Jones, A. & Black, D. L. Co-transcriptional splicing of constitutive and alternative exons. *Rna* **15**, 1896–1908 (2009).
183. Bhatt, D. M. *et al.* Transcript dynamics of proinflammatory genes revealed by sequence analysis of subcellular RNA fractions. *Cell* **150**, 279–290 (2012).
184. Tong, A. J. *et al.* A Stringent Systems Approach Uncovers Gene-Specific Mechanisms Regulating Inflammation. *Cell* **165**, 165–179 (2016).
185. Lee, J. E., Lee, J. Y., Wilusz, J., Tian, B. & Wilusz, C. J. Systematic analysis of Cis-elements in unstable mRNAs demonstrates that CUGBP1 is a key regulator of mRNA decay in muscle cells. *PLoS One* **5**, (2010).
186. Figueroa, A. *et al.* Role of HuR in skeletal myogenesis through coordinate regulation of muscle differentiation genes. *Mol. Cell. Biol.* **23**, 4991–5004 (2003).
187. Zeisel, A. *et al.* Coupled pre-mRNA and mRNA dynamics unveil operational strategies underlying transcriptional responses to stimuli. *Mol. Syst. Biol.* **7**, 529 (2011).
188. Rabani, M. *et al.* Metabolic labeling of RNA uncovers principles of RNA production and degradation dynamics in mammalian cells. *Nat. Biotechnol.* **29**, 436–442 (2011).
189. Burrage, P. S., Mix, K. S. & Brinckerhoff, C. E. Matrix metalloproteinases: role in arthritis. *Front. Biosci.* **11**, 529–43 (2006).
190. Sanjana, N. E., Shalem, O. & Zhang, F. Improved vectors and genome-wide libraries for CRISPR screening. *Nat. Methods* **11**, 783–784 (2014).
191. Dogra, C. *et al.* TNF-related weak inducer of apoptosis (TWEAK) is a potent skeletal muscle-wasting cytokine. *FASEB J.* **21**, 1857–69 (2007).
192. Dobin, A. & Gingeras, T. R. Mapping RNA-seq Reads with STAR. *Curr. Protoc. Bioinforma.* **51**, 11.14.1-11.14.19 (2015).
193. Liao, Y., Smyth, G. K. & Shi, W. FeatureCounts: An efficient general purpose program for assigning sequence reads to genomic features. *Bioinformatics* **30**, 923–930 (2014).
194. Robinson, J. T. *et al.* Integrative genomics viewer. *Nat. Biotechnol.* **29**, 24–6 (2011).
195. Schwalb, B. *et al.* Measurement of genome-wide RNA synthesis and decay rates with Dynamic Transcriptome Analysis (DTA). *Bioinformatics* **28**, 884–5 (2012).
196. Chechik, G. & Koller, D. Timing of Gene Expression Responses to Environmental Changes. *J. Comput. Biol.* **16**, 279–290 (2009).